Hodell, D.A., Abrantes, F., Alvarez Zarikian, C.A., and the Expedition 397 Scientists
Proceedings of the International Ocean Discovery Program Volume 397
publications.iodp.org

Expedition 397 summary[1]

D.A. Hodell, F. Abrantes, C.A. Alvarez Zarikian, H.L. Brooks, W.B. Clark, L.F.B. Dauchy-Tric, V. dos Santos Rocha, J.-A. Flores, T.D. Herbert, S.K.V. Hines, H.-H.M. Huang, H. Ikeda, S. Kaboth-Bahr, J. Kuroda, J.M. Link, J.F. McManus, B.A. Mitsunaga, L. Nana Yobo, C.T. Pallone, X. Pang, M.Y. Peral, E. Salgueiro, S. Sanchez, K. Verma, J. Wu, C. Xuan, and J. Yu[2]

[1] Hodell, D.A., Abrantes, F., Alvarez Zarikian, C.A., Brooks, H.L., Clark, W.B., Dauchy-Tric, L.F.B., dos Santos Rocha, V., Flores, J.-A., Herbert, T.D., Hines, S.K.V., Huang, H.-H.M., Ikeda, H., Kaboth-Bahr, S., Kuroda, J., Link, J.M., McManus, J.F., Mitsunaga, B.A., Nana Yobo, L., Pallone, C.T., Pang, X., Peral, M.Y., Salgueiro, E., Sanchez, S., Verma, K., Wu, J., Xuan, C., and Yu, J., 2024. Expedition 397 summary. In Hodell, D.A., Abrantes, F., Alvarez Zarikian, C.A., and the Expedition 397 Scientists, Iberian Margin Paleoclimate. Proceedings of the International Ocean Discovery Program, 397: College Station, TX (International Ocean Discovery Program). https://doi.org/10.14379/iodp.proc.397.101.2024
[2] **Expedition 397 Scientists' affiliations.**

Contents

Keywords
International Ocean Discovery Program, IODP, *JOIDES Resolution*, Expedition 397, Iberian Margin Paleoclimate, Climate and Ocean Change, Site U1586, Site U1587, Site U1385, Site U1588

Core descriptions

Supplementary material

References (RIS)

MS 397-101
Published 11 June 2024

Funded by NSF OCE1326927, ECORD, and JAMSTEC

Abstract

During International Ocean Discovery Program Expedition 397, we recovered a total of 6176.7 m of core (104.2% recovery) at four sites (U1586, U1587, U1385, and U1588) from the Promontório dos Príncipes de Avis, a plateau located on the Portuguese continental slope that is elevated above the Tagus Abyssal Plain and isolated from the influence of turbidites. The drill sites are arranged along a bathymetric transect (4692, 3479, 2591, and 1339 meters below sea level [mbsl], respectively) to intersect each of the major subsurface water masses of the eastern North Atlantic. Multiple holes were drilled at each site to ensure complete spliced composite sections, which will be further refined postcruise by a campaign of X-ray fluorescence core scanning.

At Site U1586 (4692 mbsl), the deepest and farthest from shore, a 350 m sequence was recovered in four holes that extend as far back as the middle Miocene (14 Ma), which is nearly twice as old as initially predicted from seismic stratigraphy. Sedimentation rates are lower (averaging 5 cm/ky in the Quaternary) at Site U1586 than other Expedition 397 sites, and a few slumped intervals were encountered in the stratigraphic sequence. Despite these limitations, Site U1586 anchors the deep end-member of the bathymetric transect and provides an important reference section to study deepwater circulation, ventilation and carbon storage in the deep eastern North Atlantic.

At Site U1587 (3479 mbsl), the second deepest site along the depth transect, we recovered a 567 m sequence of late Miocene to Holocene sediments that accumulated at rates between 6.5 and 11 cm/ky. The high sedimentation rates and long continuous record at this site will permit climate reconstruction at high temporal resolution (e.g., millennial) for the past 7.8 My. The Messinian Stage (7.25–5.33 Ma) was recovered, which provides a valuable opportunity to study the Messinian Salinity Crisis in an open marine setting adjacent to the Mediterranean.

Site U1385 (Shackleton site) was a reoccupation of a position previously drilled during Integrated Ocean Drilling Program Expedition 339. Expedition 339 Site U1385 has yielded a remarkable record of millennial-scale climate change for the past 1.45 My (Marine Isotope Stage 47). During Expedition 397, we deepened the site from 156 to 400 meters below seafloor, extending the record to near the base of the Pliocene (5.3 Ma). Sedimentation rates remained high, averaging between 9 and 11 cm/ky throughout the sequence. The newly recovered cores at Expedition 397 Site U1385 will permit the study of millennial climate variability through the entire Quaternary and Pliocene, prior to the intensification of Northern Hemisphere glaciation.

Site U1588 is the shallowest, closest to shore, and youngest site drilled during Expedition 397 and is also the one with the highest sedimentation rate (20 cm/ky). The base of the 412.5 m sequence is 2.2 Ma, providing an expanded Pleistocene sequence of sediment deposited under the influence

of the lower core of the Mediterranean Outflow Water (MOW). Together with other Expedition 339 sites, Site U1588 will be important for determining how the depth and intensity of the MOW has varied on orbital and millennial timescales. In addition, it also provides a marine reference section for studying Quaternary climate variability at very high temporal resolution (millennial to submillennial).

A highlight of the expedition is that sediment at all sites shows very strong cyclicity in bulk sediment properties (color, magnetic susceptibility, and natural gamma radiation). Particularly remarkable are the precession cycles of the Pliocene that can be correlated peak-for-peak among sites. These cyclic variations will be used to derive an orbitally tuned timescale for Expedition 397 sites and correlate them into classic Mediterranean cyclostratigraphy.

The cores recovered during Expedition 397 will form the basis of collaborative postcruise research to produce benchmark paleoclimate records for the late Miocene through Quaternary using the widest range of proxy measurements. It will take many years to complete these analyses, but the records will lead to major advances in our understanding of millennial and orbital climate changes and their underlying causes and evolving contextuality.

Outreach during Expedition 397 was highly productive, reaching a record number of students and the general public across the world through several diverse platforms, including live ship-to-shore events, webinars, social media, videos, radio pieces, blog posts, and in-person activities.

Plain language summary

From 11 October to 11 December 2022, International Ocean Discovery Program Expedition 397 took place off the coast of Portugal southwest of Lisbon. The main objective was to recover the exceptional sedimentary archive preserved beneath the seafloor on the Iberian margin to study past climate change at high temporal resolution. During the expedition, which carried 26 international scientists, four sites were drilled, recovering 6.2 km of marine sediments that accumulated rapidly, thereby providing a high-fidelity record of past climate change on timescales of hundreds to thousands of years and extending back millions of years ago. Climate signals contained in these marine sediment cores will be correlated precisely to polar ice cores from both hemispheres and with European pollen records, providing a rare opportunity to link oceanic, atmospheric, and terrestrial climate and environmental changes. The four drill sites are located at different water depths (1339, 2591, 3479, and 4692 m below sea level), permitting scientists to study how deep-ocean circulation and chemistry changed in the past, including its role in deep-sea carbon storage and atmospheric CO_2 changes. The sediment cores recovered during Expedition 397 will provide benchmark records of North Atlantic climate change at high temporal resolution from the late Miocene (about 8 million years ago) to present. This period includes the last 3 million years when changes in the Earth's orbit resulted in the growth and decay of large ice sheets in the Northern Hemisphere and a warmer world before this time when atmospheric CO_2 was similar to today. All cores recovered show strong changes in physical properties (such as color) that represent a response to known cyclic changes in Earth's orbit, which will aid in accurately dating the sediment. Many years of research will be needed to extract the detailed climatic signals from the kilometers of core recovered during Expedition 397, but the records to be produced will be vital for testing numerical climate models and understanding how the climate system evolved in the past and how it might change in the future.

1. Introduction

The southwestern Iberian margin is a well-known source of rapidly accumulating sediment that contains high-fidelity records of millennial climate variability (MCV) for the late Pleistocene (Figures **F1**, **F2**), as expressed in proxy records of oxygen isotopes and sea-surface temperature (Shackleton et al., 2000, 2004; Bard et al., 2000; Pailler and Bard, 2002; Martrat et al., 2007). Previous studies have demonstrated that surface and deepwater climate signals from the region can be correlated precisely to the polar ice cores in both hemispheres. Shackleton et al. (2000) demonstrated that surface oxygen isotope and sea-surface temperature records mirror those of Green-

land ice core records, whereas the deepwater signal follows the Antarctic ice core climate signal, thereby preserving a history of both polar ice cores in a single sedimentary archive (Figure **F3**). The relative timing of surface (Greenland) and deepwater (Antarctic) signals in the same core provides a means to assess interhemispheric phasing of climate change (e.g., bipolar seesaw), which has been independently verified by methane synchronization of ice cores for the last glacial period (Blunier and Brook, 2001; WAIS Divide Project Members, 2015). Moreover, the narrow continental shelf off Portugal results in the rapid delivery of terrestrial material to the deep-sea environment, thereby permitting correlation of marine, ice core, and European terrestrial records (Margari et al., 2010, 2014; Naughton et al., 2019; Oliveira et al., 2016, 2017, 2018, 2020; Sánchez Goñi et al., 1999, 2000; Shackleton et al., 2003; Tzedakis et al., 2004, 2009).

The continuity, high sedimentation rates, and fidelity of the climate signals preserved in Iberian margin sediments make it a prime target for ocean drilling. A proof-of-concept, Site U1385 was drilled during Integrated Ocean Drilling Program Expedition 339 (Mediterranean Outflow) in late 2011 at a water depth of 2582 meters below sea level (mbsl) (Hodell et al., 2013b; Expedition 339 Scientists, 2013a). Five holes were cored using the advanced piston corer (APC) system to a maximum depth of ~155.9 meters below seafloor (mbsf). Immediately after the expedition, cores from

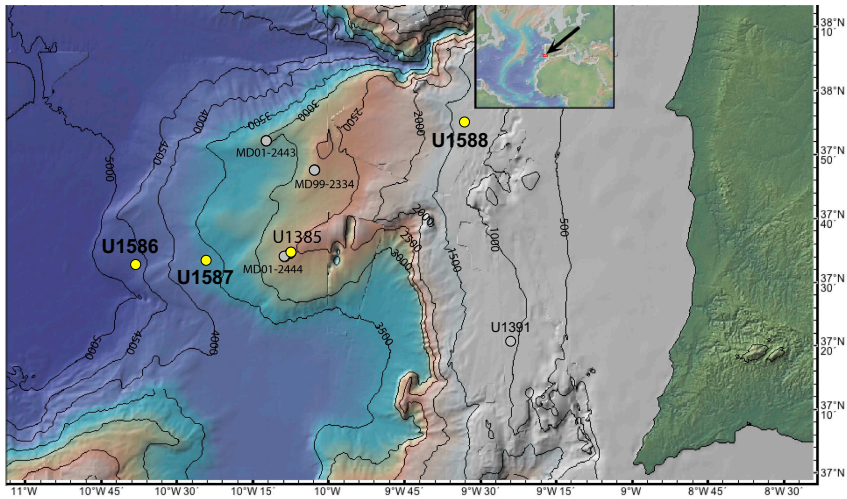

Figure F1. Bathymetry of the Promontório dos Príncipes de Avis (PPA) showing the locations of the four sites (U1586, U1587, U1385, and U1588) drilled during Expedition 397, Marion Dufrense (MD) piston cores, and IODP Site U1391. Site U1385 was occupied previously during Expedition 339, as was Site U1391. The map is modified from Hodell et al. (2015) and was made with GeoMapApp (**http://www.geomapapp.org**) using the bathymetry of Zitellini et al. (2009).

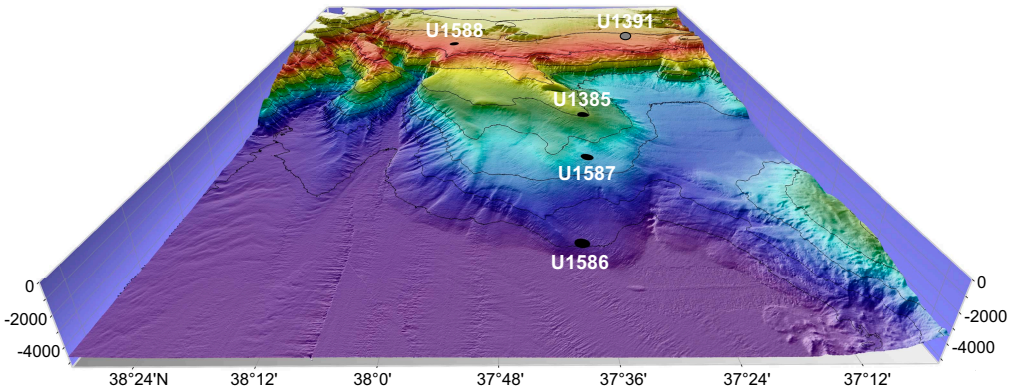

Figure F2. Depth distribution of Expedition 397 drill sites on the Promontório dos Príncipes de Avis (PPA) looking onshore to the east. The sites are located on a bathymetric transect that intersects each of the major subsurface water masses of the North Atlantic. Depths range from 1339 mbsl (Site U1588) to 4692 mbsl (Site U1586). Expedition 339 Site U1391 is also shown. (Figure made by Helder Pereira using Mirone and iVew4D software.)

all holes were analyzed by core scanning X-ray fluorescence (XRF) at 1 cm spatial resolution (Hodell et al., 2015). Ca/Ti data were used to accurately correlate hole-to-hole and construct a composite spliced section containing no gaps or disturbed intervals to 166.5 meters composite depth (mcd). A high-resolution oxygen isotope record confirms that Site U1385 contains a continuous record of MCV from the Holocene to 1.45 Ma (Marine Isotope Stage [MIS] 47) (Hodell et al., 2023) with sedimentation rates of ~10–20 cm/ky (Figure **F4**). Strong precession cycles in color and elemental XRF signals from Site U1385 were used to develop an orbitally tuned reference timescale that is independent of LR04 (Hodell et al., 2015). Although results are still emerging, Site U1385 demonstrates the great potential of the western Iberian margin to yield long, undisturbed records of millennial-scale climate change and land-sea comparisons.

Building on the success of Site U1385 and given the seminal importance of the Iberian margin for paleoclimatology and marine-ice-land correlations, International Ocean Discovery Program (IODP) Expedition 397 was designed to accomplish the following:

- Extend the record beyond the base of Site U1385 (1.45 Ma) and recover the high-fidelity Iberian margin sedimentary archive for study of climate variability from the Quaternary through the late Miocene and
- Recover a bathymetric transect of sites from 1339 to 4692 mbsl that spans the range of the major subsurface water masses of the eastern North Atlantic (Figure **F5**).

The depth transect is designed to complement those sites drilled during Expedition 339 where sediment was recovered at intermediate water depths (560–1073 mbsl) under the influence of Mediterranean Outflow Water (MOW). Together, the Expedition 339 and 397 sites will constitute a complete depth transect from 560 to 4692 mbsl with which to study past variability of all the major subsurface water masses of the eastern North Atlantic.

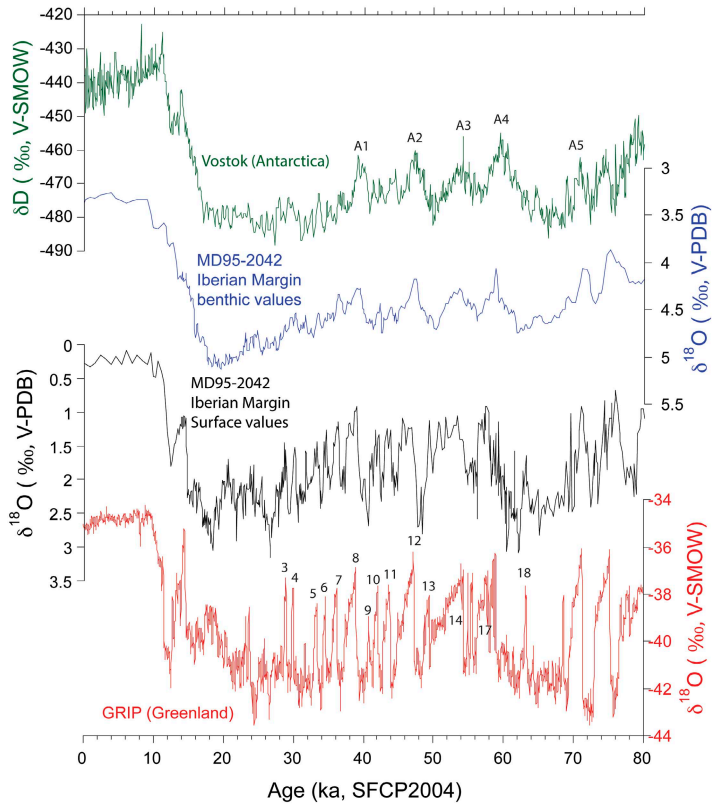

Figure F3. Correlation of $\delta^{18}O$ record of Greenland ice core (GRIP; red) to $\delta^{18}O$ of *Globigerina bulloides* (black) in Core MD95-2042 (Shackleton et al., 2000). Selected Dansgaard-Oeschger events are labeled in GRIP record and Antarctic isotope maxima (A1–A5) are labeled in Vostok. Timescale is SFCP2004 published by Shackleton et al. (2004). V-SMOW = Vienna standard mean ocean water, V-PDB = Vienna Peedee belemnite. From Hodell et al. (2013b).

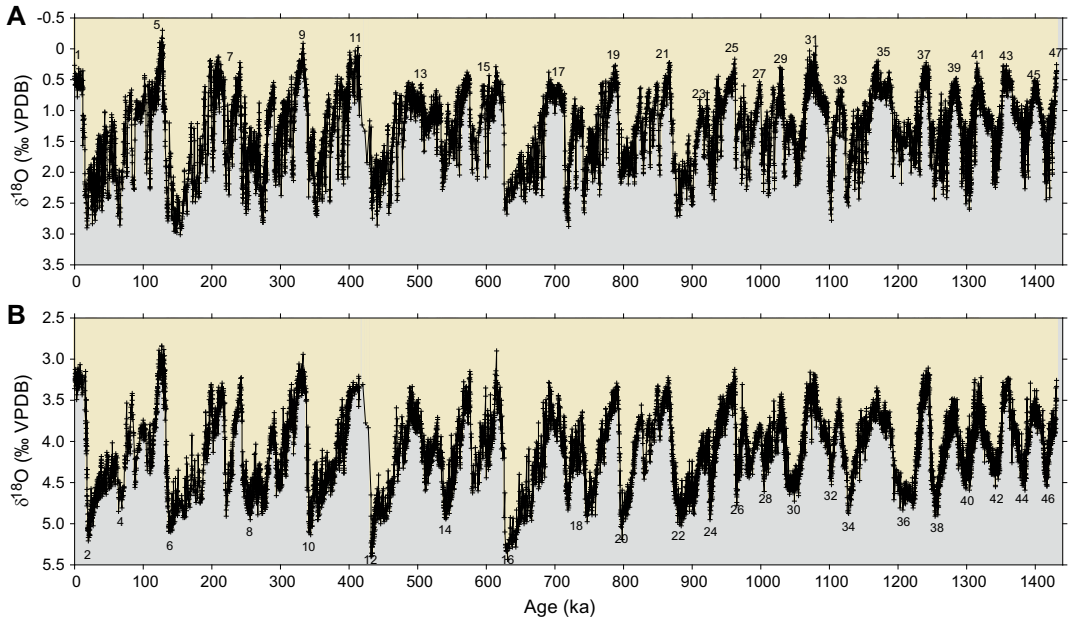

Figure F4. Oxygen isotope record of (A) *Globigerina bulloides* and (B) mixed benthic foraminifer species mostly consisting of *Cibicidoides wuellerstorfi*, spanning the last 1.45 My (to MIS 47) at Expedition 339 Site U1385. Marine isotope stages are numbered: interglacial in (A) and glacial in (B). Figure from Hodell et al. (2023). VPDB = Vienna Peedee belemnite.

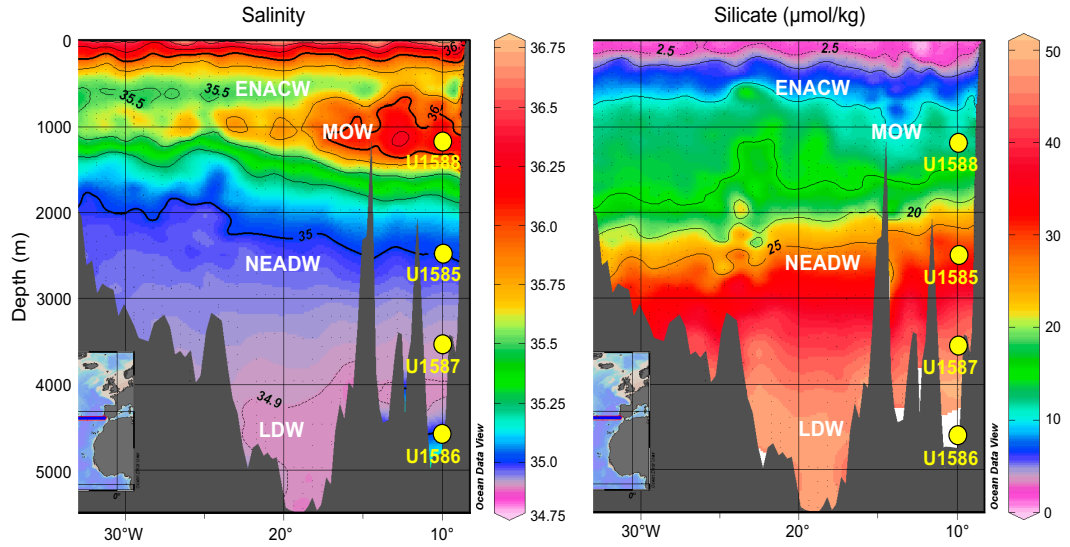

Figure F5. Salinity and silicate profiles on WOCE Line A03 (36°N) showing proposed site locations on the Iberian margin (Schlitzer, 2000). Tongue of high salinity water between 600 and 1200 m is MOW. High Si (>35 µmol/kg) below 3000 m represents a contribution from LDW sourced from the Southern Ocean. Water masses do not have clearly defined boundaries but rather consist of a series of core layers bordered by transition (mixing) zones between adjacent layers. The positions of Expedition 397 sites are shown relative to each of the identified subsurface water masses.

2. Preliminary scientific assessment

Expedition 397 accomplished almost all of its primary objectives and was a great success overall. We recovered 6176.7 m of sediment (104.2% recovery) at four primary sites (U1586, U1587, U1385, and U1588) (Table **T1**). Multiple holes were drilled at each site, and complete composite sections were constructed. Sites U1586 and U1385 were drilled to the planned depths of 350 and 400 mbsf, respectively (Figure **F6**).We recovered much older sediment (14 Ma) than anticipated at

Site U1586 (Figure F7), which extended the expedition objectives into the middle Miocene (Figure F8). At Site U1587, we sought and were granted permission from the Environmental Protection and Safety Panel (EPSP) to deepen the hole from 400 to 450 mbsf to ensure complete recovery of the Messinian Stage (7.25–5.33 Ma). Site U1588 could only be drilled to 412.5 mbsf out of the planned 500 mbsf because severe gas expansion of the sediment forced us to alter our strategy and drill half advances (4.8 m) with the extended core barrel (XCB) system, which significantly slowed the recovery rate.

The decision to use a polycrystalline diamond compact (PDC) bit and cutting shoe with the XCB system proved pivotal to the expedition's success, resulting in very high recovery and good quality XCB cores (Figure F9). The exceptional percent recovery (104%) was aided by half advances of the

Table T1. Hole summary, Expedition 397. **Download table in CSV format.**

Hole	Latitude	Longitude	Water depth (m)	Total penetration (m)	Cored interval (m)	Recovered length (m)	Recovery (%)	Drilled interval (m)	Total cores (*N*)	APC cores (*N*)	HLAPC cores (*N*)	XCB cores (*N*)	XCB half-cores (*N*)
U1586A	37°37.3108′N	10°42.5987′W	4691.1	350.0	350.0	339.6	97		42	19	7	16	0
U1586B	37°37.3478′N	10°42.5506′W	4690.5	350.0	350.0	335.1	96		40	16	0	24	0
U1586C	37°37.2911′N	10°42.6216′W	4692.4	349.1	349.1	334.4	96		38	13	0	25	0
U1586D	37°37.2835′N	10°42.6289′W	4693.6	350.0	350.0	337.8	97		38	12	0	26	0
		Site U1586 totals:		1399.1	1399.1	1346.9	96		158	60	7	91	0
U1587A	37°34.8602′N	10°21.5400′W	3480.5	500.0	500.0	478.1	96		53	15	0	38	0
U1587B	37°34.8650′N	10°21.5314′W	3478.0	547.8	547.8	534.3	98		59	11	0	48	0
U1587C	37°34.8750′N	10°21.5205′W	3479.0	567.9	567.9	553.3	97		61	12	0	49	0
		Site U1587 totals:		1615.7	1615.7	1565.7	97		173	38	0	135	0
U1385F	37°33.9999′N	10°7.6587′W	2589.1	400.0	303.1	290.8	96	96.9	32	0	0	32	0
U1385G	37°34.0108′N	10°7.6656′W	2592.4	397.3	397.3	396.3	100		42	12	0	30	0
U1385H	37°34.0223′N	10°7.6641′W	2592.4	399.2	284.6	285.0	100	114.6	31	0	0	31	0
U1385I	37°34.0205′N	10°7.6505′W	2589.1	152.5	152.5	145.4	95		16	11	0	5	0
U1385J	37°34.0103′N	10°7.6513′W	2593.1	400.0	400.0	397.8	99		43	11	0	32	0
		Site U1385 totals:		1749.0	1537.5	1515.2	99	211.5	164	34		130	0
U1588A	37°57.6044′N	9°30.9961′W	1339.3	353.0	353.0	378.4	107		49	17	0	9	23
U1588B	37°57.6149′N	9°30.9956′W	1339.3	350.0	350.0	456.1	130		64	9	0	0	55
U1588C	37°57.6160′N	9°30.9814′W	1339.3	353.6	261.6	345.0	132	92.0	53	0	0	0	53
U1588D	37°57 60.23′N	9°30.9820′W	1338.5	412.5	412.5	569.4	138		76	11	0	0	65
		Site U1588 totals:		1469.1	1377.1	1748.9	127	92.0	242	37	0	9	196
		Expedition 397 totals:		6232.9	5929.4	6176.7	104	303.5	737	169	7	365	196

Hole	Date started (2022)	Start time UTC (h)	Date finished (2022)	End time UTC (h)	Time on hole (h)	Time on hole (d)
U1586A	16 Oct	1730	20 Oct	0830	87.12	3.63
U1586B	21 Oct	0900	25 Oct	1220	99.36	4.14
U1586C	25 Oct	1220	28 Oct	0345	63.36	2.64
U1586D	28 Oct	0345	1 Nov	0710	99.36	4.14
U1587A	1 Nov	1130	5 Nov	0250	87.36	3.64
U1587B	5 Nov	0250	10 Nov	1530	132.72	5.53
U1587C	10 Nov	1530	15 Nov	1000	114.48	4.77
U1385F	16 Nov	0120	19 Nov	2235	93.36	3.89
U1385G	19 Nov	2235	22 Nov	0200	51.36	2.14
U1385H	22 Nov	0200	23 Nov	2315	45.36	1.89
U1385I	26 Nov	0800	27 Nov	0215	18.24	0.76
U1385J	27 Nov	0215	30 Nov	0140	71.52	2.98
U1588A	30 Nov	0600	2 Dec	0145	43.68	1.82
U1588B	2 Dec	0145	3 Dec	2145	43.92	1.83
U1588C	3 Dec	2145	5 Dec	1550	42.00	1.75
U1588D	5 Dec	1550	8 Dec	0038	56.88	2.37

XCB system at Site U1588 that recovered a greater length of core than that drilled because of gas expansion.

A primary objective of Expedition 397 was to recover marine sequences that could be compared with existing and future polar ice core records. If the Beyond EPICA-Oldest Ice (BE-OI) Project and/or Center for Oldest Ice Exploration (COLDEX) are successful, the Antarctic ice core record will span the last 1.5 My (Fischer et al., 2013). Figure **F10** shows the natural gamma radiation (NGR) records of all Expedition 397 sites along the bathymetric transect for the last ~1.5 My. With few exceptions, such as the slump at Site U1586, the records correlate peak-for-peak among the sites despite a nearly four-fold difference in sedimentation rates. These sites will serve as marine reference sections of Pleistocene climate variability (Alley, 2003) and are important for linking to the polar ice cores (Wolff et al., 2022) and European terrestrial sequences.

Sediments at all sites show strong cyclic variations in physical properties (color, magnetic susceptibility (MS), and NGR) that are related to changes in Earth's orbital cycles. Particularly notable are

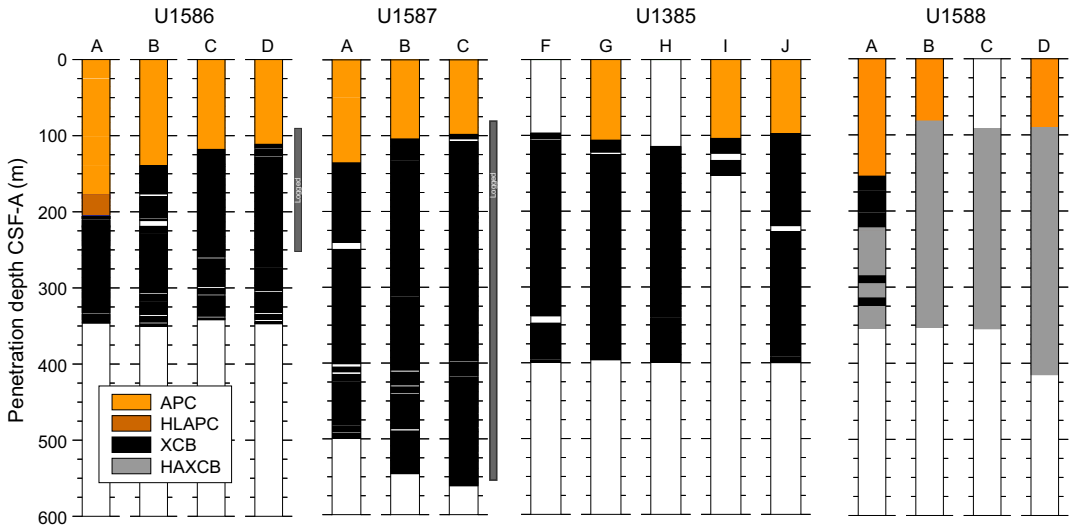

Figure F6. Core recovery for each hole drilled during Expedition 397. Holes U1385F, U1385H, and U1588C were washed down without recovery before XCB coring. HAXCB = half advance extended core barrel. Gray bar alongside Holes U1586D and U1587C = portion of the hole logged using the triple combo tool string.

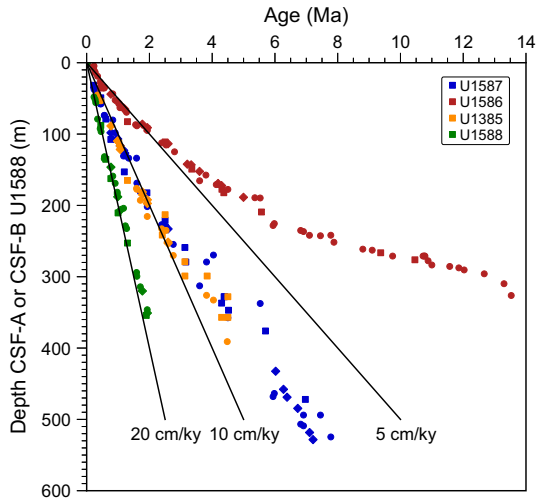

Figure F7. Age-depth points based on biostratigraphy and magnetostratigraphy for each Expedition 397 site. Sedimentation rates of 5, 10, and 20 cm/ky are shown for reference. Squares = planktonic foraminifer markers, circles = nannofossil markers, diamonds = magnetostratigraphic markers.

the precession cycles of the Pliocene that can be correlated peak-for-peak among sites (Figure **F11**) and the exceptional late Miocene cycles at Site U1587. These cyclic variations will be invaluable for deriving orbitally tuned timescales for Expedition 397 sites and correlating them with classic Mediterranean cyclostratigraphy. The cycles are also evident in the downhole logging NGR data of Site U1587, which will be important for core-log integration.

Although Expedition 397 was overall highly successful, no expedition is without its compromises, and Expedition 397 is no exception. We had planned to produce two complete stratigraphic splices at each site for sampling purposes, but this was impossible because of time lost to waiting on weather, which totaled 8 days (192 h or 14.5% of operating days). Logging was successful at only two of the four sites because of problems with the tools becoming lodged in the drill pipe. Some slumps were encountered at Site U1586 that disturbed the continuity of the stratigraphic section. Site U1588 could only be drilled to 412.5 mbsf out of the planned 500 mbsf because of severe gas expansion of the sediment. The basal age of the cored section at Site U1588 is considerably younger (2.2 Ma) than the original objective of reaching the Pliocene. These shortcomings do not detract from the invaluable >6 km sediment archive recovered from the Iberian margin that will provide raw material (mud) for paleoclimate studies for generations to come.

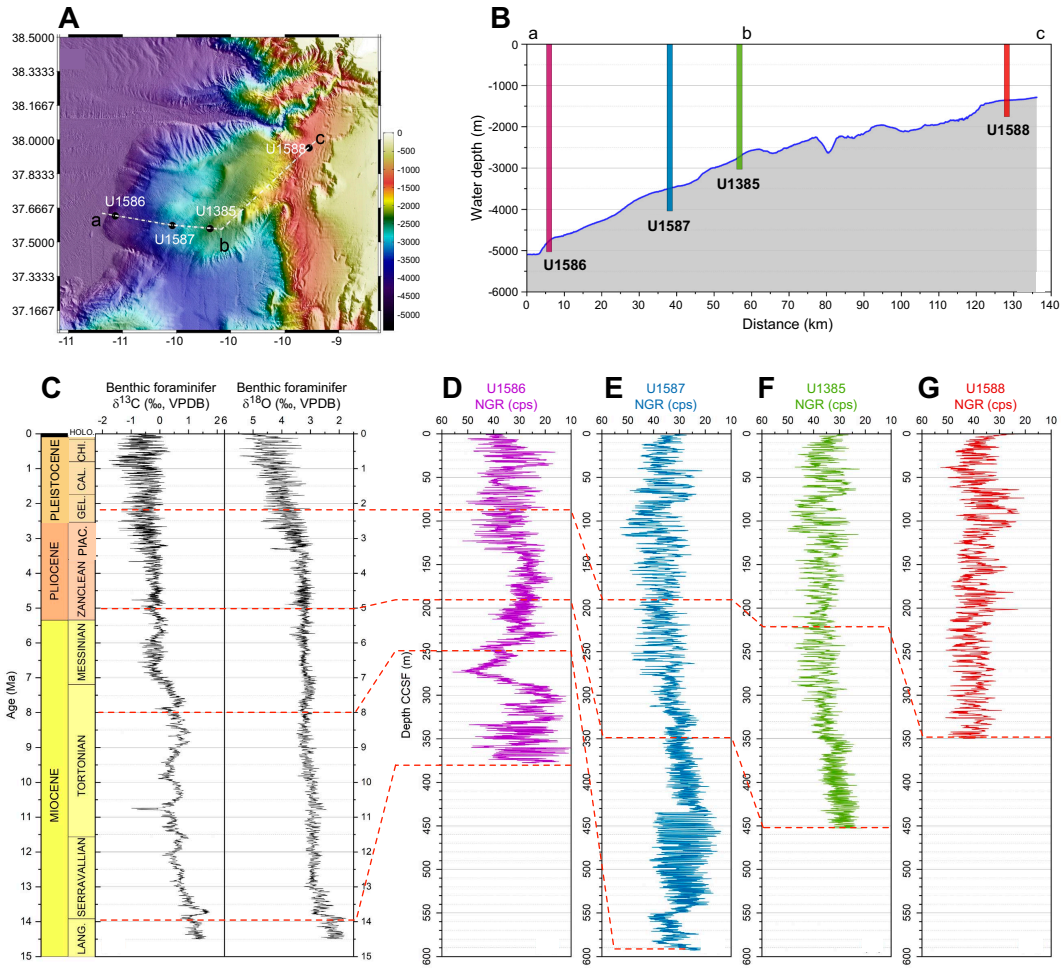

Figure F8. D–G. NGR data for each Expedition 397 site relative to (C) the global carbon and oxygen stable isotope curves (Westerhold et al., 2020) showing (A, B) the depth transect of sites and relative age of the sequences. VPDB = Vienna Peedee belemnite, cps = counts per second.

Figure F9. Comparison of XCB and APC cores, Site U1586. Archive halves are shown. 397-U1586A-19H-5, 0–150 cm, spans 173.88–175.38 m CSF-A. 397-U1586B-21X-3, 28–150 cm, spans 173.88–175.1 m CSF-A. 397-U1586B-21X-4, 0–28 cm, spans 175.1–175.38 m CSF-A. 397-U1586A-19H-5 (APC) exhibits slight up-arching between 0 and 75 cm and basal flow-in between 75 and 150 cm. 397-U1586B-21X-3 and 21X-4 (XCB) exhibit slight biscuiting.

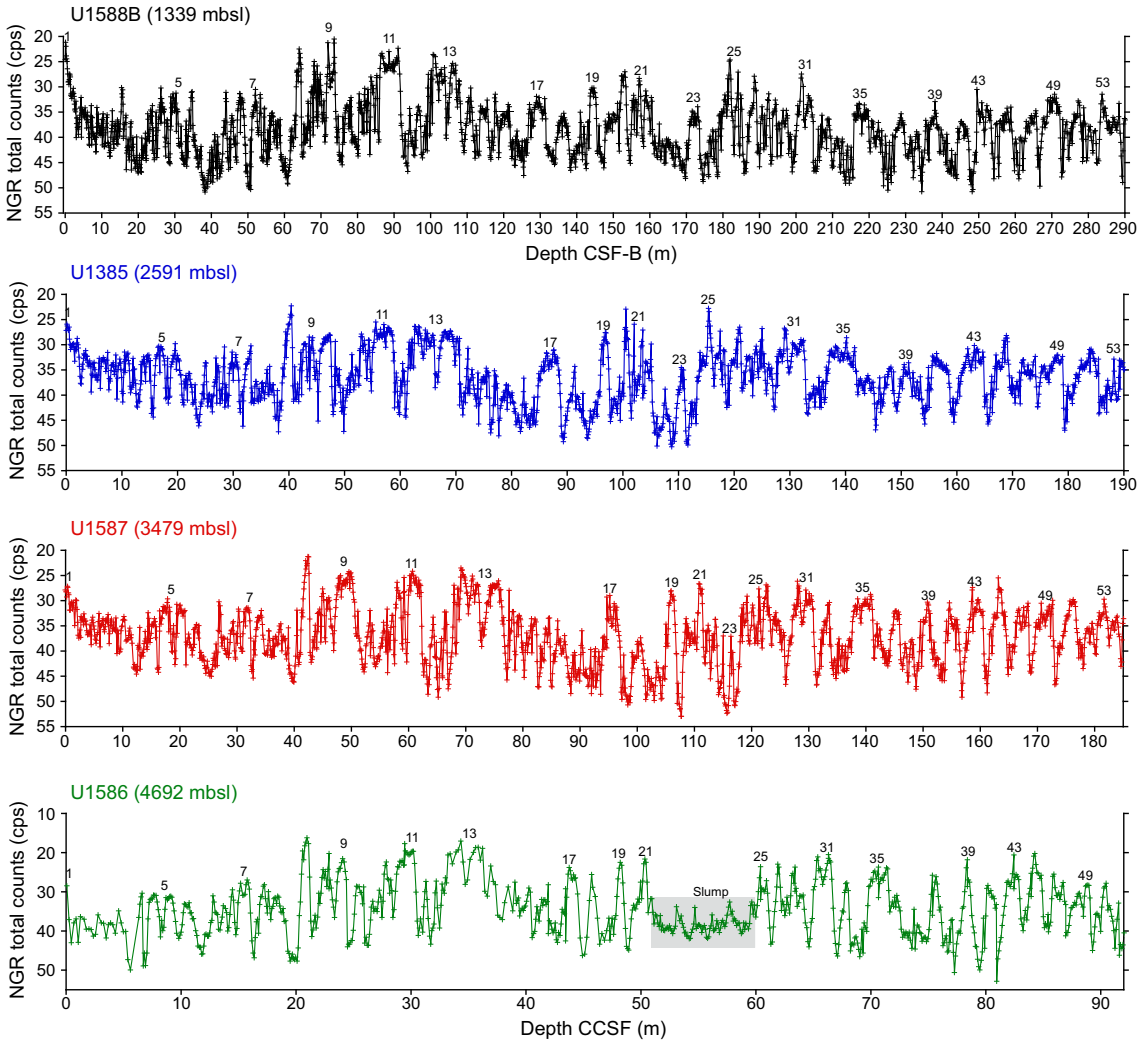

Figure F10. NGR data for each Expedition 397 site showing the approximate location of selected marine oxygen isotope stages. cps = counts per second. NGR data have been cleaned for outliers and spurious data at section ends.

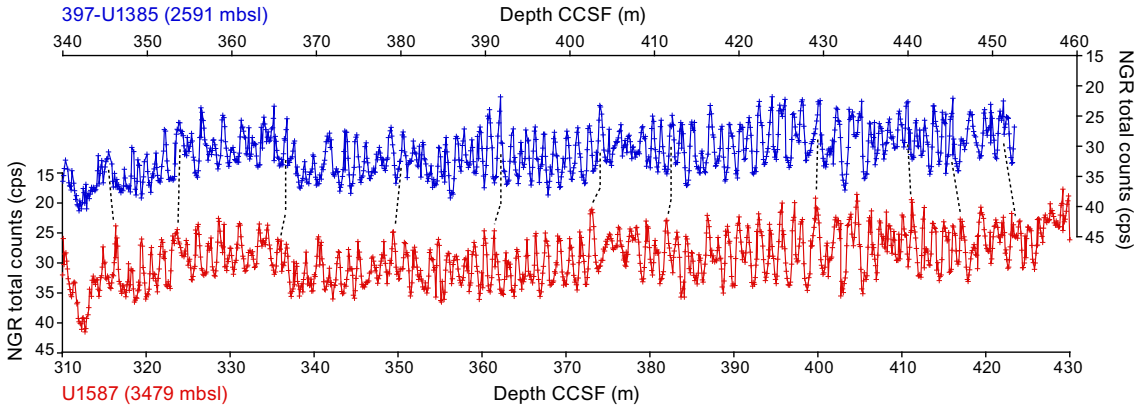

Figure F11. Correlation of Pliocene NGR cycles between Sites U1587 and 397-U1385. cps = counts per second. NGR data have been cleaned for outliers and spurious data at section ends.

3. Background

3.1. Geological setting

The Expedition 397 drill sites are located on a plateau, Promontório dos Príncipes de Avis (PPA), on the southwestern Iberian margin (Figure **F1**). The PPA protrudes from the continental shelf and slope and extends seaward toward the Tagus Abyssal Plain (Vanney and Mougenot, 1981). The PPA is approximately 100 km long by 50 km wide with a bathymetric relief of 4 km above the abyssal plain (Figure **F2**). It is topographically isolated from the turbidites that are funneled to the Tagus Abyssal Plain via the bordering submarine canyons to the north and south.

Sites were selected for Expedition 397 by examining available seismic data. Geophysical coverage of the PPA is good with a dense network of multichannel seismic lines. Furthermore, a dedicated site survey cruise aboard the RSS *James Cook*, conducted in 2013, provided high-resolution seismic lines at each of the proposed site locations (Hodell et al., 2014). Piston cores, recovered during the same cruise, supplied evidence for hemipelagic sediments consisting of nannofossil muds and clays with varying proportions of biogenic carbonate and terrigenous components on the entire PPA (Abrantes et al., 1998; Baas et al., 1997; Expedition 339 Scientists, 2013a). High sedimentation rates, ranging 10–20 cm/ky (Figure **F7**), occur during both glacial and interglacial periods and are attributed to the copious pelagic sediment supply and lateral transport of sediment by bottom and contour currents. Enhanced lateral transport and deposition of finer sediments (i.e., clay and silt) on the Iberian margin are affected by an enhanced nepheloid layer associated with the MOW (Ambar et al., 2002; Abrantes, 2000; Magill et al., 2018). Detrital input from the Tagus and Sado Rivers are mainly channeled by turbidity currents through submarine canyon systems to the abyssal plains (Lebreiro et al., 1997, 2009) and have relatively little effect on open slope deposition.

3.2. Surface hydrography

The western Iberian margin is at the northern limit of the Canary Current/Northwest African eastern boundary upwelling system (Figure **F12**). Coastal upwelling driven by northerly winds occurs predominantly from late May/early June to late September/early October (Fiúza et al., 1998; Haynes et al., 1993). As a result, the current flow direction is equatorward with the offshore presence of the perennial Portugal Current (PC), the eastern boundary recirculation from the North Atlantic Drift, and the nearshore seasonal Portugal Coastal Current (PCC). The PC is centered at 10°W and slowly advects surface and subsurface waters equatorward (Pérez et al., 2001), whereas the PCC is a jet-like slope current transporting the upwelled waters southward (Fiúza, 1984).

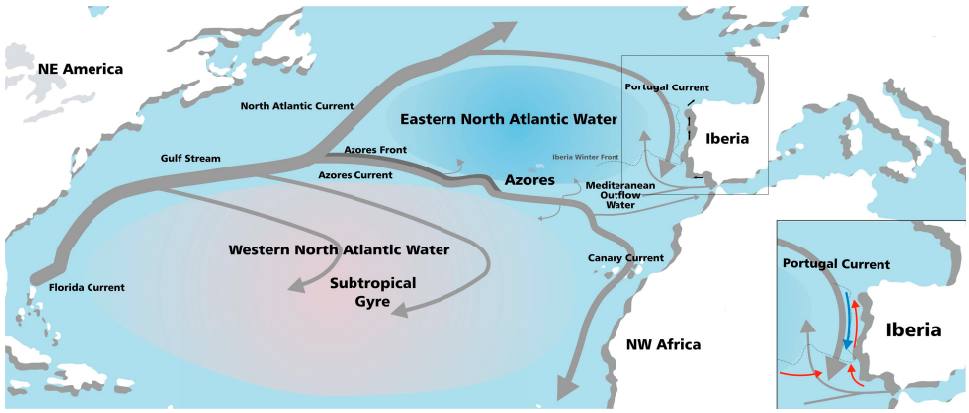

Figure F12. Gulf Stream and its relation to the Azores Current and Azores Front system and Portugal and Canary Currents. Also shown are the MOW, Iberian Winter Front, and the river plumes' flow direction (small arrows). Lower inset: more detail of the changing surface circulation on the western Iberian margin in summer (Portugal Coastal Current; blue arrows) and winter (Iberian Poleward Current; red arrows).

Eastern North Atlantic Central Water (ENACW) is the PC's subsurface component and forms by winter cooling in the eastern North Atlantic (Brambilla et al., 2008). The second major perennial current influencing the margin, especially the southwestern regions, is the Azores Current (AC). The AC, whose northern boundary is associated with the subtropical front, diverges from the Gulf Stream and flows as a jet with large meanders between 35 and 37°N across the North Atlantic. Although most of the AC recirculates southward, its eastern branch flows into the Gulf of Cádiz (Peliz et al., 2005). During the winter months, a northward bending of this subtropical front deflects it toward the SW Portuguese margin and feeds the Iberian Poleward Current (IPC) (Peliz et al., 2005). As the PC, the IPC's subsurface or undercurrent component also transports ENACW of subtropical origin. This subtropical ENACW flows poleward year round and is formed by strong evaporation and winter cooling along the Azores front (Ríos et al., 1992); it is poorly ventilated and warmer and saltier than the PC's subpolar counterpart.

The oceanographic conditions along the western Iberian Peninsula have important implications for primary production, biodiversity and biogeochemical cycles in the region. Moreover, the upwelling fronts are not simple continuous features, but rather punctuated by mesoscale structures (filaments) that can extend 200 km offshore, generating a transition zone between the oligotrophic offshore water and the highly productive coastal region, where particle accumulation leads to biogeochemical and productivity hotspots (Woodson and Litvin, 2015). This upwelling process leaves a clear imprint in the sediments deposited on the seafloor in the area, including physical properties, geochemistry, and diatom and planktonic foraminifer assemblages (Abrantes, 1988; Abrantes and Moita, 1999; Salgueiro et al., 2008).

3.3. Subsurface hydrography

The flanks of the PPA intersect each of the major subsurface water masses of the North Atlantic and are ideal for the placement of a depth transect of sites (Figure **F2**). During Cruise JC089, 13 conductivity-temperature-depth (CTD) casts were made and subsurface water masses were recognized by their temperature-salinity characteristics (Figure **F13**). ENACW occupies the depth interval below the thermocline between ~50 and 500 m (van Aken, 2000). Between 500 and 1500 m, warm, salty water derived from the Mediterranean (MOW) dominates. MOW flows over the Strait of Gibraltar into the Gulf of Cádiz and splits into two core branches centered at ~800 and 1200 mbsl (Ambar and Howe, 1979), flowing north along the western Iberian margin. Below 2000 mbsl, recirculated Northeast Atlantic Deep Water (NEADW) prevails, representing a mixture of Labrador Sea Water, Iceland Scotland Overflow Water, Denmark Strait Overflow Water, and to a lesser extent MOW and Lower Deep Water (LDW) (van Aken, 2000). The deepest water mass is southern-sourced LDW, which is modified Antarctic Bottom Water (AABW) that enters the eastern Atlantic Basin through the Vema Fracture Zone at 11°N (Saunders, 1987).

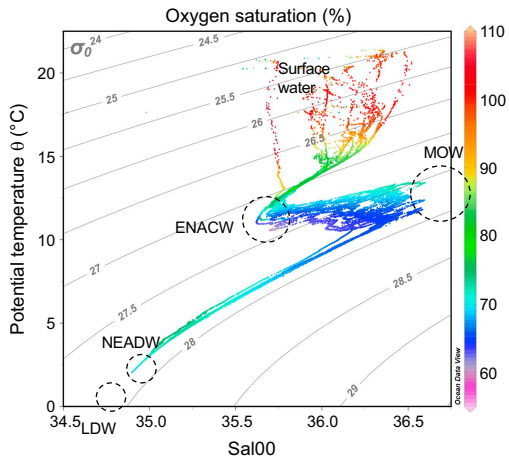

Figure F13. Temperature vs. salinity of CTD casts made during Cruise JC089 to the Iberian margin showing major subsurface water masses (Hodell et al., 2014). Color bar = percent oxygen saturation, contours = potential density.

Jenkins et al. (2015) performed an optimum multiparameter analysis (OMPA) for the stations along the GEOTRACES North Atlantic transect. OMPA assesses the relative contributions of end-member water masses by a least-square optimization using input values for conservative properties. We used this analysis to identify the optimal site locations based on the relative contribution of end-member water masses at each of the proposed drill sites.

3.4. Paleo-conductivity-temperature-depth strategy

We employed a paleo-conductivity-temperature-depth (paleo-CTD) approach whereby the seabed was sampled beneath each of the major subsurface water masses (Foreman, 2017; Lund et al., 2011). The PPA provides the bathymetric relief that in a limited area intersects all the principal water masses involved in the Atlantic thermohaline circulation (Figure **F5**). Water depths at the sites range 1339–4692 mbsl, permitting the sampling of paleowater mass properties of intermediate-water (Mediterranean Overflow) and deepwater masses (NEADW and LDW). The water depth range also complements those sites drilled during Expedition 339, which focused on the variability of MOW at five sites (U1386–U1390) in the Gulf of Cádiz at 566–980 mbsl and Site U1391 on the southwest Iberian margin at 1074 mbsl (Figures **F1**, **F2**). Together with Expedition 339, the proposed sites constitute a complete depth transect from 566 to 4686 mbsl on the eastern margin of the North Atlantic Basin. Because the depth ranges of water masses differed in the past, it is important to sample the sediment column under a wide range of bathymetric and hydrographic conditions. The paleo-CTD approach permits a comprehensive reconstruction of past water mass variability in the North Atlantic, much of which appears to be related to spatial redistributions on both glacial–interglacial and millennial timescales (Adkins, 2013). Understanding the role of the deep ocean in climate change and carbon storage is necessary to identify the underlying mechanisms of glacial–interglacial cycles and millennial-scale climate variation.

4. Scientific objectives

The overall objective of the Expedition 397 drilling proposal is to recover the late Miocene–Pleistocene sediment archive located offshore Portugal in a range of water depths to document past changes in vertical water mass structure and its relation to global climate change (Figures **F1**, **F2**). By producing multiproxy time series at each site and placing them on an integrated stratigraphy, these sediments provide the information needed to study MCV over the Pliocene–Pleistocene and understand its underlying causes and evolving contextuality.

Some of the specific scientific objectives include the following:

- Document the occurrence of MCV for older glacial cycles beyond the limit of Site U1385 (1.45 Ma) and how MCV evolved as glacial boundary conditions changed with the progressive intensification of Northern Hemisphere glaciation (NHG) since the late Pliocene.
- Derive a marine sediment proxy record for Greenland and Antarctic ice cores to examine the amplitude and pacing of MCV during the Quaternary.
- Determine interhemispheric phase relationships (leads/lags) by comparing the timing of proxy variables that monitor surface (Greenland) and deepwater (Antarctic) components of the climate system.
- Study how changes in orbital forcing and glacial boundary conditions affect the character of MCV and, in turn, how MCV interacts with orbital geometry to produce the observed glacial-to-interglacial patterns of climate change.
- Reconstruct the history of changing local dominance of northern-sourced versus southern-sourced deep water using the depth transect of Expedition 397 and 339 sites on orbital and suborbital timescales during the Quaternary.
- Develop orbitally tuned timescales for each of the sites and correlate them into the classic Mediterranean cyclostratigraphy.
- Document changes in the coastal upwelling system from the Miocene to the present, including its impact on primary production, carbon export, and biogeochemical cycling.
- Reconstruct the evolution of continental vegetation and hydroclimate using pollen and terrestrial biomarkers that are delivered to the deep-sea environment of the Iberian margin.

- Link terrestrial, marine, and ice core records by comparing proxy signals of different components of the Earth system that are coregistered in a single sediment archive.

A more comprehensive explanation of the scientific objectives follows.

4.1. Integrated global stratigraphy

Precise stratigraphy is the main limitation to our ability to determine phase relationships (leads/lags) among various variables in the ocean-atmosphere system, which is essential for testing causal mechanisms of global climate change. A great strength of the Iberian margin sediment record is that it contains proxies of marine, atmospheric (ice core), and terrestrial signals coregistered in a single archive. It is thus possible to determine the relative phasing of changes in proxy variables that monitor different components of the ocean climate system in the same core (Shackleton et al., 2000, 2004). For example, temporal comparisons between marine stable isotope and pollen records in the same core have allowed the evaluation of phase relationships between global climate and European terrestrial change during the last 420 ky (Sánchez Goñi et al., 1999, 2000, 2016; Margari et al., 2010, 2014; Oliveira et al., 2020; Roucoux et al., 2001; Shackleton et al., 2000, 2003, 2002; Tzedakis et al., 2004). A similar strategy can be applied to the entire sequence recovered by Expedition 397, circumventing many problems associated with core-to-core correlation and developing age models on millennial timescales (Blaauw, 2012).

At Expedition 339 Site U1385, variations in sediment color contain an eccentricity-modulated precession signal over the past 1.45 My (Hodell et al., 2013a, 2013b, 2023), and shipboard data indicates this cyclicity continues for older time periods. The modulation of precession by eccentricity provides a powerful tool for developing orbitally tuned age models (Shackleton et al., 1995). An astronomically tuned timescale will be developed at each of the Expedition 397 sites by correlating variations in shipboard physical properties and postcruise XRF results to orbital target curves (e.g., Hodell et al., 2015). This also will allow the sites to be correlated to the classic Mediterranean cyclostratigraphy (Hilgen, 1991; Konijnendijk et al., 2015). In addition, the correlation of Iberian margin proxy records with European speleothems will provide a novel opportunity to tie marine records into a radiometrically dated chronology using U-Th and U-Pb isotopes (e.g., Tzedakis et al., 2018; Bajo et al., 2020).

4.2. Marine sediment analog to the polar ice cores

Ice cores offer the most detailed records available for reconstructing changes in climate and greenhouse gases in the latest Pleistocene. However, many of the mechanisms that control atmospheric composition and climate are rooted in the oceans. The answers to Pleistocene climate questions require a coupled ocean-atmosphere approach where ice core data are integrated with marine sediment cores. In this regard, Iberian margin sediments are important for comparison to existing and future ice core records from Greenland and Antarctica (Nehrbass-Ahles et al., 2020; Wolff et al., 2022). Given that the Greenland ice core is limited to the last glacial cycle and the oldest ice core in Antarctica (EPICA Dome C) is limited to the last 800 ky, we must rely on marine sediment records to provide the longer term history of changes in polar climate.

If we assume the correlation between rapid temperature changes on the Iberian margin and over Greenland has held for older glacial periods, then sediment recovered during Expedition 397 can serve as a marine sediment proxy record for the Greenland ice core beyond the age of the oldest undisturbed ice (~122 ka). Comparing surface water signals from the Iberian margin with the synthetic Greenland reconstruction (Barker et al., 2011) demonstrated a strong similarity for the last 400 ky (Hodell et al., 2013a). Millennial-scale variability in benthic $\delta^{18}O$ from the Iberian margin is similar to EPICA δD for the last 800 ky (Hodell et al., 2023). Beyond the last three glacial cycles, the temporal resolution of the EPICA Dome C record diminishes because of compression and diffusion, which hinders clear detection of millennial to submillennial events for older glacial periods depending on sampling resolution (Jouzel et al., 2007; Pol et al., 2010). Problems of diffusion and compression will undoubtedly be more severe in older ice to be recovered by the BE-OI Project (Fischer et al., 2013; Bereiter et al., 2014; Wolff et al., 2022) and COLDEX (COLDEX, 2022). Comparison of the ice core record from BE-OI and proxies measured in Expedition 397 sediment will

allow an assessment of whether there has been significant loss of climate information at higher frequencies due to diffusion and migration in the ice core record.

4.3. Millennial-scale climate variability during the Pliocene–Pleistocene

Much progress has been made toward understanding the orbital effects on climate, but a complete theory of the ice ages remains elusive (Raymo and Huybers, 2008). Understanding how climate changes on shorter (i.e., suborbital) timescales interact with the effects of orbital forcing to produce the observed patterns of glacial–interglacial cycles through the Pleistocene may be an important piece of the puzzle. For example, MCV may play an important role in longer term climate transitions, such as glacial terminations (Cheng et al., 2009; Denton et al., 2010; Wolff et al., 2009; Barker and Knorr, 2021). Studying the coevolution of orbital and suborbital variability requires a new caliber of sediment archives with a high level of chronological precision. With few exceptions, deep-sea sedimentary records generally lack the resolution needed to delineate such variability; however, exceptions do exist, such as those from the Iberian margin. MCV has been well documented for the last glacial cycle in the North Atlantic, but relatively little is known about similar variability during older glacial periods of the Pleistocene (de Abreu et al., 2003; Margari et al., 2010; Martrat et al., 2007; Rodrigues et al., 2011). Some marine records of MCV exist beyond the last glacial cycle (Alonso-Garcia et al., 2011; Barker et al., 2015, 2011; Hodell et al., 2008; Jouzel et al., 2007; Kawamura et al., 2007; Dome Fuji Ice Core Project Members, 2017; Margari et al., 2010; Martrat et al., 2007; McManus et al., 1999; Oppo et al., 1998), but only a few extend beyond 800 ka into the early Pleistocene (Barker et al., 2021; Billups and Scheinwald, 2014; Birner et al., 2016; Hodell and Channell, 2016; Hodell et al., 2008, 2023; Mc Intyre et al., 2001; Raymo et al., 1998; Rodrigues et al., 2017) and none for the Pliocene.

MCV is thought to be a pervasive feature of Quaternary climate change (Jouzel et al., 2007; Weirauch et al., 2008; Hodell et al., 2015, 2023; Sun et al., 2021), but its pacing and amplitude are likely to be influenced by changing orbital and ice sheet boundary conditions (Zhang et al., 2021). MCV can exert an upscale influence on orbital timescales through its effect on ice sheet dynamics (Verbitsky et al., 2018) or atmospheric CO_2 by changing carbon storage in the deep sea. MCV is also a source of high-frequency variability (noise) on glacial–interglacial timescales that may affect the resonance of internal climate change with external orbital forcing. Sediments recovered during Expedition 397 will be important for documenting how orbital and millennial variability coevolved through the Quaternary and Pliocene (Hodell et al., 2023).

4.4. Testing the thermal bipolar seesaw hypothesis

Millennial-scale variations in Greenland temperature have a counterpart variation in Antarctic ice cores, which are smaller in magnitude and have a different shape than the signals found in Greenland (Blunier and Brook, 2001; EPICA Community Members, 2006; WAIS Divide Project Members, 2015). The phasing between Greenland and Antarctic temperature is often explained by changes in interhemispheric heat transport caused by changes in the strength of Atlantic Meridional Overturning Circulation (AMOC), referred to as the thermal bipolar seesaw (Stocker, 1998). Temperature records from the Iberian margin, when used as inputs to a thermal bipolar seesaw model, produce synthetic Southern Hemisphere temperature records that greatly resemble Antarctic temperature records (Davtian and Bard, 2023).

Determining phase relationships of MCV in glacial periods beyond the last climate cycle is challenging because absolute dating of marine cores is too imprecise to correlate and resolve small differences in the timing of paleoclimate signals (Blaauw, 2012; Andrews et al., 1999; Wunsch, 2006). An alternative approach is to determine the relative phasing of changes in proxy variables in the same core that monitor different components of the ocean climate system. A great strength of the Iberian margin sediment record is the fact that it contains signals of both Greenland and Antarctic ice cores in a single archive and it is possible to determine the relative phasing of polar climate by comparing proxy signals in the same core (Figure **F1**). Expedition 397 sediments provide an opportunity to test whether similar phasing patterns existed in older glacial periods, consistent with the operation of a bipolar seesaw (e.g., Margari et al., 2010; Hodell et al., 2023).

4.5. North Atlantic thermohaline circulation

Northern Component Water is thought to have extended deeper in the water column during the warmer, longer Greenland interstadials (e.g., IS 8, 12, and 14) and shoaled during Greenland stadials, especially during Heinrich events (Hodell et al., 2010; Kissel et al., 2008; Piotrowski et al., 2008; Henry et al., 2016). Previous work using sediments from the Iberian margin has confirmed (with particularly firm chronostratigraphic constraints) the link between past interhemispheric climate change and perturbations to the deep Atlantic hydrography. Thus, changes in deepwater radiocarbon concentration (Skinner and Shackleton, 2004; Skinner et al., 2021), oxygenation (Martrat et al., 2007; Skinner et al., 2003; Thomas et al., 2022), temperature (Skinner et al., 2003, 2007; Davtian and Bard, 2023), remineralized nutrient content (Shackleton et al., 2000; Skinner et al., 2007; Willamowski and Zahn, 2000), and lateral export rates (Gherardi et al., 2005) have all been linked to abrupt climatic changes that occurred in the recent geological past.

Indeed, it is precisely the tight connection between deepwater circulation on the Iberian margin and the bipolar seesaw that lies at the heart of Shackleton's initial observation of northern and southern signals recorded simultaneously in Core MD95-2042 (Shackleton et al., 2000).

Expedition 397 sites permit the types of reconstructions noted above, such as benthic $\delta^{13}C$ as a proxy for deepwater sourcing and ventilation (Thomas et al., 2022), to be extended beyond the 1.45 Ma of Site U1385. Furthermore, the range of water depths of the Expedition 397 sites (1339–4692 mbsl) allow the study of past changes in vertical water mass structure of the North Atlantic with especially strong stratigraphic constraints.

The cores recovered during Expedition 397, together with those drilled during Expedition 339, provide the basis for marine reference sections of temporal water column variability in the northeast Atlantic. Postcruise studies of this material will prove invaluable for assessing the expression and impacts of abrupt ocean circulation change in the past, especially as this relates to interhemispheric climate phasing and glacial–interglacial climate evolution.

4.6. Continental vegetation and hydroclimate changes

Marine archives recovered adjacent to the continents have the potential to link continental and marine climate records because they are influenced directly by continental inputs, such as from rivers and winds. The western Iberian margin has emerged as a critical area for studying continent-ocean connections because of the combined effects of major river systems and a narrow continental shelf that lead to the rapid delivery of terrestrial material (e.g., pollen and organic biomarkers) to the deep-sea environment (Margari et al., 2014, 2020; Oliveira et al., 2016, 2017, 2018, 2020; Rodrigues et al., 2017; Sánchez Goñi et al., 2016; Tzedakis et al., 2015). In the southern Portuguese margin, pollen enters the ocean mainly as particulate suspended matter through the Tagus and Sado rivers and upwelling filaments (Naughton et al., 2007). A comparison of modern marine and terrestrial samples along western Iberia has shown that the marine pollen assemblages provide an integrated picture of the regional vegetation on the adjacent continent. Moreover, modern biogeographical differences in the distribution of Atlantic and Mediterranean plant communities are reflected in the pollen signal of northern and southern marine pollen spectra, respectively (Naughton et al., 2007). Thus, the Portuguese margin provides a rare opportunity to (1) enhance the study of ocean-continent linkages by analyzing proxies for continental hydrology and vegetation (e.g., pollen, elemental ratio data in bulk sediments, and molecular and isotopic composition of leaf waxes) in marine sediment cores that can be precisely correlated to polar ice cores and (2) construct the longest continuous record of late Miocene–Pleistocene vegetation changes available anywhere to date. A detailed pollen record from the Portuguese margin linked to the marine isotopic stratigraphy and record of millennial-scale variability will be an invaluable resource that can be used to place vegetation changes in the context of global and North Atlantic climate changes. Comparisons with terrestrial pollen reference sequences, such as Tenaghi Philippon, Greece (Tzedakis et al., 2006), and with International Continental Scientific Drilling Program (ICDP) sites from Lake Ohrid (Albania/Macedonia) (Donders et al., 2021) and Lake Van (Turkey) (Litt et al., 2014), will assess patterns of geographical variation. Furthermore, it will also allow us to

investigate major vegetation changes throughout the Pliocene–Pleistocene with shifts in climatic regimes (e.g., intensification of NHG, mid-Pleistocene transition, etc.).

4.7. History of upwelling on the Portuguese margin

The Iberian margin is a coastal upwelling region where primary production increases in response to seasonal (May–September) wind intensity and direction, which in turn results in the upward flow of nutrient-rich subsurface waters, such as ENACW. Although upwelling centers are mainly coastal, upwelled water spreads seaward through filaments extending up to 200 km offshore depending on northerly wind intensity (Fiúza, 1984; Relvas et al., 2009). These nutrient-rich waters generate a transition zone between the oligotrophic water offshore and the highly productive area near the coast.

The upwelling process leaves a clear imprint in the sediments deposited on the seafloor in the area, including physical properties, geochemistry, diatom and planktonic foraminifer assemblages, and their geographic distribution (Abrantes, 1988; Abrantes and Moita, 1999; Salgueiro et al., 2008). The past geological variability of the upwelling has been studied both at orbital and millennial timescales. At the glacial–interglacial scale, an increase in diatom accumulation rates, which is in good agreement with other independent productivity proxies, has been interpreted to represent an order of magnitude increase in productivity during the previous glacial and deglaciation periods, not only on the Portuguese margin but in both hemispheres of the eastern Atlantic (Abrantes, 1991, 2000). For millennial timescales, Abrantes et al. (1998) suggested increased primary production associated with Heinrich events off the Portuguese coast, whereas the high-resolution planktonic foraminifer study of three sites along the Iberian margin indicates a more complex north–south pattern (Salgueiro et al., 2010). Primary production decreased markedly during stadials and Heinrich events on the northern margin but increased off Sines in the region of influence of the Cabo da Roca filament and near the Expedition 397 sites.

Expedition 339 Sites U1391 and U1385 are located in the area influenced by the Cape Sines and Cape St. Vicente filaments (Sousa and Bricaud, 1992) and constitute a transect across a productivity gradient, allowing for the investigation of the impact of climate variations on marine production. Site 339-U1385 is mostly barren of biogenic silica, whereas Site U1391 has diatom abundance peaks during some deglaciation–early interglacial periods, such as MIS 2/MIS 1, MIS 10/MIS 9, and the mid-Pleistocene transition (MIS 22/MIS 21 to MIS 32/MIS 31) (Abrantes et al., 2017).

Increased values of upwelling-related diatom species at the shallower and coastal location of Site U1391 support a coastal upwelling-related increase in primary production in accordance with the Si/Al record of Ocean Drilling Program (ODP) Site 658 off Northwest Africa (Meckler et al., 2013). Its co-occurrence with deep waters of southern origin at Site U1385 may suggest that intermediate and upwelled source waters were also of southern origin (Thomas et al., 2022). Furthermore, equally high diatom abundances found at the North Atlantic Site U1334 point to a widespread pattern rather than a regional one (Hernández-Almeida et al., 2013). Large oligotrophic warm-water species at the base of MIS 25 at Site U1391 (Abrantes et al., 2017) and the nearby Site U1387 (Ventura et al., 2017) point to significantly different surface ocean circulation dynamics at the southern Portuguese coast during early MIS 25.

Expedition 397 sites will provide information about the regional coastal upwelling system and the biotic response to global climate change from the Miocene to the Quaternary. The new core material will also elucidate how the upwelling system evolved through changing boundary conditions such as warmer temperatures and equal or higher atmospheric CO_2 concentrations at present.

4.8. Connections to the 2050 Scientific Framework

IODP Expedition 397 is highly relevant to many of the strategic objectives and initiatives proposed by the IODP 2050 Scientific Framework, including Themes 3 (Earth's Climate System), 4 (Feedback in the Earth System), and 5 (Tipping Points in Earth History). The sediment cores recovered during Expedition 397 and those of Expedition 339 from the same region constitute an invaluable sedimentary archive with which to study past climate variability at high temporal resolution. The Iberian margin sedimentary archive will be used to document orbital and suborbital variability in

climate and AMOC and its relation to carbon storage in the deep ocean and atmospheric CO_2 changes, as recorded in Antarctic ice cores. The long continuity, high resolution, and precise chronology offered by Iberian margin cores will enhance our understanding of how Earth's climate system operates and responds to various forcing and feedback processes across a wide array of background states, including those warmer than today and with atmospheric CO_2 concentrations equal to or greater than at present. By comparing marine and ice core records with their European terrestrial counterparts, Expedition 397 research will document the response of European hydroclimate and vegetation to regional and global climate change. These outcomes will advance the IODP 2050 scientific framework's objective of obtaining the data necessary to calibrate and improve numerical models to project future climate impacts and inform mitigation strategies.

5. Site summaries

5.1. Site U1586

5.1.1. Background and objectives

Site U1586 is the deepest (4692 mbsl) and farthest from shore of all the Expedition 397 sites. It is located at the toe of the PPA in a slightly elevated region protected from bottom currents and turbidite deposition (Figure **F14**). As the deepest site in the bathymetric transect, it is bathed by LDW that consists of AABW (Figure **F5**), which has been modified by mixing during its transit from the South Atlantic.

Because of relatively lower sedimentation rates at Site U1586 compared to other sites (Figure **F7**), drilling at this site represents our best opportunity to obtain the oldest sediment (Miocene) to be recovered during Expedition 397. The main drilling objective was to recover a high-resolution record of the late Miocene–Pleistocene with which to study the evolution of the surface and deepest water masses of the northeast Atlantic. Of specific interest are the time periods associated with (1) the water exchange between the Mediterranean and the Atlantic before, during, and following the Messinian Salinity Crisis (latest Miocene to the base of the Pliocene); (2) the mid-Pliocene warm period characterized by atmospheric CO_2 concentrations similar to present values (400 ppm); (3) the late Pliocene intensification of the NHG (~2.9 Ma); and (4) the Pleistocene (last 2.6 Ma) when MCV was superimposed upon glacial–interglacial cycles.

Site U1586 is positioned at Common Midpoint 1330 on Seismic Line 2 of Cruise JC089 in a region with good continuity of reflectors (Figure **F15**). The objective was to drill to the package of high-amplitude reflectors represented by the pink and green reflectors in Figure **F15**. A target drilling depth of 350 mbsf was approved by the EPSP.

5.1.2. Operations

Expedition 397 began on 11 October 2022 at 1045 h (UTC +1 h) upon the arrival of the R/V *JOIDES Resolution* at Rocha Pier in Lisbon, Portugal, at the end of Expedition 397T. On 16 October,

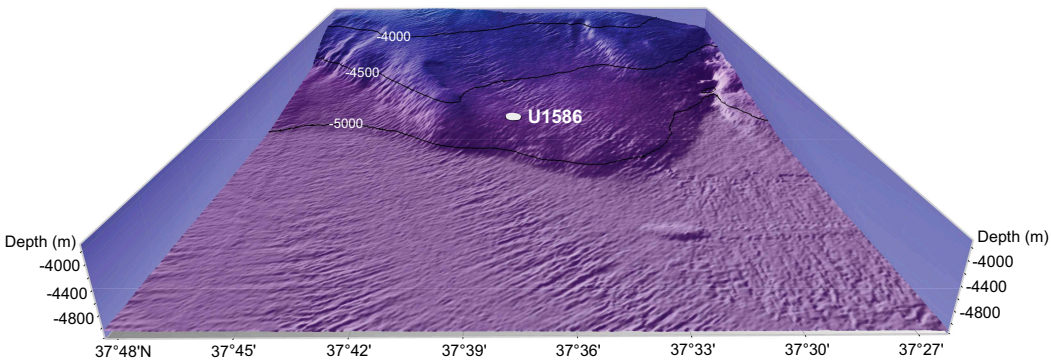

Figure F14. Location of Site U1586 at the toe of the Promontório dos Príncipes de Avis (PPA) at a water depth of 4692 mbsl. See Figure F2 for broader bathymetric context. (Figure made by Helder Pereira using Mirone and iVew4D software.)

JOIDES Resolution left port by 0830 h Portuguese time, reaching Site U1586 at 1834 h. A water depth reading with the ship's precision depth recorder (PDR) was taken as the vessel arrived on site, giving a seafloor depth of 4702.4 meters below rig floor (mbrf)/4691.4 mbsl.

The plan for Site U1586 was to core five holes. Holes U1586A–U1586C were to be cored with the APC and half-length APC (HLAPC) systems to refusal (estimated at approximately 250 m core depth below seafloor, Method A [CSF-A]), and then cored to a maximum depth of 350 mbsf using the XCB system. Holes U1586C and U1586D were to be cored to APC/HLAPC refusal. Formation temperature measurements were planned for Hole U1586A and downhole wireline logging measurements were planned for Hole U1586C.

Once on site, weather conditions and high seas caused a ~48 h delay over the planned 14.8 days of operations, and the coring strategy was adjusted. High core quality obtained using the XCB system fitted with a PDC bit and cutting shoe in Hole U1586A allowed for it to be deployed earlier than normal in Holes U1586B–U1586D, eliminating the need to use the HLAPC system. Therefore, a revised plan was executed, using the APC system until the first partial stroke and then extending the holes to total depth using the XCB system. Site U1586 consisted of four holes to 350 mbsf (Figure **F6**). Formation temperature was measured at 34.9, 63.4, 82.4, and 120.4 mbsf in Hole U1586A with the advanced piston corer temperature (APCT-3) tool, and Hole U1586D was logged using the triple combination (triple combo) tool string. All APC and HLAPC cores used nonmagnetic core barrels, and APC cores were oriented using the Icefield orientation tool. In total, 1399.1

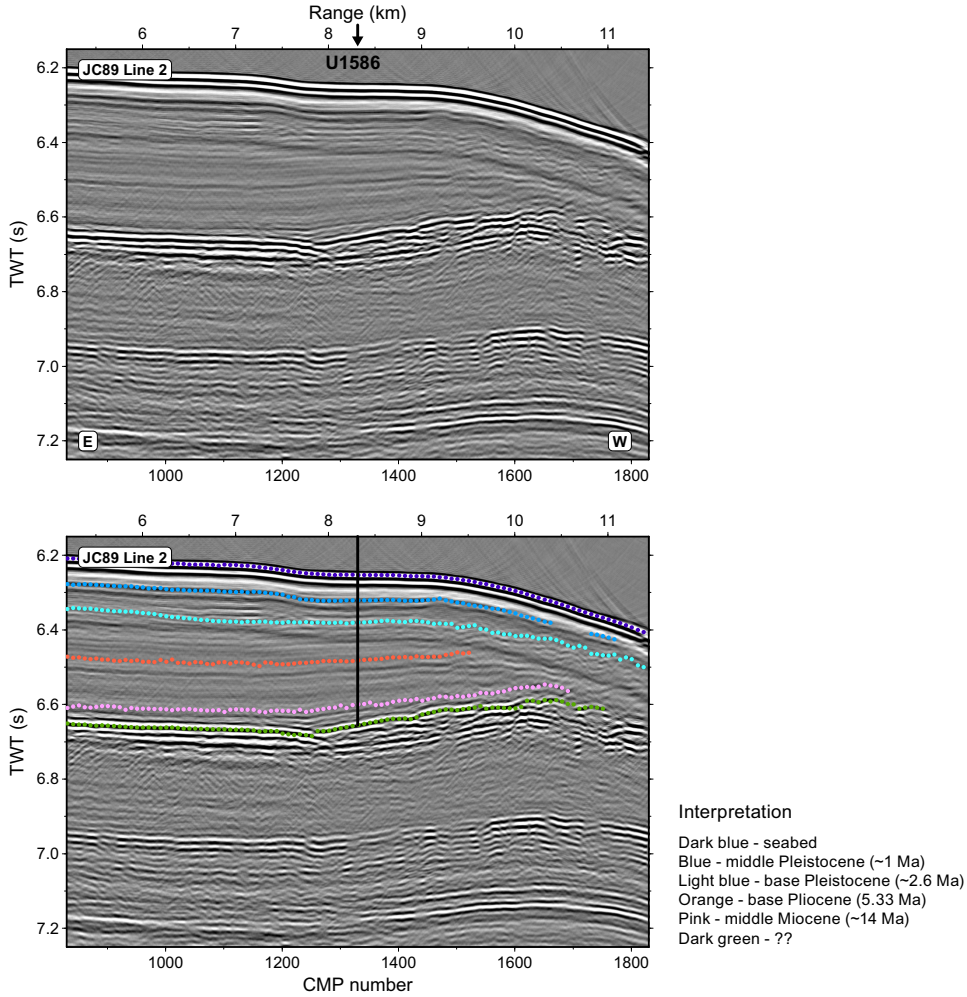

Figure F15. Original and interpreted seismic profile (JC89-2) showing the location of Site U1586 with penetration to 350 mbsf. The ages of the reflectors have been revised during the expedition to reflect the ages of the recovered sediment. TWT = two-way traveltime, CMP = common midpoint.

m were cored using the three coring systems with an overall recovery rate of 96% across all holes. Operations at Site U1586 took 349.5 h (14.6 days) to complete.

5.1.3. Principal results

Site U1586 yielded several significant findings and observations, some of which were unexpected:

- Operationally, the quality of the cores recovered using the XCB system was surprisingly good with high recovery and relatively minor disturbance (biscuiting), which is attributed to the use of a PDC bit and cutting shoe.
- A ~350 m middle Miocene–Holocene spliced sedimentary sequence (14 Ma) was recovered (Figure **F16**), nearly twice the age (7 Ma; late Miocene) predicted from the interpretation of the seismic profiles.

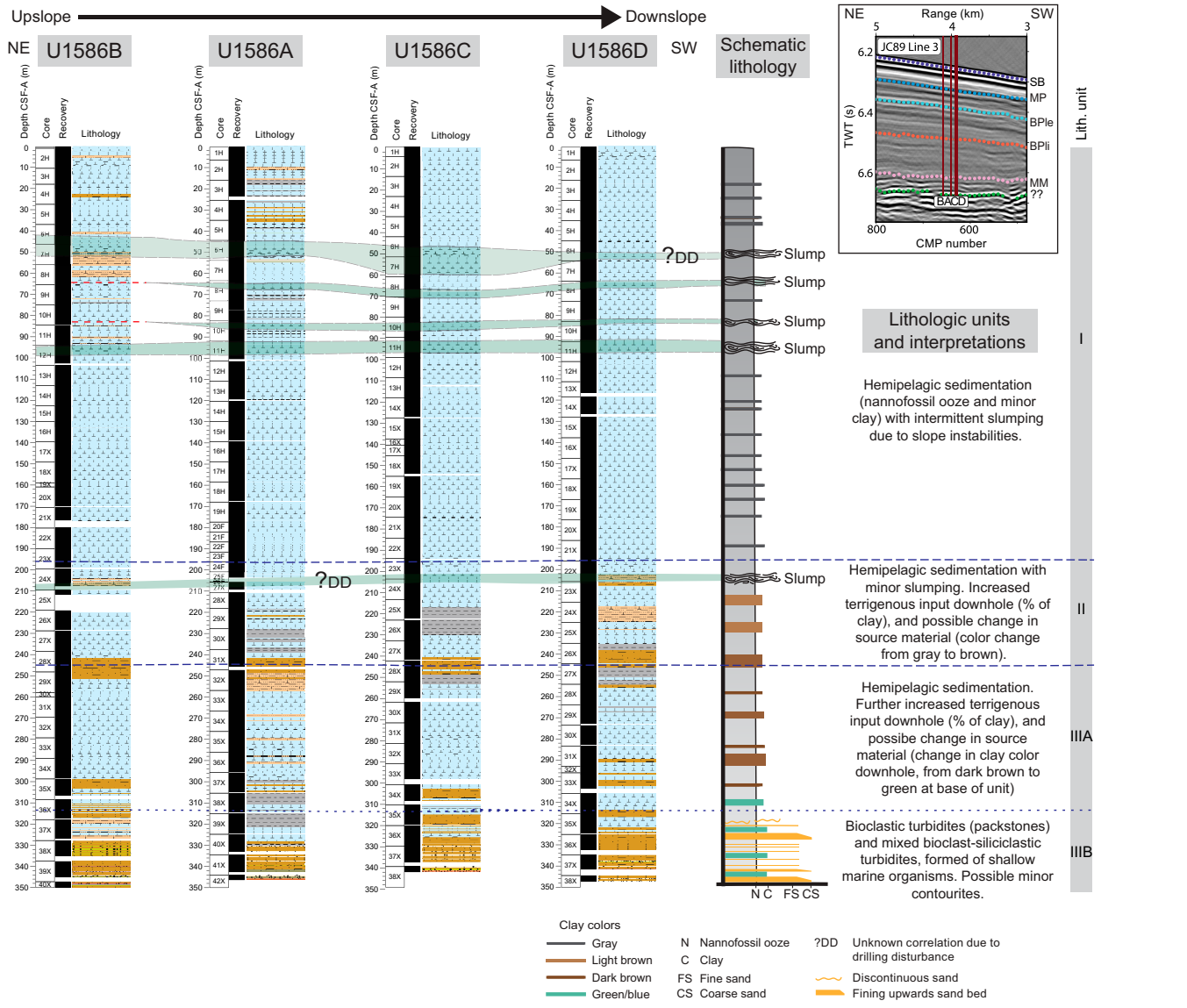

Figure F16. Lithologic summary, Site U1586. Left: summary lithostratigraphic logs of Holes U1586A–U1586AD, ordered left to right from northeast to southwest (upslope to downslope). Blue dashed line = divisions of lithostratigraphic units, blue dotted line = division of subunits (not slump related), green overlay = correlation of slumped intervals (Subunits IB, ID, IF, and IH and Subunit IIB). Right: lithologic unit names and preliminary interpretations of depositional processes. Colors are based on visual description as well as L*a*b* values. Unit and subunit boundaries are primarily based on sedimentary structures as well as changes and color and banding thickness. Color is independent of lithology and is related to relative amounts of minor constituents such as pyrite and glauconite. Inset: cropped section of Seismic Line JC89 Line 3 showing location along transect and depth of Holes U1586A–U1586D. TWT = two-way traveltime, CMP = common midpoint, SB = seabed, MP = Middle Pleistocene, BPle = base Pleistocene, BPli = base Pliocene, MM = Middle Miocene.

- The occurrence of convoluted banded sediment interpreted as slumps was found in all the holes at the same stratigraphic position, indicating slope instability associated with possible sea level fluctuations or tectonic activity. Slumped intervals were carefully noted by sedimentologists and can be recognized by the low-amplitude signal of physical properties measurements. Although the occurrence of slumps interrupts the stratigraphic section, many continuous intervals, suitable for paleoclimate studies, are identified (Figure **F16**).
- The Pliocene sequence at Site U1586 is remarkably complete and unaffected by slumping. Sediments are marked by very strong cyclic variations in color, MS, and NGR, which are dominated by an apparent precession signal and offer much promise for developing an orbitally tuned age model and correlating to Mediterranean sequences (Figure **F17**).
- A serendipitous finding was an exceptionally high peak in MS that was detected at the same stratigraphic interval in all the holes. The sediments were found to contain abundant metallic particles, some of which are spherical and interpreted to be of cosmic origin. The estimated age of the layer is 3.6 Ma by correlation of the color reflectance signal to precession and the identification of the Gilbert-Gauss polarity reversal boundary.

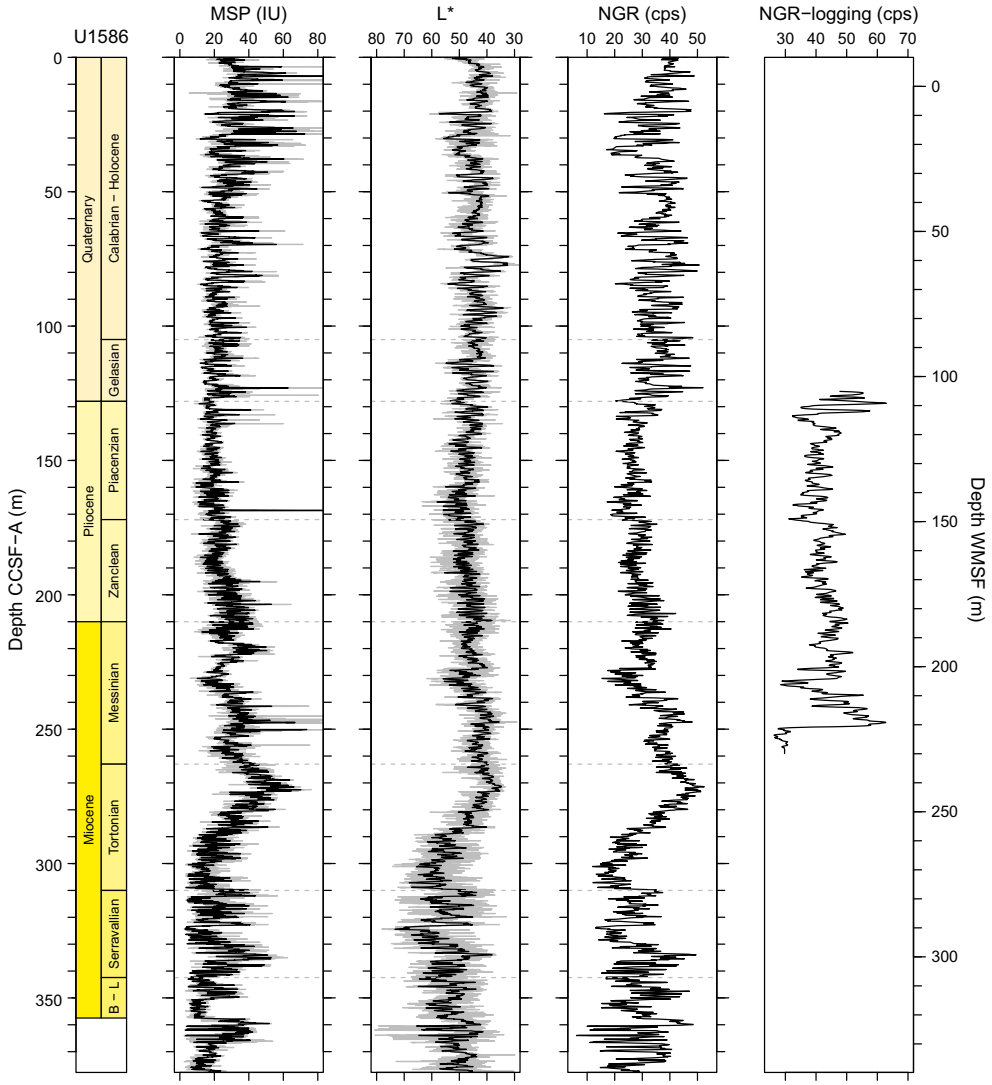

Figure F17. Core composite downhole trends of physical properties data, Site U1586. B-L = Burdigalian–Langhian. MSP = section-half point MS, NGR = whole-round NGR, cps = counts per second, NGR-logging = NGR data from the triple combo logging tool. WMSF = wireline log matched depth below seafloor. MSP and L* panels: a smoothed curve (black line; 20-point moving average) is shown over the original data (gray line). NGR panels: only the original data is shown.

At Site U1586, four holes (U1586A–U1586D) were drilled to 350 mbsf and a total of 1346.85 m of sediment was recovered. The primary lithology consisted of various proportions of nannofossil ooze and clay/silt. Very fine to coarse calcareous sands were found near the base of the holes below 310 mbsf (Figure **F16**) and may have resulted from sediment gravity flows (turbidites). Different types and intensities of drilling disturbance were observed in the cores, with the most common being up-arching, flow-in, soupy, and slurry in the APC cores and biscuiting and fall-in for the XCB cores. Bioturbation varied from absent to complete disturbance of sedimentary layers. Pyrite nodules filling burrows are commonly observed in X-ray images.

A well-constrained biostratigraphic age model was developed for Site U1586 based on analyses of calcareous nannofossils and planktonic foraminifers (Figure **F18A**). Overall, 51 calcareous nannofossil and planktonic foraminifer bioevents were identified. The integrated biostratigraphy suggests a reasonably complete sequence from middle Miocene to Holocene.

Magnetostratigraphy of Site U1586 was established based on the natural remanent magnetization (NRM) (after 20 mT demagnetization) inclination and (orientation-corrected) declination data from archive-half core sections and stepwise NRM demagnetization data from discrete cube samples. The following polarity reversals and subchrons were generally well identified in APC cores from Holes U1586A–U1586C: the Brunhes/Matuyama (B/M) boundary (0.773 Ma), the Jaramillo Subchron (0.99–1.07 Ma), and the Matuyama/Gauss (M/G) boundary (2.595 Ma). APC cores from Hole U1586A also recorded the Mammoth Subchron (3.207–3.33 Ma) and the Gauss/Gilbert (G/G) boundary (3.596 Ma). The Cobb Mountain (1.18–1.215 Ma), Olduvai (1.775–1.934 Ma),

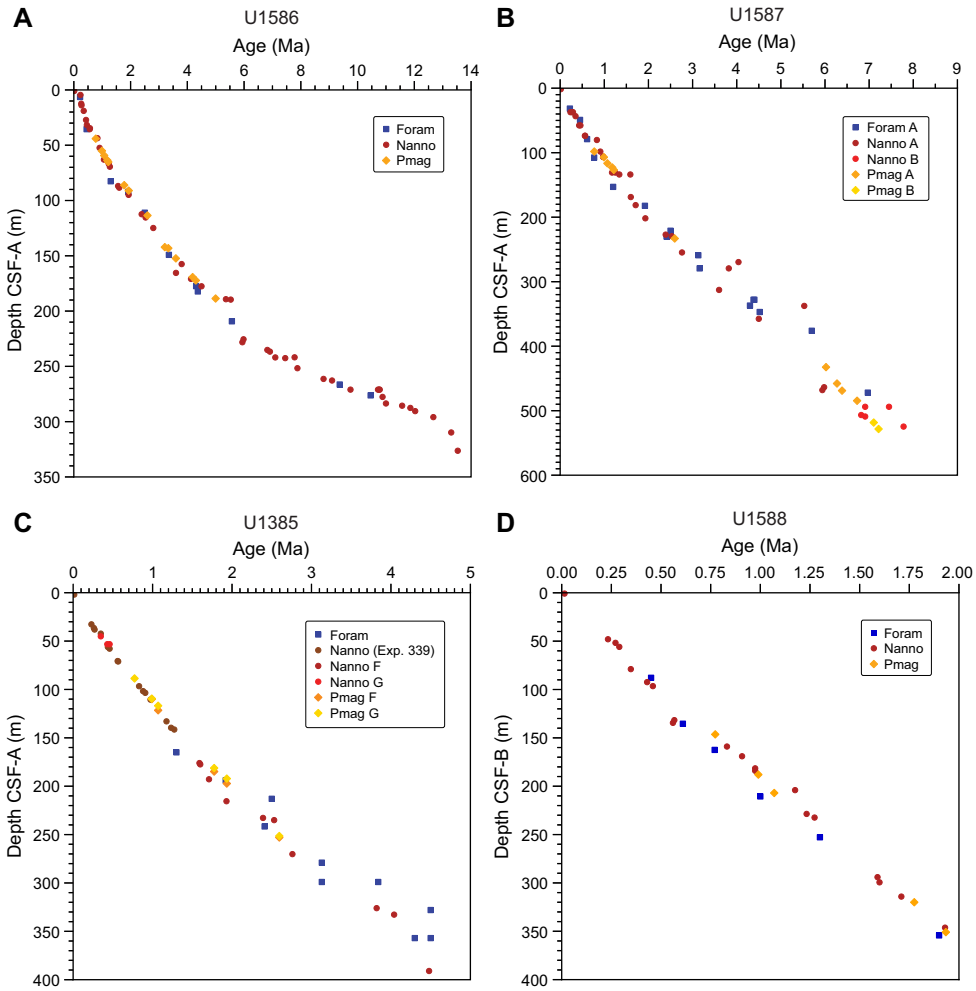

Figure F18. Preliminary age model based on calcareous nannofossils (Nanno) and planktonic foraminifer (Foram) biostratigraphic events and magnetostratigraphic (Pmag) transitions for Sites (A) U1586, (B) U1587, (C) U1385, and (D) U1588.

Feni (2.116–2.14 Ma), Cochiti (4.187–4.3 Ma), and Thvera (4.997–5.235 Ma) Subchrons (or part of these subchrons) were recorded in one or more holes at the site. Magnetostratigraphy is poorly resolved for XCB cores from all four holes at the site due to strong drilling overprint and for APC cores from Hole U1586D because of strong coring disturbance in cores from near the polarity boundaries.

Whole round samples (5–10 cm thick) were taken for interstitial water (IW) analysis from the base of every section for the uppermost 34 m and then from the penultimate section recovered from every core from Hole U1586A. IW analysis shows relatively constant salinity, sodium, and chloride throughout Hole U1586A, with values close to seawater, whereas potassium declines downhole with a relatively constant slope. Decreasing sulfate concentration is indicative of organic matter respiration via sulfate reduction; however, unlike other sites, sulfate at Site U1588 never reaches zero and methane concentration never exceeds 15 ppmv (Figure **F19**). A decrease in calcium and magnesium in the upper 50 m reflects authigenic carbonate precipitation driven by high pore water alkalinity and associated sulfate reduction. Peaks in redox-sensitive elements, such as iron and manganese, are similarly indicative of microbially mediated respiration reactions within the sediments. Below 200 mbsf, Ca, Sr, and Si concentrations increase while Mg decreases. Although dolomitization may explain the Mg, Ca and Sr profiles, by liberating Ca and Sr and using Mg, the high silicon concentration near the bottom of the hole indicates important Si dissolution within the silty clay layers of Lithostratigraphic Unit III. Mean $CaCO_3$ in Hole U1586A is 37.4 wt%, and values increase steadily but nonlinearly with depth. Total organic carbon values in Hole U1586A are generally low (mean = 0.48 ± 0.32 wt%), ranging 0–2.02 wt%; they are highest in the upper 50 m (0.57 ± 0.21 wt%) and steadily decline with depth (0.33 ± 0.27 wt% in the bottom 50 m). Methane is the only detectable gas, and its concentration ranges 0–14.10 ppmv with a peak between 100 and 150 mbsf (Figure **F19**).

Inductively coupled plasma–atomic emission spectroscopy (ICP-AES) data from bulk sediment analysis show strong correlations between SiO_2, K_2O, Fe_2O_3, MgO, and TiO_2 with Al_2O_3, indicating the dominance of local detritus. Barium is weakly correlated with Al or Ca, likely due to barite in sediments. Elemental ratios of Si/Al, K/Al, Si/Al, Sr/Ca, and estimated biogenic Ba are highlighted as potential proxies for provenance, weathering, and productivity.

Sediment physical properties data acquired from whole-round measurements for Site U1586 are generally in good agreement with those from split core measurements for gamma ray attenuation (GRA) and moisture and density (MAD) bulk densities, *P*-wave logger (PWL) and *P*-wave caliper (PWC) velocities, and MS loop and point count measurements. The cyclic variations in MS, NGR and L* color reflectance values are particularly distinct throughout all holes (Figure **F17**), showing

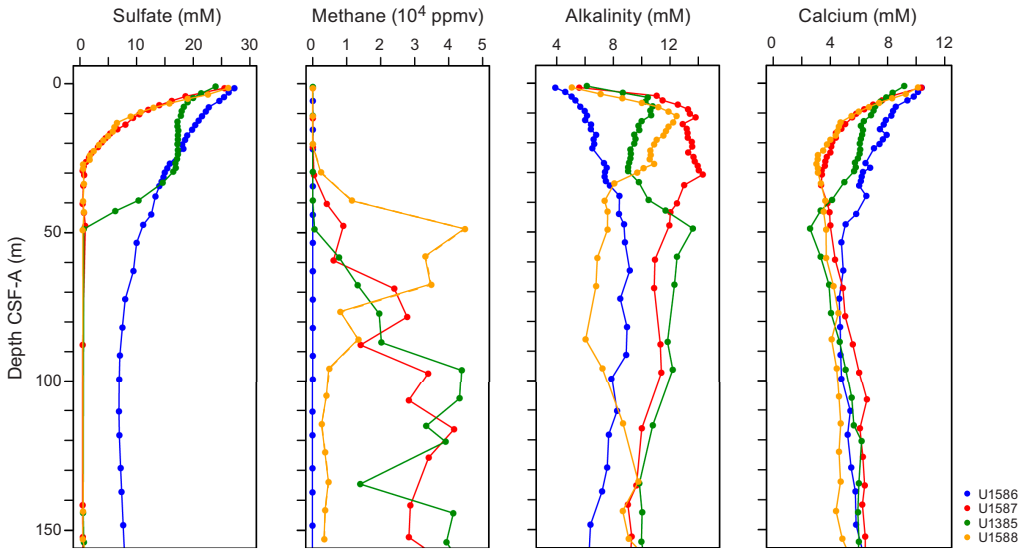

Figure F19. Comparison of IW sulfate, headspace methane, alkalinity, and calcium among Expedition 397 sites.

lower MS and NGR values in carbonate-rich sediments with higher L* values, whereas higher MS and NGR values occur in clay-rich sediments with lower L* values. The gradual increasing trend of bulk densities, thermal conductivity, and *P*-wave velocities and decreasing trend of porosity are attributed to compaction of sediments with depth. Downhole changes in physical properties overall are coherent with the defined lithofacies based on sedimentological observations. MS gradually declines over the upper ~100 m, coinciding with a decrease in pore water sulfate. This reflects the reaction of fine-grained magnetite with hydrogen sulfide, produced by sulfate reduction, to form iron sulfides (e.g., pyrite).

Downhole logging was conducted in Hole U1586D with the triple combo tool string between 84.6 (bottom of the pipe) and 255.3 mbsf. Comparison of the processed logging and core physical properties data reveal a good correlation in the NGR (Figure **F17**) and less so for density and MS. Four downhole formation temperature measurements were made in Hole U1586A. The calculated in situ sediment temperatures resulted in a geothermal gradient of 26.9°C/km and a heat flow of 32.0 m W/m2, which are slightly lower than the published value for the region.

Stratigraphic correlation among holes at Site U1586 was accomplished using Correlator software. Tie points were established using L* color reflectance, MS, and the blue channel extracted from the color images (RGB-blue). A splice was constructed from 0 to 320 m core composite depth below seafloor, Method A (CCSF-A) using four holes (U1586A–U1586D). The splice is complete except for one potential small gap in the Upper Pliocene where overlap is equivocal. Slump intervals noted by the sedimentologists were correlatable among all holes and have disturbed/removed variable amounts of intact stratigraphy. These include four in the Middle to Upper Pleistocene sequence and two in the Upper Miocene. Gaps in core recovery were evident when offset holes were compared and appear to correlate with sea state.

In summary, the preliminary age model based on biostratigraphy and magnetostratigraphy suggests that the sedimentary sequence recovered at Site U1586 spans the last 14 My. The combination of nearly continuous recovery, moderate sedimentation rates, clear cyclic variations in physical properties and sediment color, and a rich array of well-preserved calcareous microfossils suggest Site U1586 will provide an important record of North Atlantic surface and deepwater variability for the Middle Miocene to Pleistocene.

5.2. Site U1587

5.2.1. Background and objectives

Site U1587 is positioned at 3479 mbsl (Figure **F20**) and bathed today by a mixture of 75% North Atlantic Deep Water (NADW) and 25% LDW sourced from the Southern Ocean (Jenkins et al., 2015) (Figure **F5**). The mixing ratio of these water masses has changed in the past, as well as their vertical position in the water column, which has implications for ventilation and carbon storage in the deep Atlantic. Site U1587 is the second deepest site along the Expedition 397 bathymetric

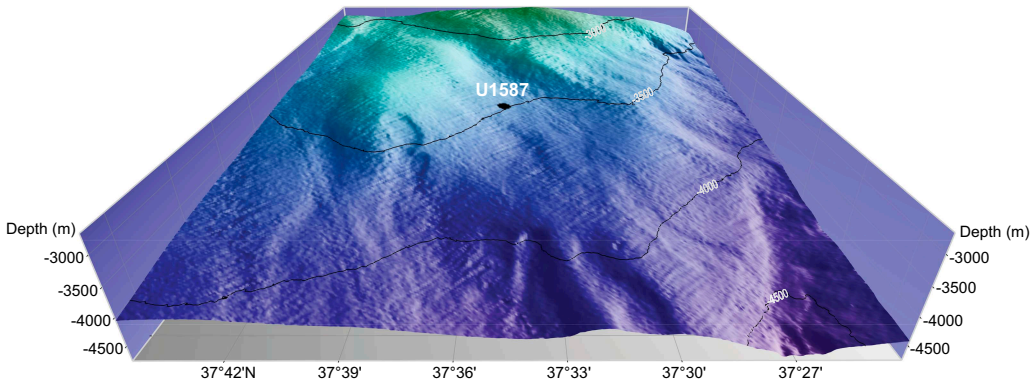

Figure F20. Location of Site U1587 on the Promontório dos Príncipes de Avis (PPA) at a water depth of 3479 mbsl. See Figure F2 for broader bathymetric context. (Figure made by Helder Pereira using Mirone and iVew4D software.)

transect (paleo-CTD) and will be important for reconstructing changes in the physical and chemical properties of the deep eastern North Atlantic on both long and short timescales.

The Upper Miocene to Quaternary sequence is expanded at Site U1587 and more than 500 m thick (Figure **F21**). Sedimentation rates are estimated to average ~10 cm/ky (Figure **F7**). We received permission from the EPSP to drill to 500 mbsf at this site but requested and were granted permission to drill an additional 50 m to extend the record well into the late Miocene.

Site U1587 was designed to recover an expanded sequence of late Miocene to Quaternary sediments with which to address several expedition objectives related to the history of MCV, orbital forcing of glacial–interglacial cycles, cyclostratigraphy, warm Pliocene climate, and the Messinian salinity crisis. The high sedimentation rates and long continuous record at Site U1587 will permit paleoceanographic reconstruction at millennial resolution as the climate system evolved from the warm Pliocene, through the intensification of NHG in the late Pliocene, the obliquity-dominated "41-kyr world," the middle Pleistocene transition, and the Great Ice Ages of the "100-kyr world."

5.2.2. Operations

We arrived at Site U1587 at 1121 h on 1 November 2022 after completing the 16.9 nmi transit from Site U1586 with the thrusters down and the vessel heading controlled by dynamic positioning (DP). The drill crew made up an APC/XCB bottom-hole assembly (BHA) using the same APC/XCB PDC bit used at Site U1586.

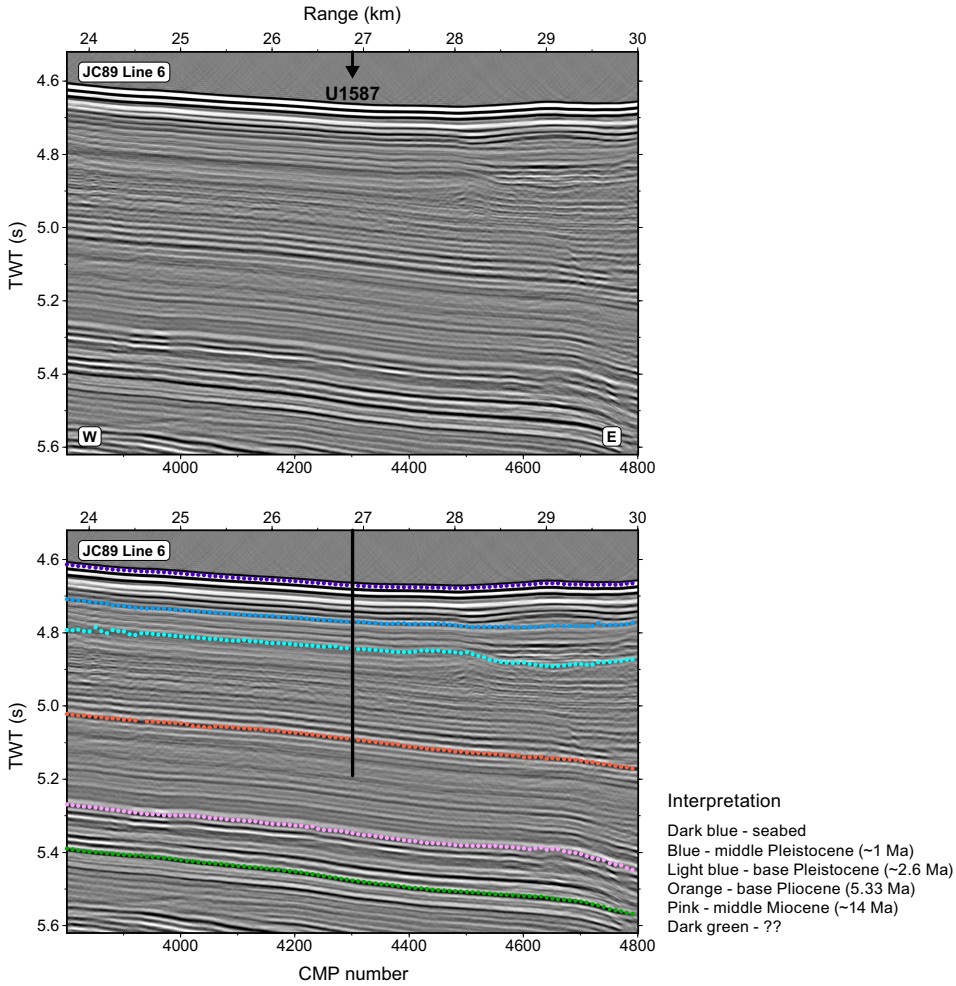

Figure F21. Original and interpreted seismic profile (JC89-6) showing the location of Site U1587 with penetration to 500 mbsf. The age of the reflectors have been revised to reflect the age of the recovered sediment. TWT = two-way traveltime, CMP = common midpoint.

The plan for Site U1587 was to core four holes with the APC and HLAPC systems to refusal (~250 mbsf) and then core to a maximum depth of 500 mbsf using the XCB system. Formation temperature measurements (APCT-3) were planned for the first hole and downhole logging (triple combo tool string) was planned for Hole U1587D.

Once on site, weather conditions and high seas caused some delays and the coring strategy was adjusted by removing the fourth hole from the plan after all site objectives had been met. Permission to deepen the site was requested from and approved by the EPSP while coring in Hole U1587B. Finally, the site consisted of three holes. Hole U1587A was cored to 500 mbsf, Hole U1587B was cored to 547.8 mbsf, and Hole U1587C was cored to 567.9 mbsf. As at Site U1586, the drilling strategy consisted of APC coring until the first partial stroke and then XCB coring to extend the hole to total depth. Hole U1587C was successfully logged with the triple combo tool string to 558 mbsf, roughly 10 m above the total depth of the hole. The drill string was raised, clearing the seafloor at 0850 h on 15 November and ending Hole U1587C and the site. The bit was raised to 2484 mbrf, and at 1115 h, we started moving to Site U1385 under DP navigation mode.

All APC cores used nonmagnetic core barrels and were oriented with the Icefield orientation tool. In total, 1615.7 m were cored at Site U1587 using the APC and XCB systems with a recovery rate of 97%. The site took 335.5 h (14.0 days) to complete.

5.2.3. Principal results

Principal results for Site U1587 are as follows:

- Recovery of a 567 m sequence ranging in age from the late Miocene (Tortonian; ~7.8 Ma) to Quaternary with sedimentation rates from 6.5 to 11 cm/ky (Figures **F18B**, **F22**).
- Continuous deposition and high sedimentation rates for the last 1.5 My are ideal for studying MCV and correlating Site U1587 to the polar ice core records.
- Pliocene sediments contain very strong precession-scale cycles in color and other physical properties (MS, density, and NGR) (Figures **F11**, **F23**). Amplitude modulation of these presumed precession cycles by eccentricity provides a powerful tool for developing an orbitally tuned timescale for Site U1587.
- Recovery of an apparently complete Messinian Stage (7.246–5.333 Ma) of the late Miocene with strong Milankovitch cyclicity consisting of alternating dark clay-rich sediments and lighter nannofossil ooze. This sequence will permit the study of the Messinian Salinity Crisis in an open ocean setting adjacent to the Mediterranean.
- Complete logging run from 81 to 558 mbsf showing cyclic variations in NGR that will be used for core-log integration (Figure **F23**).
- Expanded late Pliocene section documenting the intensification of NHG between 3.3 (MIS M2) and 2.6 Ma (MIS 100), including the mid-Pliocene warm period (3.3–3 Ma).

Coring in Holes U1587A, U1587B, and U1587C recovered a total of 1566 m of sediment. The dominant lithologies are nannofossil ooze and clay in varying proportions (Figure **F22**), which manifest as light and dark sediment layers reflected by changes in sediment physical properties. Pyrite nodules and infilled pyrite burrows are common throughout the sedimentary sequence. Bioturbation varies from light to heavy. Drilling disturbance in a few APC cores include soupy/slurry sediments, mostly in the top of Section 1 of many cores, and slight up-arching toward the bottom of the APC interval. XCB cores are generally undisturbed, but biscuiting occurs mainly below 204 mbsf.

Nannofossils are extraordinarily abundant, and foraminifers and ostracods are also common and generally well preserved. Planktonic foraminifer preservation decreases with depth, and Miocene specimens are very small in size, recrystallized, and challenging to identify. A total of 51 biostratigraphic markers (37 nannofossils and 14 planktonic foraminifers) were recognized and suggest a continuous sequence from the late Miocene (Tortonian; 7.8 Ma) to Holocene. Nannofossil and planktonic foraminifer stratigraphic events are in good agreement with magnetostratigraphy (Figure **F18B**). Sedimentation rate varies between 11 and 6.5 cm/ky (Figure **F7**).

Remarkably abundant ichthyoliths, accompanied by a high diversity of benthic foraminifers and a monospecific ostracod assemblage consisting only of the genus *Xylocythere*, were found in Sample

397-U1587A-22X-CC (201.6 m CSF-A) from the early Pleistocene. *Xylocythere* is known from chemosynthetic environments, such as hydrothermal vents, cold seeps, and fish and whale carcasses (Karanovic and Brandão, 2015; Tanaka et al., 2019), as well as oligotrophic, deep-sea sediments (Steineck et al., 1990).

Magnetostratigraphy of Site U1587 was established based on the NRM (after 20 mT demagnetization) inclination and (orientation-corrected) declination data from archive-half core sections and stepwise NRM demagnetization data from discrete cube samples. The following polarity reversals and subchrons were identified in all three holes: the B/M boundary (0.773 Ma), the M/G boundary (2.595 Ma), and the C3An.1n (6.023–6.272 Ma) and the C3An.2n (6.386–6.727 Ma) Subchrons. The Jaramillo (0.99–1.07 Ma) and possibly the Cobb Mountain (1.18–1.215 Ma) Subchrons were identified in APC cores from Hole U1587A. The C3Bn Chron (7.104–7.214 Ma) could be recorded

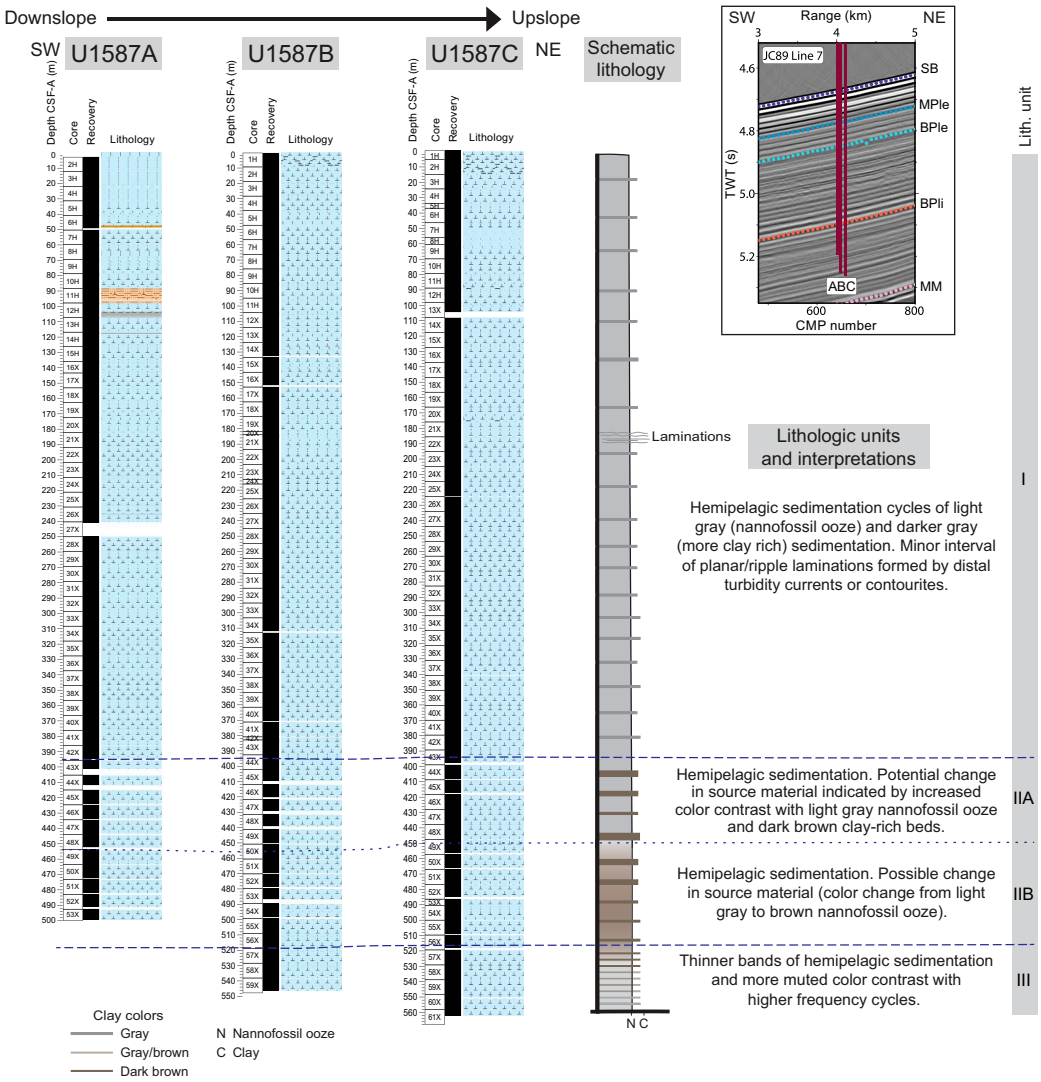

Figure F22. Lithologic summary, Site U1587. Left: summary lithostratigraphic logs of Holes U1587A–U1587C, ordered left to right from southwest to northeast (upslope to downslope). Blue dashed line = divisions of lithostratigraphic units, blue dotted line = division of subunits (not slump related). Right: lithologic unit names and preliminary interpretations of depositional processes. Colors are based on visual description as well as color (L*a*b*) values. Unit and subunit boundaries are primarily based on sedimentary structures as well as changes in color and banding thickness. Color is independent of lithology and is related to relative amounts of minor constituents such as pyrite and glauconite. Inset: cropped section of Seismic Line JC89 Line 7 showing location along transect and depth of the holes at the site. TWT = two-way traveltime, CMP = common midpoint, SB = seabed, MPle = Middle Pleistocene, BPle = base Pleistocene, BPli = base Pliocene, MM = Middle Miocene.

in Holes U1587B and U1587C, and the bottom ~20 m of sediments in Hole U1587C possibly records part of the C4n Chron (7.537–8.125 Ma).

IW samples show an increase in alkalinity, ammonium, and phosphate in the upper 50 m, whereas sulfate correspondingly decreases rapidly in the upper 30 m, indicating sulfate reduction and organic matter respiration (Figure **F19**). As sulfate reaches zero the concentration of methane begins to increase reaching about 40,000 ppmv at 125 mbsf. The decrease in calcium and magnesium in the upper 35 m reflects authigenic carbonate precipitation driven by high pore water alkalinity associated with sulfate reduction.

Sediment $CaCO_3$ content varies between 2.9 and 78.1 wt% with an average of 37.4 wt%. Total organic carbon (TOC), total nitrogen (TN), and total sulfur (TS) values are generally low, ranging within 0–2.02 wt% (mean = 0.48 wt%), 0–0.13 wt% (mean = 0.05 wt%), and 0–0.37 wt% (mean = 0.03 wt%), respectively. Organic carbon/nitrogen ratios (0–86.7; mean = 20.0) suggest that organic matter has marine and terrestrial sources.

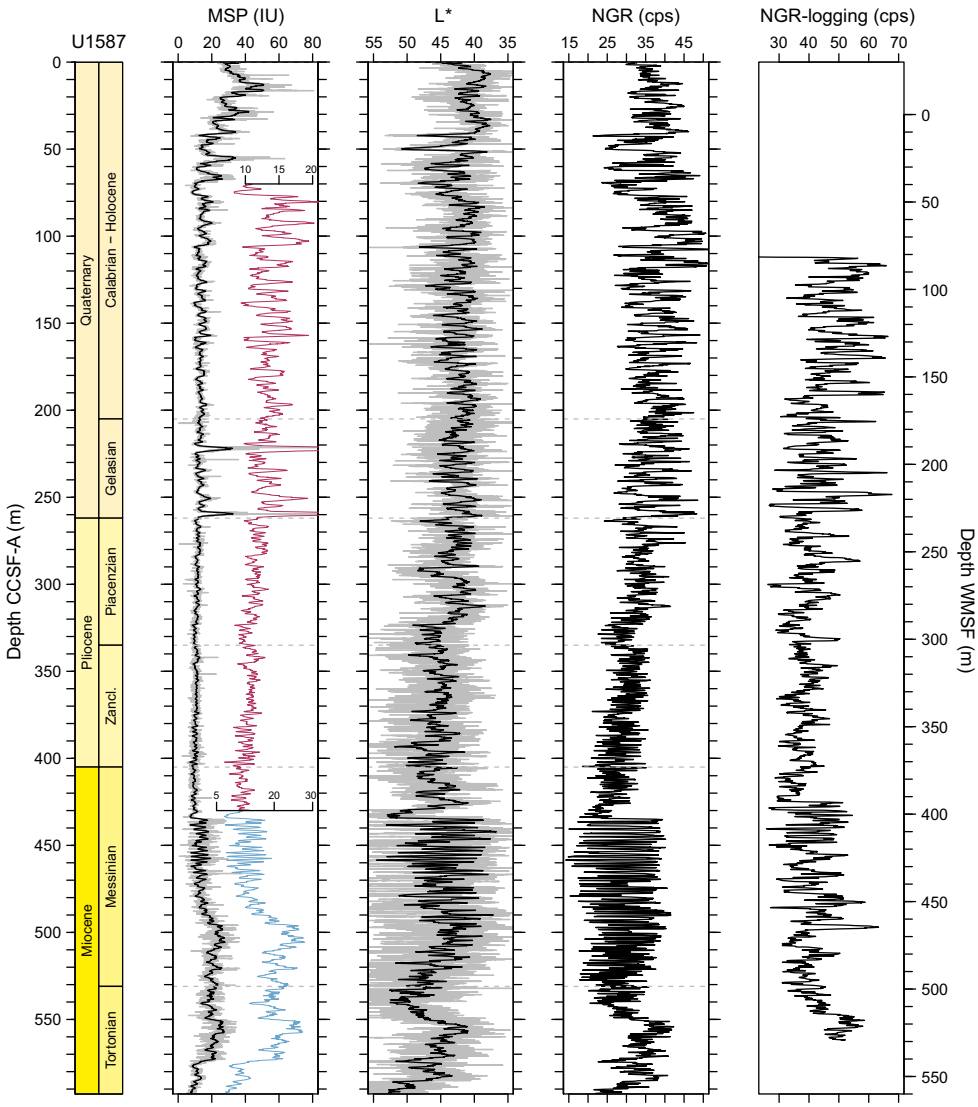

Figure F23. Core composite downhole trends of physical properties data, Site U1587. MSP = section-half point MS, NGR = whole-round NGR, cps = counts per second, NGR-logging = NGR data from the triple combo logging tool. WMSF = wireline log matched depth below seafloor. Inset MSP data (red and blue) are the same as the original signal but with an expanded scale to highlight the variability. MSP and L*: smoothed curve (black line; 50-point moving average) is shown over original data (gray line). NGR: only original data is shown.

ICP-AES data from the bulk sediment indicates elemental oxides of SiO_2, K_2O, and TiO_2 are strongly and positively correlated to Al_2O_3, reflecting the dominance of terrigenous detritus. The manganese and carbonate association in bulk sediment reinforces the IW indication of microbial mediated respiration reactions. Furthermore, elemental ratios of Ca/Ti, K/Al, Si/Al, Sr/Ca, and estimated biogenic Ba are potential proxies for provenance, weathering, and productivity.

Physical properties data acquired from whole-round measurements follow those from split core measurements. Physical properties data show strong cyclic variations in MS, NGR, and color throughout the sedimentary succession retrieved at Site U1587, reflecting variations in relative proportion of carbonate and clay (Figure **F23**). MS and NGR show lower values in lighter carbonate-rich sediments, whereas MS and NGR values are higher in darker clay-rich sediments. MS decreases in the upper ~80 m as sulfate reduction produces H_2S that reacts with magnetite to form iron sulfide minerals (e.g., pyrite). The X-ray images reveal the presence of pyrite nodules and burrow fill, diagenesis, and drilling disturbances. The gradual increasing trend of bulk densities, thermal conductivity, *P*-wave velocities, and the decreasing trend in porosity are attributed to the compaction of sediments with depth.

Following the completion of drilling Hole U1587C, the bit was raised to 80.1 mbsf for downhole logging. The triple combo tool string was deployed into the hole to 558 mbsf. We conducted an upward pass with the caliper open at a pace of 274 m/h over the entire hole to achieve the maximum possible data resolution from the Hostile Environment Natural Gamma Ray Sonde (HNGS) of the triple combo tool string. Initial evaluation of the HNGS log from Hole U1587C looks promising for correlating many of the cyclic features seen in NGR measurements on cores (Figure **F23**). Overall downhole trends of wireline logging densities, which show a gradual increase with depth, are consistent with GRA bulk densities measured on cores, although fine-scale variations are less well matched. Four downhole formation temperature measurements were made in Hole U1587A. The calculated in situ sediment temperatures yields a geothermal gradient of 43.4°C/km and a heat flow of 49.6 mW/m^2, which are comparable with those of published data from the Iberian margin.

A composite splice was constructed from 0 to 593 m CCSF-A using all three holes (U1587A–U1587C). A disturbed interval occurs from ~198 to 210 m CCSF-A, interrupting the sequence that is otherwise easy to correlate to late Pliocene and Pleistocene oxygen isotope stages. The disturbed interval appears to be in a similar stratigraphic position as the one identified at Site U1586 but removes much less section: the gap is equivalent to MIS 64–MIS 76. The late Miocene–Pliocene sequence is without apparent stratigraphic gaps, and the Pliocene sequence correlates cycle-for-cycle to Site U1586. An interval of expanded sedimentation with cycles ~1.5 m thick occupies the late Messinian. The cyclicity in sediment physical properties is remarkably strong at Site U1587 with a strong precession signal expressed throughout the late Miocene and Pliocene, which will be valuable for developing an astronomically tuned timescale.

5.3. Site U1385

5.3.1. Background and objectives

As a proof of concept for demonstrating the potential of the Iberian margin for providing long, continuous records of MCV, Site U1385 was first drilled during Expedition 339 in November 2011. As expected, a 1.45 My sequence with continuously high sedimentation rates was recovered at Site U1385 (Hodell et al., 2023). Postcruise studies demonstrated the great potential of the site to yield detailed records of MCV (Figure **F4**). On the basis of the success of Site U1385, Expedition 397 sought to extend the length of this remarkable sediment archive to 400 mbsf, spanning the entire Quaternary and Pliocene.

Expedition 397 Site U1385 is located ~1 km southwest of Expedition 339 Site U1385 (Figure **F1**) at 2591 mbsl, in the core of lower NEADW (Figure **F5**). It is the second shallowest site along the Expedition 397 bathymetric transect (paleo-CTD) (Figure **F24**), and it is positioned on Seismic Line JC089-9 (Figure **F25**). The site was designed to provide a marine reference section from the core of NEADW. During glacial periods, Site U1385 was influenced by a relatively greater proportion of deep water sourced from the Southern Ocean.

The overall objective of Expedition 397 Site U1385 is to recover a Pliocene–Pleistocene sediment sequence that can serve as a marine reference section for reconstructing the long-term history of orbital- and millennial-scale climate variability. Isotope and XRF records from Expedition 339 Site U1385 have demonstrated that MCV was a persistent feature of glacial climates over the past 1.45 My (Hodell et al., 2023). But does similar MCV persist during glacial periods beyond 1.5 Ma

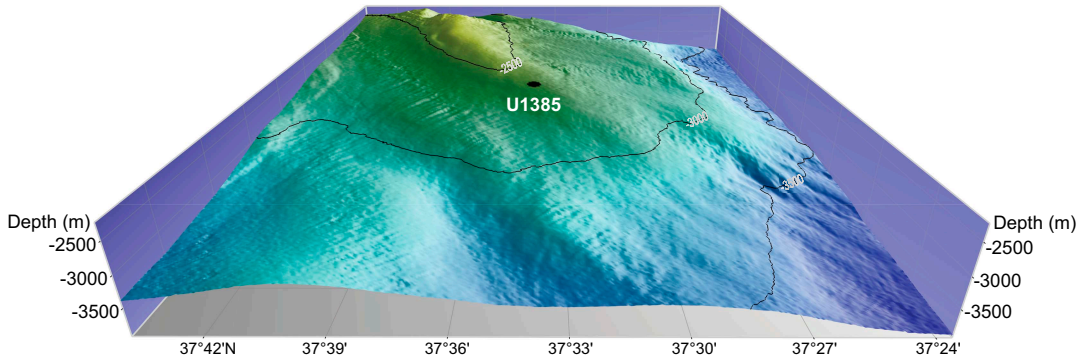

Figure F24. Location of Site U1385 on the Promontório dos Príncipes de Avis (PPA) at a water depth of 2591 mbsl. See Figure F2 for broader bathymetric context. (Figure made by Helder Pereira using Mirone and iVew4D software.)

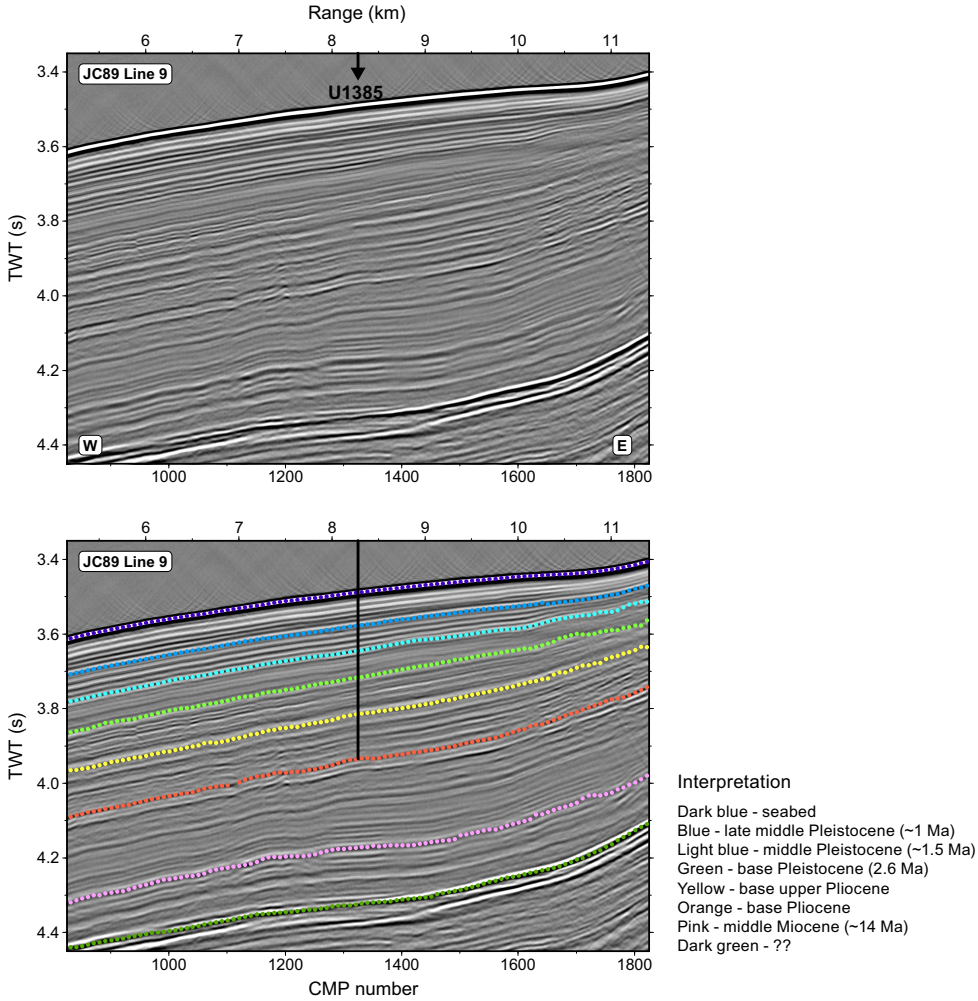

Figure F25. Original and interpreted seismic profile (JC89-9) showing the location of Site U1385 with penetration to 400 mbsf. The age of the reflectors have been revised to reflect the age of the recovered sediment. TWT = two-way traveltime, CMP = common midpoint.

throughout the entire Quaternary? How does the nature (intensity, duration, and pacing) of MCV change with orbital configuration and climate background state throughout the Quaternary? How did MCV change with the intensification of NHG during the late Pliocene? Was MCV suppressed during the warm Pliocene prior to the intensification of NHG as it was during most interglacial stages of the Pleistocene? How did millennial climate change interact with the effects of orbital forcing to produce the observed patterns of glacial–interglacial cycles through the Pliocene–Pleistocene? How did the relative importance of obliquity and precession evolve in the Pliocene–Pleistocene? What was responsible for the strong precession cycle observed in sediment color throughout the record? These are some of the questions that will be addressed by collaborative postcruise investigations among Expedition 397 scientists.

5.3.2. Operations

The vessel made the transit to Site U1385 with the thrusters deployed in DP mode between 15 and 16 November 2022 over 12.75 h and arrived on site at 0220 h. Site U1385 was previously occupied during Expedition 339 when five holes were cored (25–29 November 2011). Expedition 397 began operations in Hole U1385F. The plan for the reoccupation of Site U1385 was to core four new holes with the APC system to refusal (estimated at ~135 mbsf) and then core to 400 mbsf using the XCB system. Downhole measurements with the triple combo tool string were planned for Hole U1385I.

Once on site, weather conditions and high seas led to changes to the coring strategy, which was adjusted to take full advantage of all operational time to achieve the best possible core quality. Five holes were eventually cored. Two holes were drilled ahead without coring (Hole U1385F to 96.9 mbsf and Hole U1385H to 114.6 mbsf) to allow for XCB coring in the lower section of the holes to the total depth (400 mbsf). In the other three holes, the APC system was deployed from the seafloor until the first partial stroke was registered and then the holes were extended to 400 mbsf using the XCB system. Logging was attempted in Hole U1385J using the triple combo tool string, but a portion of a bow spring centralizer on the tool broke and wedged in the lockable float valve, trapping the tool string inside the pipe, and logging was abandoned.

All APC cores used nonmagnetic core barrels and were oriented using the Icefield MI-5 core orientation tool. In total, 1537.5 m was cored using both the APC and XCB systems with an overall core recovery of 99%. Site U1385 took 336.0 h (14.0 days) to complete, including 101.0 h (4.2 days) waiting on weather.

5.3.3. Principal results

Principal results for Site U1385 are as follows:

- Drilling at Site U1385 recovered a continuous 5.3 My record of hemipelagic sediments to the base of the Pliocene with an average sedimentation rate between 11 and 9 cm/ky (Figures **F18C**, **F26**).
- A complete spliced section was constructed to 453 m core composite depth below seafloor (CCSF) using five holes (U1385F–U1385J).
- We reproduced the upper 158 mbsf of the sequence recovered previously at Expedition 339 Site U1385, which provides additional sediment for sampling of these high-demand cores. We also recovered a more complete record of MIS 11 than was previously recovered at the site, which was partially missing in a hiatus at Expedition 339 Site U1385 (Hodell et al., 2015).
- Extension of the Site U1385 record beyond the last 1.45 My (MIS 47) permits the study of MCV for the earlier part of the Quaternary and late Pliocene, prior to the intensification of NHG, including linkages and phase relationship with the polar ice core and European terrestrial records.
- Variations in sediment color and other physical properties at Site U1385 display very strong cyclicity throughout the Pliocene and Pleistocene (Figure **F27**), permitting the development of an orbitally tuned timescale and correlation to Mediterranean cyclostratigraphy. The cycles can be matched one-for-one between Site U1385 and Sites U1586 and U1587 (Figure **F11**), providing a powerful cross check of the completeness of the stratigraphic sections.
- Complete recovery of Pliocene sediments to 5.3 Ma permits studies of variability under warmer climate conditions and atmospheric CO_2 concentrations similar to today.

A total of 1515.2 m of sediment was recovered at Site U1385 in five holes (U1385F, U1385G, U1385H, U1385I, and U1385J), four of which were drilled to a total depth of 400 mbsf. One lithostratigraphic unit was defined that primarily consists of nannofossil ooze with varying amounts of clay, indicating the dominance of hemipelagic sedimentation. Cyclic color banding is evident throughout all cores. Drilling disturbance is present in many cores from all holes, ranging from slight to severe, which varies with the drilling system, operation conditions, and gas (methane) content of the sediments.

On the basis of 15 nannofossil and 11 planktonic foraminifer bioevents, the ~400 m thick sedimentary succession at Site U1385 ranges in age from the Pleistocene to the earliest Pliocene. Both nannofossils and foraminifers show good preservation and are abundant throughout the section. The zonal schemes of the two microfossil groups are in good agreement and consistent with previous biostratigraphy of Expedition 339 Site U1385 for the upper 150 mbsf.

Magnetostratigraphy of Site U1385 was established based on the NRM (after 20 mT demagnetization) inclination and (orientation-corrected) declination data from archive-half core sections and stepwise NRM demagnetization data from discrete cube samples. The B/M boundary (0.773 Ma)

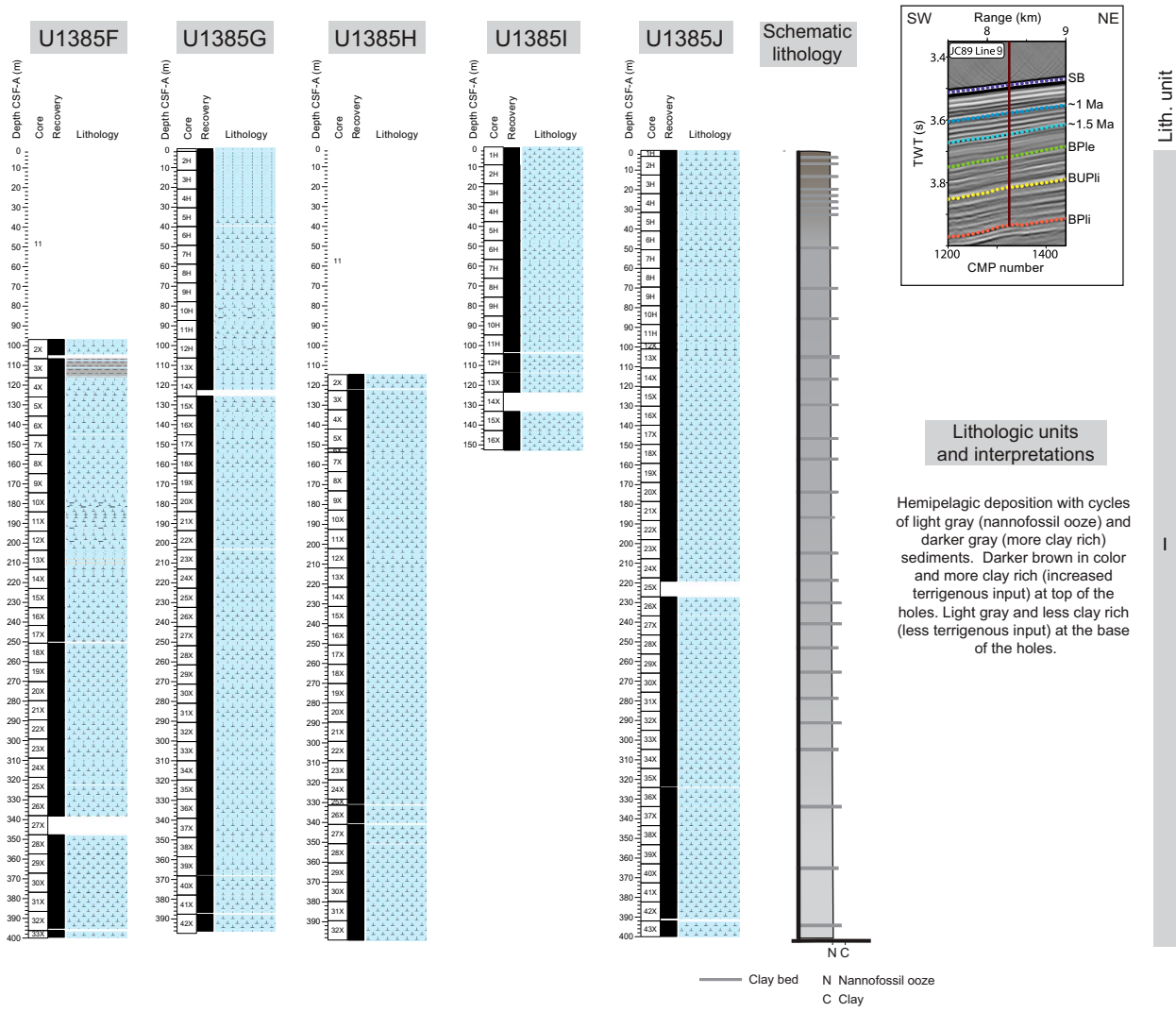

Figure F26. Lithologic summary, Site U1385. Left: summary lithostratigraphic logs of Holes U1385F–U1385J. Right: lithologic unit names and preliminary interpretations of depositional processes. Colors are based on visual description as well as L*a*b* values. Color is independent of lithology and is related to relative amounts of minor constituents such as pyrite and glauconite. Inset: cropped section of Seismic Line JC89 Line 9 showing location along transect and depth of Holes U1385F–U1385J. TWT = two-way traveltime, CMP = common midpoint, SB = seabed, BPle = base Pleistocene, BUPli = base of Upper Pliocene, BPli = base Pliocene.

is identified in APC cores from Holes U1385G, U1385I, and U1385J. The Jaramillo Subchron is recorded in XCB cores from Holes U1385F, U1385G, U1385I, and U1385J. The Olduvai Subchron (1.775–1.934 Ma) and the M/G boundary (2.595 Ma) are recorded in XCB cores from Holes U1385F, U1385G, U1385H, and U1385J. The magnetostratigraphy and biostratigraphy are generally in good agreement, and sedimentation rates vary between 9 and 11 cm/ky (Figure **F18C**).

In the upper 150 m CSF-A, the IW chemistry of Expedition 397 Site U1385 is very similar to that of Expedition 339 Site U1385 (Expedition 339 Scientists, 2013b). Sulfate shows a two-step decrease before reaching values of zero by 48.8 m CSF-A (Figure **F19**). The first step represents organoclastic sulfate reduction, and the second represents anaerobic oxidation of methane (Turchyn et al., 2016). Once sulfate reaches zero, methane increases, reaching maximum values of ~35,000 between 100–280 m CSF-A. Alkalinity, ammonium, and phosphate also increase in the upper 50 m CSF-A in conjunction with sulfate reduction. Calcium declines in two steps in the upper 50 m, likely reflecting authigenic precipitation of carbonate as a consequence of increased alkalinity associated with the two-step change in sulfate reduction.

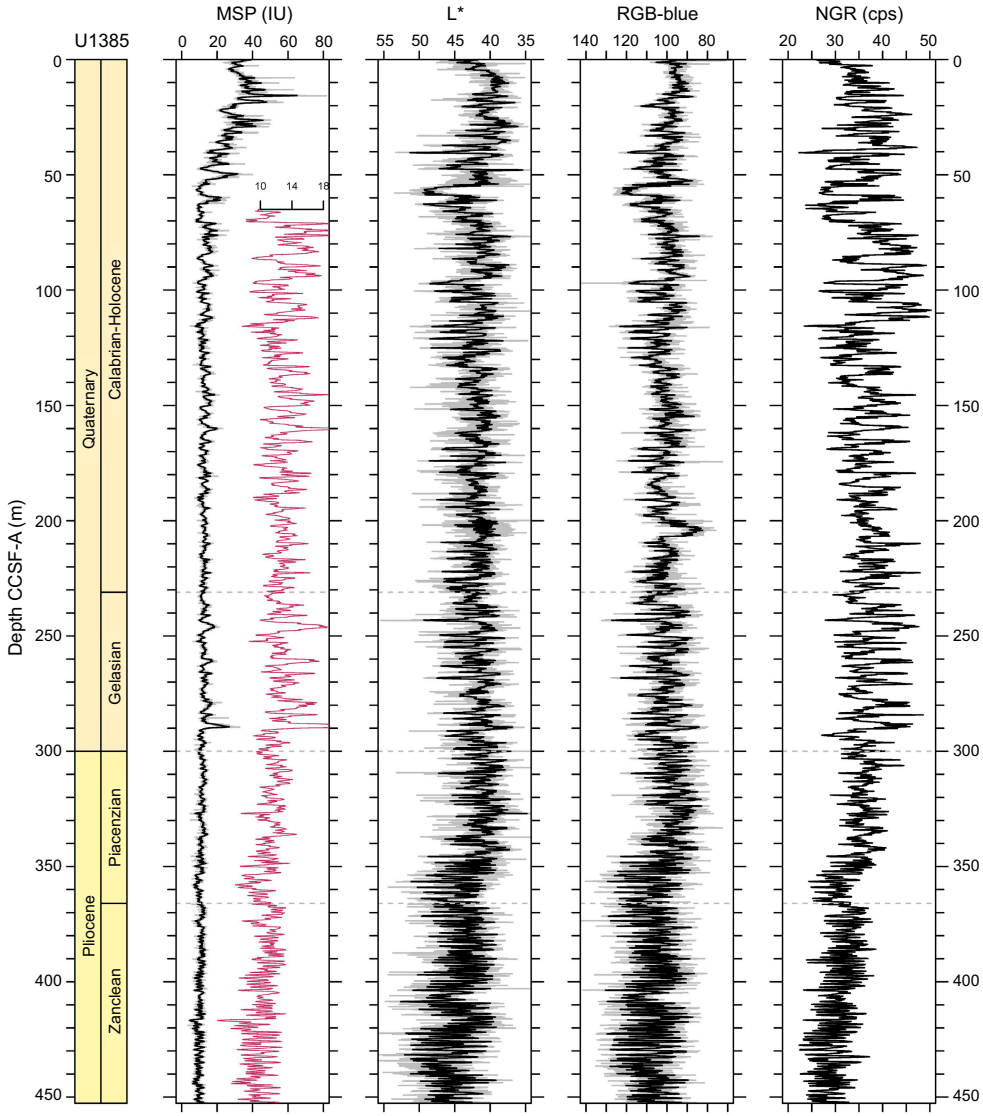

Figure F27. Core composite downhole trends of physical properties data, Site U1385. MSP = section-half point MS, NGR = whole-round NGR, cps = counts per second. The red MSP data are the same as the original signal but with an expanded scale to emphasize the cyclic variability. MSP, L*, and RGB-blue: smoothed curve (black line; 20-point moving average) is shown over original data (gray line). NGR: only original data is shown.

The $CaCO_3$ content of the sediment averages 38.8 wt%, varies between 15.2% and 63.3%, and is positively correlated with L* reflectance and negatively correlated with NGR. TOC, TN, and TS values at Site U1385 are generally low with a mean value of 0.48, 0.005, and 0.115 wt%, respectively. Organic C/N ratios (mean = 20.2) indicate that organic matter is marine dominated with higher terrestrial input in the upper 75 m CSF-A.

Bulk sediment geochemistry suggests that Ca is primarily biogenic carbonate, and because of the incorporation of Sr into biogenic carbonates, both elements show an inverse relationship with Al. Barium is weakly correlated with Al or Ca, likely due to the presence of barite. Manganese seems to be mainly associated with carbonate. Elemental ratios of Ca/Ti, Si/Al, Ti/Al, Zr/Al, K/Al, Sr/Ca, and estimated biogenic Ba are suggested as potential proxies of provenance, weathering, and productivity.

Physical properties data acquired from whole-round measurements follow those from split core measurements. A decline in MS in the upper 50 m follows sulfate reduction in the sediment pore waters, suggesting that H_2S from sulfate reduction reacts with Fe in magnetite to produce iron monosulfides and pyrite. The cyclic variations in MS, NGR, and L* color reflectance parameter values are particularly strong throughout all holes at Site U1385 (Figure **F27**), showing lower MS and NGR values in carbonate-rich sediments with higher L* values and higher MS and NGR values in clay-rich sediments with lower L* values. The gradual increasing trend of bulk densities, thermal conductivity, and *P*-wave velocity and the decreasing trend in porosity are attributed to the compaction of sediments with depth. The X-ray images reveal the presence of pyritized burrows, authigenic minerals, gas expansion, and drilling disturbance. Comparisons of physical properties measured for Expedition 339 Holes U1385A–U1385E and Expedition 397 Holes U1385F–U1385I show good agreement between expeditions.

Stratigraphic correlation between holes at Site U1385 were accomplished using Correlator software (version 4.0.1). Tie points were established using the L* color reflectance parameter, whole-round MS, and the blue color channel extracted from the core images (RGB-blue). We constructed a splice from 0 to 452.7 m CCSF-A using all five of the newly drilled holes at the site (U1385F–U1385J). The data from Site U1385 will be integrated postcruise with Expedition 339 Holes U1385A–U1385E to produce a common spliced composite section. The Pliocene sequences of Sites U1586 and U1587 correlate cycle-for-cycle (Figure **F11**).

5.4. Site U1588

5.4.1. Background and objectives

Site U1588 is the closest to the coast and the shallowest of the proposed depth transect (1339 mbsl) (Figures **F1**, **F2**, **F28**). The site is on a drift deposit formed under the influence of the lower MOW (Hernández-Molina et al., 2014). It lies on the broad, gently inclined middle-slope region of the PPA, where the seismic data indicate an extensive plastered drift deposit located on the distal part of the contourite system (Figure **F29**). The water depth of Site U1588 complements the sites

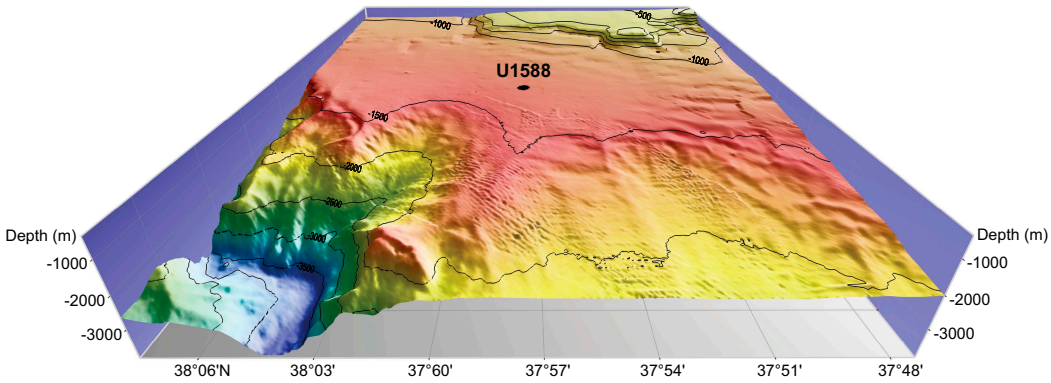

Figure F28. Location of Site U1588 on the Promontório dos Príncipes de Avis (PPA) at a water depth of 1339 mbsl. See Figure F2 for broader bathymetric context. (Figure made by Helder Pereira using Mirone and iVew4D software.)

drilled during Expedition 339 in the Gulf of Cádiz (Sites U1386–U1390) and along the Portuguese margin (Site U1391) at intermediate water depths (560–1073 mbsl) to study past variations in the depth and intensity of the MOW.

Our objective at Site U1588 was to drill multiple holes to 500 mbsf to recover a continuous and complete Pliocene–Pleistocene sedimentary succession (Figure **F29**). Sedimentation rates at Site U1588 are the highest (±20 cm/ky) of the four sites drilled during Expedition 397 (Figure **F7**), which provides a marine reference section for reconstructing climate variability at high temporal resolution (millennial to submillennial) and studying how the MOW has varied on orbital and millennial timescales.

5.4.2. Operations

The operational plan for Site U1588 was to core five holes with the APC/XCB systems. The first three were to be cored to 500 mbsf, and the final two holes were to be cored to 250 mbsf. Downhole logging measurements were to be conducted in Hole U1588D. Because of time constraints toward the end of the expedition and unexpectedly high methane gas content in the formation, the coring plan was shortened to three holes to approximately 350 mbsf and a fourth hole cored as deep as possible with the remaining time, reaching a final depth of 412.5 mbsf. Downhole logging was canceled.

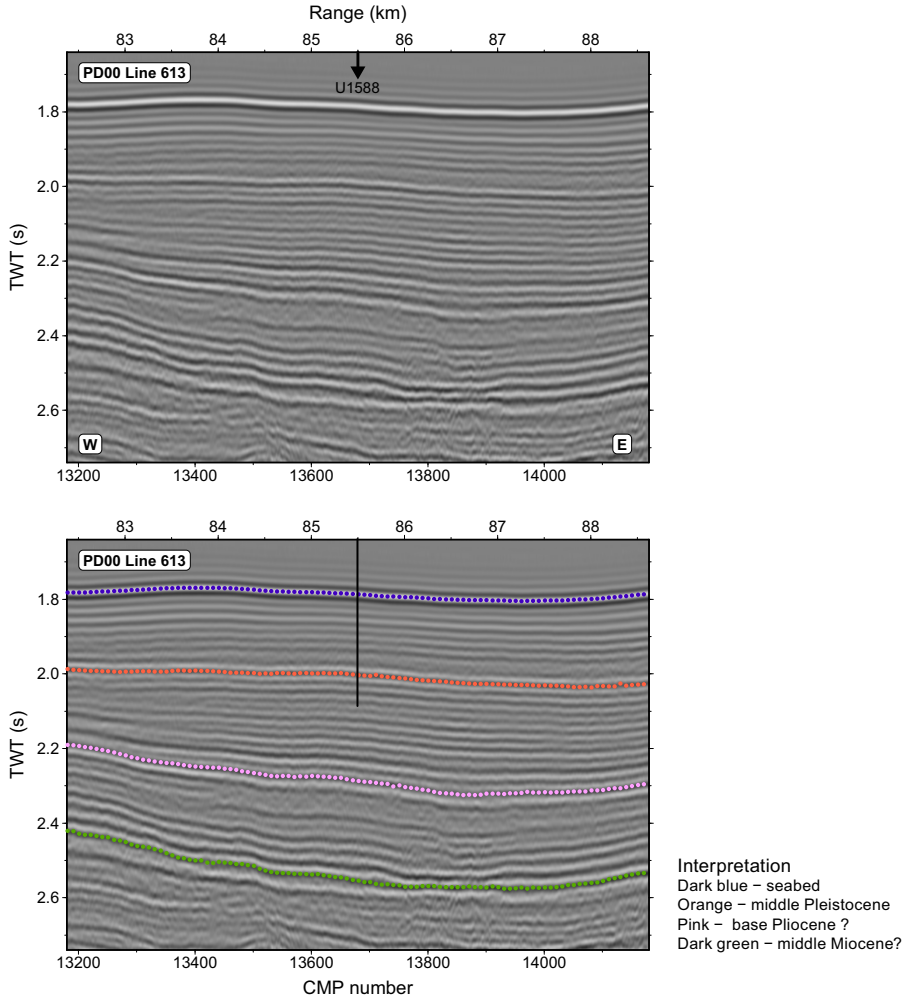

Figure F29. Original and interpreted seismic profile (TGS-NOPEC PD00-613) showing the location of Site U1588 with penetration to ~400 mbsf. The depth of penetration and age of the reflectors have been revised to reflect the actual depth and age of the recovered sediment (data courtesy of TGS-NOPAC Geophysical Company ASA). TWT = two-way traveltime, CMP = common midpoint.

Significant core expansion and curatorial difficulties encountered in Hole U1588A due to high methane gas content in the sediment led to a change in the XCB coring strategy starting with Core 397-U1588A-25X and followed at all subsequent holes at the site. XCB cores were taken using half advances, giving cores room to expand inside the core liners as gas was released.

Holes U1588A, U1588B and U1588D were APC cored to 154.2, 81.8, and 90.5 mbsf, respectively, and then XCB cored to their final depths. Because of increasing seas, APC coring was dropped in Hole U1588C in favor of drilling ahead to 92.0 mbsf before starting to XCB core the lower section.

A total of 242 cores were taken at the site, 37 APC and 205 XCB. All APC cores used nonmagnetic core barrels and were oriented using the Icefield orientation tool. In total, 1377.1 m were cored, recovering 1748.93 m (127%). Formation temperature measurements were done with the APCT-3 tool in Hole U1588A on Cores 4H, 7H, 10H, and 13H. Site U1588 took 186.75 h (7.8 days) to complete.

5.4.3. Principal results

Principal results for Site U1588 are as follows:

- Successful demonstration of an alternative coring method for gassy sediment involving half advances of the XCB, thereby allowing the core to expand into the empty part of the liner.
- Recovery of an expanded 412.5 m sequence spanning the last 2.2 My with sedimentation rates averaging 18 cm/ky (Figures **F18D**, **F30**).
- Recovery of a marine reference section for studying Quaternary climate variability at very high temporal resolution (millennial to submillennial), including changes across the mid-Pleistocene transition.
- Proxy signals of surface temperature (e.g., alkenones, planktonic $\delta^{18}O$) will constitute a marine sediment analog for the Greenland ice core.
- Contourite sedimentation under the influence of the lower MOW will, in conjunction with other Expedition 339 sites (Expedition 339 Scientists, 2013a), provide a detailed history of the response of the MOW to orbital and millennial climate change.

At Site U1588, because of the significant core expansion, all depths of the scientific results are reported in meters on the core depth below seafloor, Method B (m CSF-B), scale hereafter. The CSF-B depth scale corrects for core expansion by uniformly compressing the recovery to the advance of the bit (driller's depth).

The ~412.5 m thick sedimentary succession drilled at Site U1588 consists of one lithostratigraphic unit (Figure **F30**). Most sediments are from Lithofacies 1 and consist primarily of nannofossil ooze, with varying amounts of inorganic/detrital/recrystallized calcium carbonate of indeterminate origin (hereafter termed “carbonate”) and clay. The abundance of nannofossil ooze with substantial amounts of clay and carbonate indicates the persistence of hemipelagic sedimentation and an indeterminate (recrystallized or detrital) source of carbonate at Site U1588 through the Pleistocene. Foraminifers, diagenetic features (dark patches and pyrite), and rare, subtle color banding are disseminated throughout the cores. Bioturbation varies from absent to heavy and generally increases downhole. Deformational sedimentary structures are rare and, when present, are at a decimeter scale. Drilling disturbance is present within most cores in all holes, varies from slight to severe, and is influenced by the drilling type, operation conditions (ship heave), and methane gas contents of sediments.

Site U1588 ranges in age from the Holocene to the early Pleistocene (~2.2 Ma) based on calcareous nannofossil (21 bioevents) and planktonic foraminifer (6 bioevents) biostratigraphy. The zonal schemes of calcareous nannofossils and planktonic foraminifers generally agree, indicating an average sedimentation rate of 18 cm/ky (Figure **F18D**).

The site revealed excellent preservation for all microfossils, including biogenic Si, mainly in the form of diatoms, sponge spicules, silicoflagellates, and radiolarians at specific depth intervals that are associated with some glacial terminations (e.g., Terminations XII, VI, and V). The occurrence of biogenic silica at these terminations is in good agreement with observations from Expedition 339 Site U1391 (Abrantes et al., 2017). All calcareous microfossils, including coccoliths, plank-

tonic and benthic foraminifers, and ostracods, are abundant and are generally well distributed throughout the succession. Excellent preservation is also indicated by the presence of pteropods. Ostracod diversity increases toward the top of the sequence, and variations in planktonic foraminifer species composition throughout the Pleistocene are likely associated with glacial–interglacial or even millennial-scale climate fluctuations. Benthic foraminifer assemblages suggest variability in organic flux and/or oxygen conditions relative to changes in surface productivity and bottom water oxygenation.

Magnetostratigraphy of Site U1588 was established based on the NRM (after 20 mT demagnetization) inclination and (orientation-corrected) declination data from archive-half core sections and stepwise NRM demagnetization data from discrete cube samples. The B/M boundary (0.773 Ma) is identified in APC cores from Hole U1588A and XCB cores from Holes U1588B–U1588D. The Jaramillo Subchron (0.99–1.07 Ma) and the top of the Olduvai Subchron (1.775 Ma) appear to be recorded in XCB cores from all four holes. The bottom of the Olduvai Subchron (1.934 Ma) is only recorded in XCB cores from the deepest Hole U1588D (below 350 m CSF-B).

Geochemistry of IW samples show that alkalinity, ammonium, and phosphate increase in the upper 50 m, whereas sulfate shows a two-step decrease in the upper 50 m (Figure **F19**), indicating organic matter respiration. At this site, the sulfate reaches zero and stays low. Methane levels

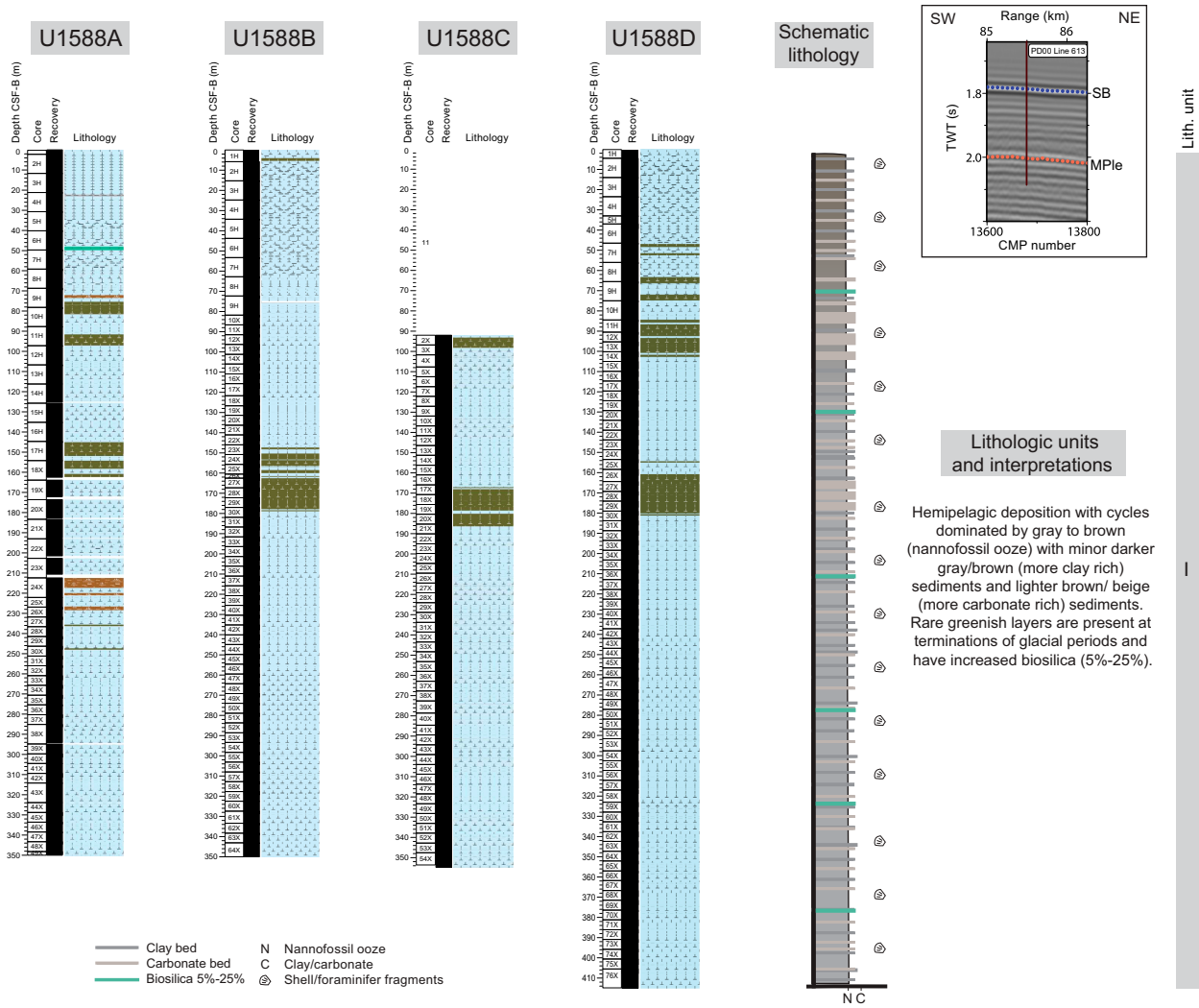

Figure F30. Lithologic summary, Site U1588. Left: summary lithostratigraphic logs of Holes U1588A–U1588D. Right: lithologic unit name and preliminary interpretation of depositional processes. Colors are based on visual description as well as L*a*b* values. Inset: cropped section of Seismic Line JC89 Line PD00-613 showing location along transect and depth of the holes at the site. TWT = two-way traveltime, CMP = common midpoint, SB = seabed, MPle = Middle Pleistocene.

increase to about 45,000 ppmv at 50 m CSF-B but decline to ~5,000 ppmv by 100 m to the bottom of the hole. Given the consistently high degassing of sediment below 50 m CSF-B, it is likely the decrease in methane concentrations measured in headspace samples does not accurately reflect the sediment gas content, which is supported by very high methane concentrations measured in void gas.

$CaCO_3$ content varies between 16.0% and 53.6% and averages 30.2 wt%. The $CaCO_3$ content determined by coulometric titration shows consistent results with stoichiometric $CaCO_3$ calculated from the Ca concentrations measured by ICP-AES, and both are positively correlated with L* reflectance and negatively correlated with NGR, TOC, TN, and TS. TOC, TN, and TS values at Site U1588 are generally low, ranging 0.30–1.89 wt% (mean = 0.74 wt%), 0.042–0.189 wt% (mean = 0.085 wt%), and 0–3.18 wt% (mean = 0.291 wt%), respectively. Organic C/N ratios (3.04–16.5; mean = 8.97) suggest that organic matter is marine dominated.

Bulk sediments SiO_2, K_2O, and TiO_2 show strong positive correlations with Al_2O_3, indicating the dominance of terrigenous detritus. Relatively weak correlations are observed for Fe_2O_3, MgO, Na_2O, MnO, and Ba against Al_2O_3 due to the widespread presence of authigenic and biogenic phases such as pyrite, dolomite and/or Mg-bearing calcite, halite (NaCl) precipitated from seawater, Mn hydroxides, and barite, respectively. Bulk sediment Ca primarily represents biogenic carbonate ($CaCO_3$), and because of the incorporation of Sr into biogenic carbonates, both elements show an inverse relationship with Al. Elemental ratios of Ca/Ti, Si/Al, Ti/Al, Zr/Al, K/Al, Sr/Ca, and estimated biogenic Ba are potentially useful proxies for provenance, weathering, and productivity.

Physical properties data acquired from whole-round core measurements for Site U1588 are in good agreement with measurements carried out on split core and discrete samples. A decrease in MS at shallower depths follows sulfate reduction in sediment pore waters. The cyclic variations in MS, NGR, and L* values are distinct throughout all holes (Figure **F31**), showing lower NGR and MS values in carbonate-rich sediments with higher L* values, whereas higher MS and NGR values occur in clay-rich sediments with lower L* values. The gradually increasing values of bulk density, thermal conductivity, *P*-wave velocity, and a decreasing trend in porosity are attributed to the compaction of sediments with increasing depth. X-ray imaging of the core sections revealed the presence of authigenic minerals and burrows, further evidence of gas expansion, and drilling disturbance.

Four downhole formation temperature measurements were made in Hole U1588A. The calculated in situ sediment temperatures yields a geothermal gradient of 33.2°C/km and a heat flow of 32.0 m W/m2, which are slightly lower than the published value for the region.

Stratigraphic correlation between holes at Site U1588 was accomplished using Correlator software (version 4.0.1). Tie points were established using MS from the Whole-Round Multisensor Logger (WRMSL) as well as NGR. A splice was constructed from 0 to 366 m core composite depth below seafloor, Method B (CCSF-B) using four holes (U1588A–U1588D). The drilling and correlation strategies were unique at this site due to the severely expanded cores. A mixture of APC, full-advanced XCB, and half-advanced XCB coring was used for different levels of core expansion at each hole. Instead of the CSF-A scale, the CSF-B scale was used for correlation, producing the CCSF-B composite depth scale. Considering the high-quality XCB cores and the high sedimentation rate at this site, the composite section was nearly complete with only one possible small gap.

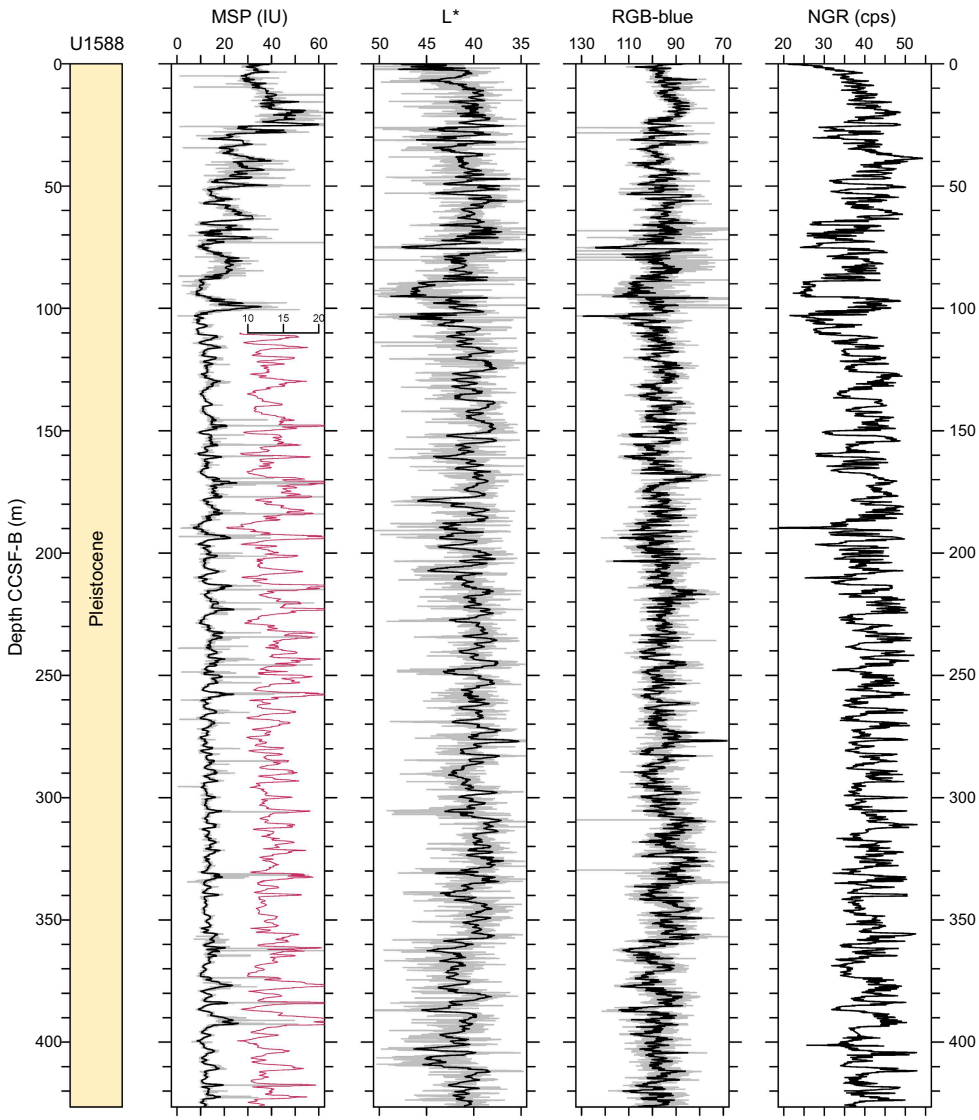

Figure F31. Core composite downhole trends of physical properties data, Site U1588. MSP = section-half point MS, NGR = whole-round NGR, cps = counts per second. Red MSP data are the same as the original signal but with an expanded scale to emphasize the cyclic variability. MSP, L*, and RGB-blue: smoothed curve (black line; 20-point moving average) is shown over original data (gray line). NGR: only original data is shown.

References

Abrantes, F., 1988. Diatom assemblages as upwelling indicators in surface sediments off Portugal. Marine Geology, 85(1):15–39. **https://doi.org/10.1016/0025-3227(88)90082-5**

Abrantes, F., 1991. Increased upwelling off Portugal during the last glaciation: diatom evidence. Marine Micropaleontology, 17(3–4):285–310. **https://doi.org/10.1016/0377-8398(91)90017-Z**

Abrantes, F., 2000. 200,000 yr diatom records from Atlantic upwelling sites reveal maximum productivity during LGM and a shift in phytoplankton community structure at 185 000 yr. Earth and Planetary Science Letters, 176(1):7–16. **https://doi.org/10.1016/S0012-821X(99)00312-X**

Abrantes, F., Baas, J., Haflidason, H., Rasmussen, T., Klitgaard, D., Loncaric, N., and Gaspar, L., 1998. Sediment fluxes along the northeastern European margin: inferring hydrological changes between 20 and 8 kyr. Marine Geology, 152(1–3):7–23. **https://doi.org/10.1016/S0025-3227(98)00062-0**

Abrantes, F., and Moita, T., 1999. Water column and recent sediment data on diatoms and coccolithophorids, off Portugal, confirm sediment record of upwelling events. Oceanologica Acta, 22:319–336. **https://doi.org/10.1016/S0399-1784(99)90007-5**

Abrantes, F., Rodrigues, T., Ventura, C., Santos, C., Roell, U., Voelker, A., and Hodell, D., 2017. Past productivity conditions off SW Iberia at the transition from the 41 ky to the 100 ky world: the record of IODP Sites U1385 and U1391. Geophysical Research Abstracts, 19:EGU2017-9743. **https://meetingorganizer.copernicus.org/EGU2017/EGU2017-9743.pdf**

Adkins, J.F., 2013. The role of deep ocean circulation in setting glacial climates. Paleoceanography and Paleoclimatology, 28(3):539–561. **https://doi.org/10.1002/palo.20046**

Alley, R.B., 2003. Raising paleoceanography. Paleoceanography and Paleoclimatology, 18(4):1085. **https://doi.org/10.1029/2003PA000942**

Alonso-Garcia, M., Sierro, F.J., and Flores, J.A., 2011. Arctic front shifts in the subpolar North Atlantic during the mid-Pleistocene (800–400 ka) and their implications for ocean circulation. Palaeogeography, Palaeoclimatology, Palaeoecology, 311(3):268–280. **https://doi.org/10.1016/j.palaeo.2011.09.004**

Ambar, I., and Howe, M.R., 1979. Observations of the Mediterranean outflow—II. The deep circulation in the vicinity of the Gulf of Cadiz. Deep Sea Research, Part A: Oceanographic Research Papers, 26(5):555–568. **https://doi.org/10.1016/0198-0149(79)90096-7**

Ambar, I., Serra, N., Brogueira, M.J., Cabeçadas, G., Abrantes, F., Freitas, P., Gonçalves, C., and Gonzalez, N., 2002. Physical, chemical and sedimentological aspects of the Mediterranean outflow off Iberia. Deep Sea Research, Part II: Topical Studies in Oceanography, 49(19):4163–4177. **https://doi.org/10.1016/S0967-0645(02)00148-0**

Andrews, J., Barber, D., and Jennings, A., 1999. Errors in generating time-series and in dating events at Late Quaternary millenial (radiocarbon) time-scales: examples from Baffin Bay, NW Labrador Sea, and east Greenland. In Clark, P.U., Webb, R.S., and Keigwin, L.D. (Eds.), Mechanisms of Global Climate Change at Millennial Time Scales. Geophysical Monograph, 112: 23–33. **https://agupubs.onlinelibrary.wiley.com/doi/10.1029/GM112p0023**

Baas, J.H., Mienert, J., Abrantes, F., and Prins, M.A., 1997. Late Quaternary sedimentation on the Portuguese continental margin: climate-related processes and products. Palaeogeography, Palaeoclimatology, Palaeoecology, 130(1–4):1–23. **https://doi.org/10.1016/S0031-0182(96)00135-6**

Bajo, P., Drysdale, R.N., Woodhead, J.D., Hellstrom, J.C., Hodell, D., Ferretti, P., Voelker, A.H.L., Zanchetta, G., Rodrigues, T., Wolff, E., Tyler, J., Frisia, S., Spötl, C., and Fallick, A.E., 2020. Persistent influence of obliquity on ice age terminations since the middle Pleistocene transition. Science, 367(6483):1235–1239. **https://doi.org/10.1126/science.aaw1114**

Bard, E., Rostek, F., Turon, J.-L., and Gendreau, S., 2000. Hydrological impact of Heinrich events in the subtropical northeast Atlantic. Science, 289(5483):1321–1324. **https://doi.org/10.1126/science.289.5483.1321**

Barker, S., Chen, J., Gong, X., Jonkers, L., Knorr, G., and Thornalley, D., 2015. Icebergs not the trigger for North Atlantic cold events. Nature, 520(7547):333–336. **https://doi.org/10.1038/nature14330**

Barker, S., and Knorr, G., 2021. Millennial scale feedbacks determine the shape and rapidity of glacial termination. Nature Communications, 12(1):2273. **https://doi.org/10.1038/s41467-021-22388-6**

Barker, S., Knorr, G., Edwards, R.L., Parrenin, F., Putnam, A.E., Skinner, L.C., Wolff, E., and Ziegler, M., 2011. 800,000 years of abrupt climate variability. Science, 334(6054):347–351. **https://doi.org/10.1126/science.1203580**

Barker, S., Zhang, X., Jonkers, L., Lordsmith, S., Conn, S., and Knorr, G., 2021. Strengthening Atlantic inflow across the mid-Pleistocene transition. Paleoceanography and Paleoclimatology, 36(4):e2020PA004200. **https://doi.org/10.1029/2020PA004200**

Bereiter, B., Fischer, H., Schwander, J., and Stocker, T.F., 2014. Diffusive equilibration of N_2, O_2 and CO_2 mixing ratios in a 1.5-million-years-old ice core. The Cryosphere, 8(1):245–256. **https://doi.org/10.5194/tc-8-245-2014**

Billups, K., and Scheinwald, A., 2014. Origin of millennial-scale climate signals in the subtropical North Atlantic. Paleoceanography and Paleoclimatology, 29(6):612–627. **https://doi.org/10.1002/2014PA002641**

Birner, B., Hodell, D.A., Tzedakis, P.C., and Skinner, L.C., 2016. Similar millennial climate variability on the Iberian margin during two early Pleistocene glacials and MIS 3. Paleoceanography and Paleoclimatology, 31(1):203–217. **https://doi.org/10.1002/2015PA002868**

Blaauw, M., 2012. Out of tune: the dangers of aligning proxy archives. Quaternary Science Reviews, 36:38–49. **https://doi.org/10.1016/j.quascirev.2010.11.012**

Blunier, T., and Brook, E.J., 2001. Timing of millennial-scale climate change in Antarctica and Greenland during the last glacial period. Science, 291(5501):109–112. **https://doi.org/10.1126/science.291.5501.109**

Brambilla, E., Talley, L.D., and Robbins, P.E., 2008. Subpolar Mode Water in the northeastern Atlantic: 2. Origin and transformation. Journal of Geophysical Research: Oceans, 113(C4). **https://doi.org/10.1029/2006JC004063**

Cheng, H., Edwards, R.L., Broecker, W.S., Denton, G.H., Kong, X., Wang, Y., Zhang, R., and Wang, X., 2009. Ice age terminations. Science, 326(5950):248–252. **https://doi.org/10.1126/science.1177840**

COLDEX, 2022. COLDEX Strategic and Implementation Plan. **https://static1.squarespace.com/static/613934d8c582e133b28e61d6/t/6351ad33a2ebab51b4689324/1666297140541/COLDEX+Strategic+Plan_July+2022_For+Website.pdf**

Davtian, N., and Bard, E., 2023. A new view on abrupt climate changes and the bipolar seesaw based on paleotemperatures from Iberian margin sediments. Proceedings of the National Academy of Sciences, 120(12):e2209558120. **https://doi.org/10.1073/pnas.2209558120**

de Abreu, L., Shackleton, N.J., Schönfeld, J., Hall, M., and Chapman, M., 2003. Millennial-scale oceanic climate variability off the western Iberian margin during the last two glacial periods. Marine Geology, 196(1–2):1–20. **https://doi.org/10.1016/S0025-3227(03)00046-X**

Denton, G.H., Anderson, R.F., Toggweiler, J.R., Edwards, R.L., Schaefer, J.M., and Putnam, A.E., 2010. The last glacial termination. Science, 328(5986):1652–1656. **https://doi.org/10.1126/science.1184119**

Dome Fuji Ice Core Project Members, 2017. State dependence of climatic instability over the past 720,000 years from Antarctic ice cores and climate modeling. Science Advances, 3(2):e1600446. **https://doi.org/10.1126/sciadv.1600446**

Donders, T., Panagiotopoulos, K., Koutsodendris, A., Bertini, A., Mercuri, A.M., Masi, A., Combourieu-Nebout, N., Joannin, S., Kouli, K., Kousis, I., Peyron, O., Torri, P., Florenzano, A., Francke, A., Wagner, B., and Sadori, L., 2021. 1.36 million years of Mediterranean forest refugium dynamics in response to glacial–interglacial cycle strength. Proceedings of the National Academy of Sciences, 118(34):e2026111118. **https://doi.org/10.1073/pnas.2026111118**

EPICA Community Members, 2006. One-to-one coupling of glacial climate variability in Greenland and Antarctica. Nature, 444(7116):195–198. **https://doi.org/10.1038/nature05301**

Expedition 339 Scientists, 2013a. Expedition 339 summary. In Stow, D.A.V., Hernández-Molina, F.J., Alvarez Zarikian, C.A., and the Expedition 339 Scientists, Proceedings of the Integrated Ocean Drilling Program. 339: Tokyo (Integrated Ocean Drilling Program Management International, Inc.). **https://doi.org/10.2204/iodp.proc.339.101.2013**

Expedition 339 Scientists, 2013b. Site U1385. In Stow, D.A.V., Hernández-Molina, F.J., Alvarez Zarikian, C.A., and the Expedition 339 Scientists, Proceedings of the Integrated Ocean Drilling Program. 339: Tokyo (Integrated Ocean Drilling Program Management International, Inc.). **https://doi.org/10.2204/iodp.proc.339.103.2013**

Fischer, H., Severinghaus, J., Brook, E., Wolff, E., Albert, M., Alemany, O., Arthern, R., Bentley, C., Blankenship, D., Chappellaz, J., Creyts, T., Dahl-Jensen, D., Dinn, M., Frezzotti, M., Fujita, S., Gallee, H., Hindmarsh, R., Hudspeth, D., Jugie, G., Kawamura, K., Lipenkov, V., Miller, H., Mulvaney, R., Parrenin, F., Pattyn, F., Ritz, C., Schwander, J., Steinhage, D., van Ommen, T., and Wilhelms, F., 2013. Where to find 1.5 million yr old ice for the IPICS "oldest-ice" ice core. Climate of the Past, 9(6):2489–2505. **https://doi.org/10.5194/cp-9-2489-2013**

Fiúza, A., 1984. Hidrologia e Dinâmica das Águas Costeiras de Portugal [PhD dissertation]. Universidade de Lisboa, Portugal.

Fiúza, A.F.G., Hamann, M., Ambar, I., Díaz del Río, G., González, N., and Cabanas, J.M., 1998. Water masses and their circulation off western Iberia during May 1993. Deep Sea Research, Part I: Oceanographic Research Papers, 45(7):1127–1160. **https://doi.org/10.1016/S0967-0637(98)00008-9**

Foreman, A.D., 2017. The evolution of glacial conditions in the Southern Atlantic Ocean: a depth transect approach [PhD dissertation]. University of California, San Diego, CA. **https://escholarship.org/uc/item/232561rg**

Gherardi, J.-M., Labeyrie, L., McManus, J.F., Francois, R., Skinner, L.C., and Cortijo, E., 2005. Evidence from the northeastern Atlantic Basin for variability in the rate of the meridional overturning circulation through the last deglaciation. Earth and Planetary Science Letters, 240(3–4):710–723. **https://doi.org/10.1016/j.epsl.2005.09.061**

Haynes, R., Barton, E.D., and Pilling, I., 1993. Development, persistence, and variability of upwelling filaments off the Atlantic coast of the Iberian Peninsula. Journal of Geophysical Research: Oceans, 98(C12):22681–22692. **https://doi.org/10.1029/93JC02016**

Henry, L.G., McManus, J.F., Curry, W.B., Roberts, N.L., Piotrowski, A.M., and Keigwin, L.D., 2016. North Atlantic ocean circulation and abrupt climate change during the last glaciation. Science, 353(6298):470–474. **https://doi.org/10.1126/science.aaf5529**

Hernández-Almeida, I., Sierro, F.J., Flores, J.-A., Cacho, I., and Filippelli, G.M., 2013. Palaeoceanographic changes in the North Atlantic during the mid-Pleistocene transition (MIS 31-19) as inferred from planktonic foraminiferal and calcium carbonate records. Boreas, 42(1):140–159. **https://doi.org/10.1111/j.1502-3885.2012.00283.x**

Hernández-Molina, F.J., Stow, D.A.V., Alvarez-Zarikian, C.A., Acton, G., Bahr, A., Balestra, B., Ducassou, E., Flood, R., Flores, J.-A., Furota, S., Grunert, P., Hodell, D., Jimenez-Espejo, F., Kim, J.K., Krissek, L., Kuroda, J., Li, B., Llave, E., Lofi, J., Lourens, L., Miller, M., Nanayama, F., Nishida, N., Richter, C., Roque, C., Pereira, H., Sanchez Goñi, M.F., Sierro, F.J., Singh, A.D., Sloss, C., Takashimizu, Y., Tzanova, A., Voelker, A., Williams, T., and Xuan, C., 2014. Onset of Mediterranean outflow into the North Atlantic. Science, 344(6189):1244–1250. **https://doi.org/10.1126/science.1251306**

Hilgen, F.J., 1991. Astronomical calibration of Gauss to Matuyama sapropels in the Mediterranean and implication for the Geomagnetic Polarity Time Scale. Earth and Planetary Science Letters, 104(2–4):226–244. **https://doi.org/10.1016/0012-821X(91)90206-W**

Hodell, D., Crowhurst, S., Skinner, L., Tzedakis, P.C., Margari, V., Channell, J.E.T., Kamenov, G., Maclachlan, S., and Rothwell, G., 2013a. Response of Iberian margin sediments to orbital and suborbital forcing over the past 420 ka. Paleoceanography and Paleoclimatology, 28(1):185–199. **https://doi.org/10.1002/palo.20017**

Hodell, D., Lourens, L., Crowhurst, S., Konijnendijk, T., Tjallingii, R., Jiménez-Espejo, F., Skinner, L., Tzedakis, P.C., and the Shackleton Site Project Members, 2015. A reference time scale for Site U1385 (Shackleton Site) on the SW Iberian Margin. Global and Planetary Change, 133:49–64. **https://doi.org/10.1016/j.gloplacha.2015.07.002**

Hodell, D.A., and Channell, J.E.T., 2016. Mode transitions in Northern Hemisphere glaciation: co-evolution of millennial and orbital variability in Quaternary climate. Climate of the Past, 12(9):1805–1828. **https://doi.org/10.5194/cp-12-1805-2016**

Hodell, D.A., Channell, J.E.T., Curtis, J.H., Romero, O.E., and Röhl, U., 2008. Onset of "Hudson Strait" Heinrich events in the eastern North Atlantic at the end of the middle Pleistocene transition (~640 ka)? Paleoceanography and Paleoclimatology, 23(4):PA4218. **https://doi.org/10.1029/2008PA001591**

Hodell, D.A., Crowhurst, S.J., Lourens, L., Margari, V., Nicolson, J., Rolfe, J.E., Skinner, L.C., Thomas, N.C., Tzedakis, P.C., Mleneck-Vautravers, M.J., and Wolff, E.W., 2023. A 1.5-million-year record of orbital and millennial climate variability in the North Atlantic. Climate of the Past, 19(3):607–636. **https://doi.org/10.5194/cp-19-607-2023**

Hodell, D.A., Elderfield, H., Greaves, M., McCave, I.N., Skinner, L., Thomas, A., and White, N. , 2014. The JC089 Cruise Report - IODP Site Survey of the Shackleton Sites, SW Iberian Margin: Liverpool, UK (British Oceanographic Data Centre).

Hodell, D.A., Evans, H.F., Channell, J.E.T., and Curtis, J.H., 2010. Phase relationships of North Atlantic ice-rafted debris and surface-deep climate proxies during the last glacial period. Quaternary Science Reviews, 29(27–28):3875–3886. **https://doi.org/10.1016/j.quascirev.2010.09.006**

Hodell, D.A., Lourens, L., Stow, D.A.V., Hernández-Molina, F. Javier, and Alvarez-Zarikian, C.A., 2013b. The "Shackleton Site" (IODP Site U1385) on the Iberian Margin. Scientific Drilling, 16:13–19. **https://doi.org/10.5194/sd-16-13-2013**

Jenkins, W.J., Smethie, W.M., Boyle, E.A., and Cutter, G.A., 2015. Water mass analysis for the U.S. GEOTRACES (GA03) North Atlantic sections. Deep Sea Research, Part II: Topical Studies in Oceanography, 116:6–20. **https://doi.org/10.1016/j.dsr2.2014.11.018**

Jouzel, J., Masson-Delmotte, V., Cattani, O., Dreyfus, G., Falourd, S., Hoffmann, G., Minster, B., Nouet, J., Barnola, J.M., Chappellaz, J., Fischer, H., Gallet, J.C., Johnsen, S., Leuenberger, M., Loulergue, L., Luethi, D., Oerter, H., Parrenin, F., Raisbeck, G., Raynaud, D., Schilt, A., Schwander, J., Selmo, E., Souchez, R., Spahni, R., Stauffer, B., Steffensen, J.P., Stenni, B., Stocker, T.F., Tison, J.L., Werner, M., and Wolff, E.W., 2007. Orbital and millennial Antarctic climate variability over the past 800,000 years. Science, 317(5839):793–796. **https://doi.org/10.1126/science.1141038**

Karanovic, I., and Brandão, S.N., 2015. Biogeography of deep-sea wood fall, cold seep and hydrothermal vent Ostracoda (Crustacea), with the description of a new family and a taxonomic key to living Cytheroidea. Deep Sea Research, Part II: Topical Studies in Oceanography, 111:76–94. **https://doi.org/10.1016/j.dsr2.2014.09.008**

Kawamura, K., Parrenin, F., Lisiecki, L., Uemura, R., Vimeux, F., Severinghaus, J.P., Hutterli, M.A., Nakazawa, T., Aoki, S., Jouzel, J., Raymo, M.E., Matsumoto, K., Nakata, H., Motoyama, H., Fujita, S., Goto-Azuma, K., Fujii, Y., and Watanabe, O., 2007. Northern Hemisphere forcing of climatic cycles in Antarctica over the past 360,000 years. Nature, 448(7156):912–916. **https://doi.org/10.1038/nature06015**

Kissel, C., Laj, C., Piotrowski, A.M., Goldstein, S.L., and Hemming, S.R., 2008. Millennial-scale propagation of Atlantic deep waters to the glacial Southern Ocean. Paleoceanography and Paleoclimatology, 23(2):PA2102. **https://doi.org/10.1029/2008PA001624**

Konijnendijk, T.Y.M., Ziegler, M., and Lourens, L.J., 2015. On the timing and forcing mechanisms of late Pleistocene glacial terminations: insights from a new high-resolution benthic stable oxygen isotope record of the eastern Mediterranean. Quaternary Science Reviews, 129:308–320. **https://doi.org/10.1016/j.quascirev.2015.10.005**

Lebreiro, S.M., McCave, I.N., and Weaver, P.P.E., 1997. Late Quaternary turbidite emplacement on the Horseshoe abyssal plain (Iberian margin). Journal of Sedimentary Research, 67(5):856–870. **https://doi.org/10.1306/D4268658-2B26-11D7-8648000102C1865D**

Lebreiro, S.M., Voelker, A.H.L., Vizcaino, A., Abrantes, F.G., Alt-Epping, U., Jung, S., Thouveny, N., and Gràcia, E., 2009. Sediment instability on the Portuguese continental margin under abrupt glacial climate changes (last 60 kyr). Quaternary Science Reviews, 28(27–28):3211–3223. **https://doi.org/10.1016/j.quascirev.2009.08.007**

Litt, T., Pickarski, N., Heumann, G., Stockhecke, M., and Tzedakis, P.C., 2014. A 600,000 year long continental pollen record from Lake Van, eastern Anatolia (Turkey). Quaternary Science Reviews, 104:30–41. **https://doi.org/10.1016/j.quascirev.2014.03.017**

Lund, D.C., Adkins, J.F., and Ferrari, R., 2011. Abyssal Atlantic circulation during the Last Glacial Maximum: constraining the ratio between transport and vertical mixing. Paleoceanography, 26(1):PA1213. **https://doi.org/10.1029/2010PA001938**

Magill, C.R., Ausín, B., Wenk, P., McIntyre, C., Skinner, L., Martínez-García, A., Hodell, D.A., Haug, G.H., Kenney, W., and Eglinton, T.I., 2018. Transient hydrodynamic effects influence organic carbon signatures in marine sediments. Nature Communications, 9(1):4690. **https://doi.org/10.1038/s41467-018-06973-w**

Margari, V., Skinner, L.C., Hodell, D.A., Martrat, B., Toucanne, S., Grimalt, J.O., Gibbard, P.L., Lunkka, J.P., and Tzedakis, P.C., 2014. Land-ocean changes on orbital and millennial time scales and the penultimate glaciation. Geology, 42(3):183–186. **https://doi.org/10.1130/G35070.1**

Margari, V., Skinner, L.C., Menviel, L., Capron, E., Rhodes, R.H., Mleneck-Vautravers, M.J., Ezat, M.M., Martrat, B., Grimalt, J.O., Hodell, D.A., and Tzedakis, P.C., 2020. Fast and slow components of interstadial warming in the North Atlantic during the last glacial. Communications Earth & Environment, 1(1):6. **https://doi.org/10.1038/s43247-020-0006-x**

Margari, V., Skinner, L.C., Tzedakis, P.C., Ganopolski, A., Vautravers, M., and Shackleton, N.J., 2010. The nature of millennial-scale climate variability during the past two glacial periods. Nature Geoscience, 3(2):127–131. **https://doi.org/10.1038/ngeo740**

Martrat, B., Grimalt, J.O., Shackleton, N.J., Abreu, L.d., Hutterli, M.A., and Stocker, T.F., 2007. Four climate cycles of recurring deep and surface water destabilizations on the Iberian margin. Science, 317(5837):502–507. **https://doi.org/10.1126/science.1139994**

Mc Intyre, K., Delaney, M.L., and Ravelo, A.C., 2001. Millennial-scale climate change and oceanic processes in the late Pliocene and early Pleistocene. Paleoceanography and Paleoclimatology, 16:535–543. **https://doi.org/10.1029/2000PA000526**

McManus, J.F., Oppo, D.W., and Cullen, J.L., 1999. A 0.5-million-year record of millennial-scale climate variability in the North Atlantic. In Science. 5404, 283: 971–975. **https://doi.org/10.1126/science.283.5404.971**

Meckler, A.N., Sigman, D.M., Gibson, K.A., François, R., Martínez-García, A., Jaccard, S.L., Röhl, U., Peterson, L.C., Tiedemann, R., and Haug, G.H., 2013. Deglacial pulses of deep-ocean silicate into the subtropical North Atlantic Ocean. Nature, 495(7442):495–498. **https://doi.org/10.1038/nature12006**

Naughton, F., Costas, S., Gomes, S.D., Desprat, S., Rodrigues, T., Sanchez Goñi, M.F., Renssen, H., Trigo, R., Bronk-Ramsey, C., Oliveira, D., Salgueiro, E., Voelker, A.H.L., and Abrantes, F., 2019. Coupled ocean and atmospheric changes during Greenland stadial 1 in southwestern Europe. Quaternary Science Reviews, 212:108–120. **https://doi.org/10.1016/j.quascirev.2019.03.033**

Naughton, F., Sanchez Goñi, M.F., Desprat, S., Turon, J.L., Duprat, J., Malaizé, B., Joli, C., Cortijo, E., Drago, T., and Freitas, M.C., 2007. Present-day and past (last 25000 years) marine pollen signal off western Iberia. Marine Micropaleontology, 62(2):91–114. **https://doi.org/10.1016/j.marmicro.2006.07.006**

Nehrbass-Ahles, C., Shin, J., Schmitt, J., Bereiter, B., Joos, F., Schilt, A., Schmidely, L., Silva, L., Teste, G., Grilli, R., Chappellaz, J., Hodell, D., Fischer, H., and Stocker, T.F., 2020. Abrupt CO_2 release to the atmosphere under glacial and early interglacial climate conditions. Science, 369(6506):1000–1005. **https://doi.org/10.1126/science.aay8178**

Oliveira, D., Desprat, S., Rodrigues, T., Naughton, F., Hodell, D., Trigo, R., Rufino, M., Lopes, C., Abrantes, F., and Sánchez Goñi, M.F., 2016. The complexity of millennial-scale variability in southwestern Europe during MIS 11. Quaternary Research, 86(3):373–387. **https://doi.org/10.1016/j.yqres.2016.09.002**

Oliveira, D., Desprat, S., Yin, Q., Naughton, F., Trigo, R., Rodrigues, T., Abrantes, F., and Sánchez Goñi, M.F., 2018. Unraveling the forcings controlling the vegetation and climate of the best orbital analogues for the present interglacial in SW Europe. Climate Dynamics, 51(1):667–686. **https://doi.org/10.1007/s00382-017-3948-7**

Oliveira, D., Desprat, S., Yin, Q., Rodrigues, T., Naughton, F., Trigo, R.M., Su, Q., Grimalt, J.O., Alonso-Garcia, M., Voelker, A.H.L., Abrantes, F., and Sánchez Goñi, M.F., 2020. Combination of insolation and ice-sheet forcing drive enhanced humidity in northern subtropical regions during MIS 13. Quaternary Science Reviews, 247:106573. **https://doi.org/10.1016/j.quascirev.2020.106573**

Oliveira, D., Sánchez Goñi, M.F., Naughton, F., Polanco-Martinez, J.M., Jimenez-Espejo, F.J., Grimalt, J.O., Martrat, B., Voelker, A.H.L., Trigo, R., Hodell, D., Abrantes, F., and Desprat, S., 2017. Unexpected weak seasonal climate in the western Mediterranean region during MIS 31, a high-insolation forced interglacial. Quaternary Science Reviews, 161:1–17. **https://doi.org/10.1016/j.quascirev.2017.02.013**

Oppo, D.W., McManus, J.F., and Cullen, J.L., 1998. Abrupt climate events 500,000 to 340,000 years ago: evidence from subpolar North Atlantic sediments. Science, 279(5355):1335–1338. **https://doi.org/10.1126/science.279.5355.1335**

Pailler, D., and Bard, E., 2002. High frequency palaeoceanographic changes during the past 140 000 yr recorded by the organic matter in sediments of the Iberian Margin. Palaeogeography, Palaeoclimatology, Palaeoecology, 181(4):431–452. **https://doi.org/10.1016/S0031-0182(01)00444-8**

Peliz, Á., Dubert, J., Santos, A.M.P., Oliveira, P.B., and Le Cann, B., 2005. Winter upper ocean circulation in the Western Iberian Basin—fronts, eddies and poleward flows: an overview. Deep Sea Research, Part I: Oceanographic Research Papers, 52(4):621–646. **https://doi.org/10.1016/j.dsr.2004.11.005**

Pérez, M.E., Lin, H.-L., Lange, C.B., and Schneider, R., 2001. Pliocene-Pleistocene opal records off Southwest Africa, Sites 1082 and 1084: a comparison of analytical techniques. In Wefer, G., Berger, W.H., and Richter, C. (Eds.), Proceedings of the Ocean Drilling Program, Scientific Results. 175: College Station, TX (Ocean Drilling Program). **https://doi.org/10.2973/odp.proc.sr.175.221.2001**

Piotrowski, A.M., Goldstein, S.L., Hemming, S.R., Fairbanks, R.G., and Zylberberg, D.R., 2008. Oscillating glacial northern and southern deep water formation from combined neodymium and carbon isotopes. Earth and Planetary Science Letters, 272(1–2):394–405. **https://doi.org/10.1016/j.epsl.2008.05.011**

Pol, K., Masson-Delmotte, V., Johnsen, S., Bigler, M., Cattani, O., Durand, G., Falourd, S., Jouzel, J., Minster, B., Parrenin, F., Ritz, C., Steen-Larsen, H.C., and Stenni, B., 2010. New MIS 19 EPICA Dome C high resolution deuterium data: hints for a problematic preservation of climate variability at sub-millennial scale in the "oldest ice". Earth and Planetary Science Letters, 298(1):95–103. **https://doi.org/10.1016/j.epsl.2010.07.030**

Raymo, M.E., Ganley, K., Carter, S., Oppo, D.W., and McManus, J., 1998. Millennial-scale climate instability during the early Pleistocene epoch. Nature, 392(6677):699–702. **https://doi.org/10.1038/33658**

Raymo, M.E., and Huybers, P., 2008. Unlocking the mysteries of the ice ages. Nature, 451(7176):284–285. **https://doi.org/10.1038/nature06589**

Relvas, P., Luís, J., and Santos, A.M.P., 2009. Importance of the mesoscale in the decadal changes observed in the northern Canary upwelling system. Geophysical Research Letters, 36(22):L22601. **https://doi.org/10.1029/2009GL040504**

Ríos, A.F., Pérez, F.F., and Fraga, F., 1992. Water masses in the upper and middle North Atlantic Ocean east of the Azores. Deep Sea Research, Part A. Oceanographic Research Papers, 39(3):645–658. **https://doi.org/10.1016/0198-0149(92)90093-9**

Rodrigues, T., Alonso-Garcia, M., Hodell, D.A., Rufino, M., Naughton, F., Grimalt, J.O., Voelker, A.H.L., and Abrantes, F., 2017. A 1-Ma record of sea surface temperature and extreme cooling events in the North Atlantic: a perspective from the Iberian Margin. Quaternary Science Reviews, 172:118–130. **https://doi.org/10.1016/j.quascirev.2017.07.004**

Rodrigues, T., Voelker, A.H.L., Grimalt, J.O., Abrantes, F., and Naughton, F., 2011. Iberian margin sea surface temperature during MIS 15 to 9 (580–300 ka): glacial suborbital variability versus interglacial stability. Paleoceanography and Paleoclimatology, 26(1):PA1204. **https://doi.org/10.1029/2010PA001927**

Roucoux, K.H., Shackleton, N.J., de Abreu, L., Schönfeld, J., and Tzedakis, P.C., 2001. Combined marine proxy and pollen analyses reveal rapid Iberian vegetation response to North Atlantic millennial-scale climate oscillations. Quaternary Research, 56(1):128–132. **https://doi.org/10.1006/qres.2001.2218**

Salgueiro, E., Voelker, A., Abrantes, F., Meggers, H., Pflaumann, U., Lončarić, N., González-Álvarez, R., Oliveira, P., Bartels-Jónsdóttir, H.B., Moreno, J., and Wefer, G., 2008. Planktonic foraminifera from modern sediments reflect upwelling patterns off Iberia: insights from a regional transfer function. Marine Micropaleontology, 66(3–4):135–164. **https://doi.org/10.1016/j.marmicro.2007.09.003**

Salgueiro, E., Voelker, A.H.L., de Abreu, L., Abrantes, F., Meggers, H., and Wefer, G., 2010. Temperature and productivity changes off the western Iberian margin during the last 150 ky. Quaternary Science Reviews, 29(5–6):680–695. **https://doi.org/10.1016/j.quascirev.2009.11.013**

Sánchez Goñi, M.F., Eynaud, F., Turon, J.L., and Shackleton, N.J., 1999. High resolution palynological record off the Iberian margin: direct land-sea correlation for the Last Interglacial complex. Earth and Planetary Science Letters, 171(1):123–137. **https://doi.org/10.1016/S0012-821X(99)00141-7**

Sánchez Goñi, M.F., Llave, E., Oliveira, D., Naughton, F., Desprat, S., Ducassou, E., Hodell, D.A., and Hernández Molina, F.J., 2016. Climate changes in south western Iberia and Mediterranean Outflow variations during two contrasting cycles of the last 1 myrs: MIS 31-MIS 30 and MIS 12-MIS 11. Global and Planetary Change, 136:18–29. **https://doi.org/10.1016/j.gloplacha.2015.11.006**

Sánchez Goñi, M.F., Turon, J.-L., Eynaud, F., and Gendreau, S., 2000. European climatic response to millennial-scale changes in the atmosphere–ocean system during the last glacial period. Quaternary Research, 54(3):394–403. **https://doi.org/10.1006/qres.2000.2176**

Saunders, P.M., 1987. Flow through Discovery Gap. Journal of Physical Oceanography, 17(5):631–643. **https://doi.org/10.1175/1520-0485(1987)017%3C0631:FTDG%3E2.0.CO;2**

Schlitzer, R., 2000. Electronic atlas of WOCE hydrographic and tracer data now available. Eos, Transactions of the American Geophysical Union, 81(5):45. **https://doi.org/10.1029/00EO00028**

Shackleton, N.J., Hall, M.A., and Pate, D., 1995. Pliocene stable isotope stratigraphy of Site 846. In Pisias, N.G., Mayer, L.A., Janecek, T.R., Palmer-Julson, A., and van Andel, T.H. (Eds.), Proceedings of the Ocean Drilling Program, Scientific Results. 138: College Station, TX (Ocean Drilling Program), 337–355. **https://doi.org/10.2973/odp.proc.sr.138.117.1995**

Shackleton, N.J., Chapman, M., Sánchez-Goñi, M.F., Pailler, D., and Lancelot, Y., 2002. The classic Marine Isotope Substage 5e. Quaternary Research, 58(1):14–16. **https://doi.org/10.1006/qres.2001.2312**

Shackleton, N.J., Fairbanks, R.G., Chiu, T., and Parrenin, F., 2004. Absolute calibration of the Greenland time scale: implications for Antarctic time scales and for $\Delta^{14}C$. Quaternary Science Reviews, 23(14–15):1513–1522. **https://doi.org/10.1016/j.quascirev.2004.03.006**

Shackleton, N.J., Hall, M.A., and Vincent, E., 2000. Phase relationships between millennial-scale events 64,000–24,000 years ago. Paleoceanography and Paleoclimatology, 15(6):565–569. **https://doi.org/10.1029/2000PA000513**

Shackleton, N.J., Sánchez-Goñi, M.F., Pailler, D., and Lancelot, Y., 2003. Marine Isotope Substage 5e and the Eemian interglacial. Global and Planetary Change, 36(3):151–155. **https://doi.org/10.1016/S0921-8181(02)00181-9**

Skinner, L.C., Elderfield, H., and Hall, M., 2007. Phasing of millennial climate events and northeast Atlantic deep-water temperature change since 50 Ka Bp. In Schmittner, A., Chiang, J.C.H., and Hemming, S.R. (Eds.), Ocean Circulation: Mechanisms and Impacts—Past and Future Changes of Meridional Overturning. Geophysical Monograph, 173: 197–208. **https://doi.org/10.1029/173GM14**

Skinner, L.C., Freeman, E., Hodell, D., Waelbroeck, C., Vazquez Riveiros, N., and Scrivner, A.E., 2021. Atlantic Ocean ventilation changes across the last deglaciation and their carbon cycle implications. Paleoceanography and Paleoclimatology, 36(2):e2020PA004074. **https://doi.org/10.1029/2020PA004074**

Skinner, L.C., and Shackleton, N.J., 2004. Rapid transient changes in northeast Atlantic deep water ventilation age across Termination I. Paleoceanography and Paleoclimatology, 19(2):PA2005. **https://doi.org/10.1029/2003PA000983**

Skinner, L.C., Shackleton, N.J., and Elderfield, H., 2003. Millennial-scale variability of deep-water temperature and $\delta^{18}O_{dw}$ indicating deep-water source variations in the northeast Atlantic, 0–34 cal. ka BP. Geochemistry, Geophysics, Geosystems, 4(12):1098. **https://doi.org/10.1029/2003GC000585**

Sousa, F.M., and Bricaud, A., 1992. Satellite-derived phytoplankton pigment structures in the Portuguese upwelling area. Journal of Geophysical Research: Oceans, 97(C7):11343–11356. **https://doi.org/10.1029/92JC00786**

Steineck, P.L., Maddocks, R.F., Coles, G.P., and Whatley, R.C., 1990. Xylophile ostracoda in the deep sea. In Whatley, R.C., and Maybury, C. (Eds.), Ostracoda and Global Events. London (Chapman and Hall), 307–319.

Stocker, T.F., 1998. The Seesaw Effect. Science, 282(5386):61–62. **https://doi.org/10.1126/science.282.5386.61**

Sun, Y., McManus, J.F., Clemens, S.C., Zhang, X., Vogel, H., Hodell, D.A., Guo, F., Wang, T., Liu, X., and An, Z., 2021. Persistent orbital influence on millennial climate variability through the Pleistocene. Nature Geoscience, 14(11):812–818. **https://doi.org/10.1038/s41561-021-00794-1**

Tanaka, H., Lelièvre, Y., and Yasuhara, M., 2019. Xylocythere sarrazinae, a new cytherurid ostracod (Crustacea) from a hydrothermal vent field on the Juan de Fuca Ridge, northeast Pacific Ocean, and its phylogenetic position within Cytheroidea. Marine Biodiversity, 49(6):2571–2586. **https://doi.org/10.1007/s12526-019-00987-3**

Thomas, N.C., Bradbury, H.J., and Hodell, D.A., 2022. Changes in North Atlantic deep-water oxygenation across the Middle Pleistocene Transition. Science, 377(6606):654–659. **https://doi.org/10.1126/science.abj7761**

Turchyn, A.V., Antler, G., Byrne, D., Miller, M., and Hodell, D.A., 2016. Microbial sulfur metabolism evidenced from pore fluid isotope geochemistry at Site U1385. Global and Planetary Change, 141:82–90. **https://doi.org/10.1016/j.gloplacha.2016.03.004**

Tzedakis, P.C., Drysdale, R.N., Margari, V., Skinner, L.C., Menviel, L., Rhodes, R.H., Taschetto, A.S., Hodell, D.A., Crowhurst, S.J., Hellstrom, J.C., Fallick, A.E., Grimalt, J.O., McManus, J.F., Martrat, B., Mokeddem, Z., Parrenin, F., Regattieri, E., Roe, K., and Zanchetta, G., 2018. Enhanced climate instability in the North Atlantic and southern Europe during the last interglacial. Nature Communications, 9(1):4235. **https://doi.org/10.1038/s41467-018-06683-3**

Tzedakis, P.C., Frogley, M.R., Lawson, I.T., Preece, R.C., Cacho, I., and de Abreu, L., 2004. Ecological thresholds and patterns of millennial-scale climate variability: the response of vegetation in Greece during the last glacial period. Geology, 32(2):109–112. **https://doi.org/10.1130/G20118.1**

Tzedakis, P.C., Hooghiemstra, H., and Pälike, H., 2006. The last 1.35 million years at Tenaghi Philippon: revised chronostratigraphy and long-term vegetation trends. Quaternary Science Reviews, 25(23–24):3416–3430. **https://doi.org/10.1016/j.quascirev.2006.09.002**

Tzedakis, P.C., Margari, V., and Hodell, D.A., 2015. Coupled ocean-land millennial scale changes 1.26 million years ago, recorded at Site U1385 off Portugal. Global and Planetary Change, 135:83–88. **https://doi.org/10.1016/j.gloplacha.2015.10.008**

Tzedakis, P.C., Pälike, H., Roucoux, K.H., and de Abreu, L., 2009. Atmospheric methane, southern European vegetation and low-mid latitude links on orbital and millennial timescales. Earth and Planetary Science Letters, 277(3–4):307–317. **https://doi.org/10.1016/j.epsl.2008.10.027**

van Aken, H.M., 2000. The hydrography of the mid-latitude Northeast Atlantic Ocean: II: the intermediate water masses. Deep Sea Research, Part I: Oceanographic Research Papers, 47(5):789–824. **https://doi.org/10.1016/S0967-0637(99)00112-0**

Vanney, J.R., and Mougenot, D., 1981. La plate-forme continentale du portugal et les provinces adjacentes: analyse géomorphologique. Memórias dos Serviços Geológicos de Portugal, 28:109.

Ventura, C., Abrantes, F., Loureiro, I., and Voelker, A.H.L., 2017. Data report: diatom and silicoflagellate records of marine isotope stages 25–27 at IODP Site U1387, Faro Drift. In Stow, D.A.V., Hernández-Molina, F.J., Alvarez Zarikian, C.A., and the Expedition 339 Scientists, Proceedings of the Integrated Ocean Drilling Program. 339: Tokyo (Integrated Ocean Drilling Program Management International, Inc.). **https://doi.org/10.2204/iodp.proc.339.202.2017**

Verbitsky, M.Y., Crucifix, M., and Volobuev, D.M., 2018. A theory of Pleistocene glacial rhythmicity. Earth System Dynamics, 9(3):1025–1043. **https://doi.org/10.5194/esd-9-1025-2018**

WAIS Divide Project Members, 2015. Precise interpolar phasing of abrupt climate change during the last ice age. Nature, 520(7549):661–665. **https://doi.org/10.1038/nature14401**

Weirauch, D., Billups, K., and Martin, P., 2008. Evolution of millennial-scale climate variability during the mid-Pleistocene. Paleoceanography and Paleoclimatology, 23(3):PA3216. **https://doi.org/10.1029/2007PA001584**

Westerhold, T., Marwan, N., Drury, A.J., Liebrand, D., Agnini, C., Anagnostou, E., Barnet, J.S.K., Bohaty, S.M., De Vleeschouwer, D., Florindo, F., Frederichs, T., Hodell, D.A., Holbourn, A.E., Kroon, D., Lauretano, V., Littler, K., Lourens, L.J., Lyle, M., Pälike, H., Röhl, U., Tian, J., Wilkens, R.H., Wilson, P.A., and Zachos, J.C., 2020. An astronomically dated record of Earth's climate and its predictability over the last 66 million years. Science, 369(6509):1383–1387. **https://doi.org/10.1126/science.aba6853**

Willamowski, C., and Zahn, R., 2000. Upper ocean circulation in the glacial North Atlantic from benthic foraminiferal isotope and trace element fingerprinting. Paleoceanography and Paleoclimatology, 15(5):515–527. **https://doi.org/10.1029/1999PA000467**

Wolff, E.W., Fischer, H., and Röthlisberger, R., 2009. Glacial terminations as southern warmings without northern control. Nature Geoscience, 2(3):206–209. **https://doi.org/10.1038/ngeo442**

Wolff, E.W., Fischer, H., van Ommen, T., and Hodell, D.A., 2022. Stratigraphic templates for ice core records of the past 1.5 Myr. Climate of the Past, 18(7):1563–1577. **https://doi.org/10.5194/cp-18-1563-2022**

Woodson, C.B., and Litvin, S.Y., 2015. Ocean fronts drive marine fishery production and biogeochemical cycling. Proceedings of the National Academy of Sciences of the United States of America, 112(6):1710–1715. **https://doi.org/10.1073/pnas.1417143112**

Wunsch, C., 2006. Abrupt climate change: an alternative view. Quaternary Research, 65(2):191–203. **https://doi.org/10.1016/j.yqres.2005.10.006**

Zhang, X., Barker, S., Knorr, G., Lohmann, G., Drysdale, R., Sun, Y., Hodell, D., and Chen, F., 2021. Direct astronomical influence on abrupt climate variability. Nature Geoscience, 14(11):819–826. **https://doi.org/10.1038/s41561-021-00846-6**

Zitellini, N., Gràcia, E., Matias, L., Terrinha, P., Abreu, M.A., DeAlteriis, G., Henriet, J.P., Dañobeitia, J.J., Masson, D.G., Mulder, T., Ramella, R., Somoza, L., and Diez, S., 2009. The quest for the Africa–Eurasia plate boundary west of the Strait of Gibraltar. Earth and Planetary Science Letters, 280(1–4):13–50. **https://doi.org/10.1016/j.epsl.2008.12.005**